ELECTROCHEMICAL AND RHEOLOGICAL PROPERTIES OF PHTHALOYL STARCH AND HYDROXYETHYL CELLULOSE BLEND- BASED GEL POLYMER ELECTROLYTE FOR APPLICATION IN QUASI-SOLID DYE-SENSITIZED SOLAR CELL

VIDHYA A/P SELVANATHAN

FACULTY OF SCIENCE
UNIVERSITY OF MALAYA
KUALA LUMPUR

2018

ELECTROCHEMICAL AND RHEOLOGICAL PROPERTIES OF PHTHALOYL STARCH AND HYDROXYETHYL CELLULOSE BLEND- BASED GEL POLYMER ELECTROLYTE FOR APPLICATION IN QUASI-SOLID DYE-SENSITIZED SOLAR CELL

VIDHYA A/P SELVANATHAN

THESIS SUBMITTED IN FULFILMENT OF THE REQUIREMENTS FOR THE DEGREE OF DOCTOR OF PHILOSOPHY

DEPARTMENT OF CHEMISTRY
FACULTY OF SCIENCE
UNIVERSITY OF MALAYA
KUALA LUMPUR

2018

UNIVERSITY OF MALAYA

ORIGINAL LITERARY WORK DECLARATION

Name of Candidate: **VIDHYA A/P SELVANATHAN**

Matric No: **SHC 160032**

Name of Degree: **DOCTOR OF PHILOSOPHY**

Title of Project Paper/Research Report/Dissertation/Thesis ("this Work"):

ELECTROCHEMICAL AND RHEOLOGICAL PROPERTIES OF PHTHALOYL STARCH AND HYDROXYETHYL CELLULOSE BLEND-BASED GEL POLYMER ELECTROLYTE FOR APPLICATION IN QUASI-SOLID DYE-SENSITIZED SOLAR CELL

Field of Study: **POLYMER CHEMISTRY**

I do solemnly and sincerely declare that:

(1) I am the sole author/writer of this Work;
(2) This Work is original;
(3) Any use of any work in which copyright exists was done by way of fair dealing and for permitted purposes and any excerpt or extract from, or reference to or reproduction of any copyright work has been disclosed expressly and sufficiently and the title of the Work and its authorship have been acknowledged in this Work;
(4) I do not have any actual knowledge nor do I ought reasonably to know that the making of this work constitutes an infringement of any copyright work;
(5) I hereby assign all and every rights in the copyright to this Work to the University of Malaya ("UM"), who henceforth shall be owner of the copyright in this Work and that any reproduction or use in any form or by any means whatsoever is prohibited without the written consent of UM having been first had and obtained;
(6) I am fully aware that if in the course of making this Work I have infringed any copyright whether intentionally or otherwise, I may be subject to legal action or any other action as may be determined by UM.

Candidate's Signature Date:

Subscribed and solemnly declared before,

Witness's Signature Date:

Name:

Designation:

ELECTROCHEMICAL AND RHEOLOGICAL PROPERTIES OF PHTHALOYL STARCH AND HYDROXYETHYL CELLULOSE BLEND-BASED GEL POLYMER ELECTROLYTE FOR APPLICATION IN QUASI-SOLID DYE-SENSITIZED SOLAR CELL

ABSTRACT

In this work, a simple phthaloylation process involving reaction of starch with phthalic anhydride is proposed to transform starch into organosoluble material. FTIR and NMR spectroscopy results verifies the formation of phthaloyl starch (PhSt). The resulting starch derivative, was then blend with hydroxyethyl cellulose (HEC) to fabricate polymer gel electrolytes. Rheological analyses such as amplitude sweep studies and tack tests indicate that gels with good rigidity, strength and adhesiveness were attained upon blending 20 to 60 wt.% HEC. Gels within this optimum range of composition were then fabricated into quasi-solid dye-sensitized solar cell (QSDSSC) with the addition of 5 wt.% of tetrapropylammonium iodide and iodine. EIS of the QSDSSC reveal that the adhesive property of the gels plays a crucial role in affecting charge transfer processes at the electrode/electrolyte interfaces. The highest efficiency of 3.02% was recorded with the gels consisting 70 wt.% of PhSt and 30 wt.% of HEC. This polymer blend composition was then used to study the effect of salt composition on the electrolyte properties in which two series of polymer gels containing different amounts of tetrapropylammonium iodide (TPAI) and lithium iodide (LiI) respectively were prepared. Storage modulus values from rheological studies showed that the size of cations in the electrolytes affects the mechanical property of the gels. Best performing solar cells with the efficiency of 3.94 % was achieved by addition of 12.5 wt.% of TPAI. As an initiative to further boost the efficiency values, 1-butyl-3-methylimidazolium iodide (BMII) was included into the PhSt-HEC-TPAI system. The ionic liquid greatly enhanced the short circuit current of the cells, leading to an optimum efficiency of 5.20 % upon addition of 8 wt.% of BMII.

Keywords: starch; cellulose; electrolyte; rheology; solar cell

CIRI-CIRI ELEKTROKIMIA DAN REOLOGI ELEKTROLIT GEL POLIMER BERASASKAN GABUNGAN KANJI PHTHALOYL DAN SELULOSA HIDROKSIETIL UNTUK APLIKASI SEL SURIA PEKA PEWARNA KUASI-PEPEJAL

ABSTRAK

Dalam kerja ini, proses "phthaloylation" yang mudah melibatkan tindak balas kanji dengan anhidrid phthalik dicadangkan untuk mengubah kanji menjadi bahan yang larut dalam pelarut organik. Hasil spektroskopi FTIR dan NMR mengesahkan pembentukan kanji phthaloyl. Derivatif kanji yang dihasilkan, kemudiannya digabungkan dengan selulosa hidroksietil untuk membuat elektrolit gel polimer. Analisis rheologi seperti kajian amplitud dan ujian kelekitan menunjukkan bahawa gel dengan ketegaran, kekuatan dan perekatan yang baik telah dicapai dengan penggabungan 20 hingga 60% HEC. Gel dalam julat komposisi optimum ini kemudiannya diaplikasikan ke dalam sel suria peka pewarna kuasi-pepejal dengan penambahan 5% berat tetrapropilammonium iodida dan iodin. Kajian EIS dari sel suria mendedahkan bahawa sifat pelekat gel memainkan peranan penting dalam mempengaruhi proses pemindahan caj di antara muka elektrod / elektrolit. Kecekapan tertinggi sebanyak 3.02% dicatatkan dengan gel yang mengandungi 70% berat PhSt dan 30% berat HEC. Komposisi campuran polimer ini kemudiannya digunakan untuk mengkaji kesan komposisi garam pada sifat-sifat elektrolit di mana dua siri gel polimer mengandungi jumlah tetrapropillammonium iodide (TPAI) dan litium iodide (LiI) yang berbeza. Nilai modulus penyimpanan dari kajian rheologi menunjukkan bahawa saiz kation dalam elektrolit mempengaruhi sifat mekanikal gel tersebut. Sel solar terbaik dengan kecekapan 3.94% dicapai dengan penambahan 12.5% berat TPAI. Sebagai inisiatif untuk meningkatkan lagi nilai kecekapan, 1-butil-3-methilimidazolium iodide (BMII) dimasukkan ke dalam sistem PhSt-HEC-TPAI. Cecair ionik sangat meningkatkan arus litar pintas sel-sel, yang membawa kepada kecekapan optimum 5.04% selepas penambahan 8% berat BMII.

Kata kunci: kanji; selulosa; elecktrolit; reologi; sel suria

ACKNOWLEDGEMENTS

First and foremost, I am grateful to the God for bestowing me with good health and wellbeing that were essential in this journey. That being said, I am eternally grateful to my supervisor Prof. Dr. Rosiyah Yahya for being the main aspiring guidance in this research. A famous quote mentions that "The whole purpose of education is to turn mirrors into windows". In that way, Prof. Rosiyah is a true educator in every sense, as she not only taught me scientific knowledge but also the essential values in life. Without her support and enthusiastic involvement in every step, this dissertation would have never been accomplished. Thank you so much Prof. for bringing out the best in me.

I truly believe that my family is the biggest gift in life. No matter how bad my day is, each time when I'm home, it always turns better. Thank you *Amma* and *Appa* for creating that "home" for me. It's my mission in life to make you proud, and this will be the beginning of it. Most importantly, one person deserves a special mention for being there at both moments of pressure and pleasure. My dear little sister, *Shanmol*, thank you for all the patience with my mood swings, "DJing" in the car, late night take-outs, last minute favors and proofreading services. The greatest present our parents gave us was each other.

I would like to express my gratitude to my labmates; Danial, Rizwan, Cheyma, Kak Farhana and Kak Shafiza for your valuable constructive criticism and friendly advice throughout the project. I also owe a great sense of gratitude to fellow friends from Centre of Ionics UM, particularly, Syaza, Najla, Dila and Ammar for all the knowledge and extensive moral support. All the tea-breaks, late-night characterizations and failed experiments were so much more fun with you guys. I wish that such sheer goodwill will bring all of you many success in life.

Last but not least, I would also like to expand my deepest gratitude to University of Malaya for supporting this study under the University of Malaya PPP Grant (PG181-2015A)

Yours sincerely,

Vidhya

TABLE OF CONTENTS

LIST OF FIGURES

LIST OF TABLES

LIST OF EQUATIONS

LIST OF SYMBOLS AND ABBREVIATIONS

AST	:	Amplitude sweep test
BMII	:	1-butyl-3-methylimidazolium iodide
CB	:	Conduction band
CE	:	Counter electrode
DES	:	Deep eutectic solvent
DMF	:	N,N-dimethylformamide
DS	:	Degree of substitution
DSSC	:	Dye-sensitized solar cell
QSDSSC	:	Quasi-solid dye-sensitized solar cell
E_a	:	Activation energy
EIS	:	Electrochemical impedance spectroscopy
FF	:	Fill factor
FTIR	:	Fourier Transform Infrared Spectroscopy
FTO	:	Fluorine Tin Oxide
G′	:	Storage modulus
G″	:	Loss modulus
GPE	:	Gel polymer electrolyte
HEC	:	Hydroxyethyl cellulose
HOMO	:	Highest occupied molecular orbital
I_2	:	Iodine
I_3^-	:	Triiodide ion
IL	:	Ionic liquid
J_{SC}	:	Short-circuit current
LiI	:	Lithium iodide

LUMO	:	Lowest unoccupied molecular orbital
LVE	:	Linear viscoelastic
N719	:	Ruthenium dye
NMR	:	Nuclear magnetic resonance
PhSt	:	Phthaloyl starch
R_{CT}	:	Charge transfer resistance
R_D	:	Diffusion resistance
R_{PT}	:	Counter electrode resistance
R_S	:	Sheet resistance
tan δ	:	Loss factor
TiO_2	:	Titanium dioxide
TPAI	:	Tetrapropylammonium iodide
V_{OC}	:	Open circuit voltage
XRD	:	X-ray diffraction
η	:	Photoconversion efficiency
σ	:	Ionic conductivity
γ_c	:	Critical strain

LIST OF APPENDICES

CHAPTER 1: INTRODUCTION

1.1 Motivation

Dye-sensitized solar cells (DSSC) are third generation photovoltaic devices which are highly celebrated for their cost effectiveness and ease of fabrication. The electrolyte is one of the most salient components in DSSC as it controls the internal charge transport within the electrodes; enabling the dye to be regenerated throughout the device operation. So far, the traditional liquid electrolyte based DSSC continues to be the most successful, producing efficiencies as high as 13 % (Chen *et al.*, 2009). Yet, practical drawbacks such as leakage and solvent evaporation posed by these liquid electrolytes trigger the need to explore other types of electrolytes. In such quest, fabrication of quasi-solid DSSC (QSDSSC) by the solidification of liquid electrolytes with polymers has been proposed as a prospective method (Sharma *et al.*, 2017; Wu *et al.*, 2015; Yun *et al.*, 2016). Gel polymer electrolytes (GPE) based QSDSSC provide the combined advantages of both solid and liquid electrolytes such as steady mechanical stability and high ionic conductivity (Mahmood, 2015).

In recent times, starch based polymer electrolytes are emerging as an active research field mainly due to its cost efficiency, biodegradability and natural abundance (Marcondes *et al.*, 2010; Selvanathan *et al.*, 2018; Song *et al.*, 2017). The natural adhesive, gel-like property of starch makes it an interesting choice to be experimented as polymer host in quasi-solid electrolytes. Despite possessing such desirable properties, the employment of starch based quasi-solid electrolytes has not been attempted before due to two major drawbacks. Firstly, starch is a highly hydrophilic material and this prevents its dissolution in organic solvents. However, starch chains are rich in hydroxyl groups which serve as potential modification site and by simply attaching hydrophobic groups to these sites, organosolubility can be imparted. In this work, a simple phthaloylation process is proposed to transform starch into organosoluble material.

Secondly, electrolytes based on starch solely, exhibit poor mechanical properties and in literature it has been documented that blending starch with other polysaccharides is an efficient method to resolve this issue (Hamsan *et al.*, 2017; Shukur & Kadir, 2015; Sudhakar & Selvakumar, 2012). On the other hand, the incorporation of cellulose derivatives into GPE has shown positive impact in reinforcing the mechanical aspects of the gels. Sato et al. found that combining cellulose derivatives, which has a rigid backbone, with poly(oxyethylene) methacrylates produces GPE of considerable mechanical strength even at polymer concentration of 7 wt.% (Sato *et al.*, 2005). Thus, in this work, phthaloyl starch was blended with hydroxyethyl cellulose to serve as the polymer host in the GPE. To the best of our knowledge, this is the pioneer attempt to fabricate quasi-sloid electrolytes based on starch for DSSC application.

The most vital aspect in the fabrication of polymer gel electrolytes is striking the right balance between the solid and liquid characters of the gels. By far in literature, most studies on QSDSSC focus only on analyzing the electrochemical properties of the gels (Wu *et al.*, 2015). The mechanical aspects of the gels are either completely neglected or simplified into just viscosity measurement. However, the viscoelastic properties of the polymer gels are worth exploring in a detailed manner and this can be done by rheological characterizations. In this context, the aim of this work is to provide an in-depth analyses of the effect of the polymer blends, salt composition and ionic liquid addition on the rheological characteristics alongside the electrochemical and photovoltaic properties of the GPE. This ensures that the best composition with good electrical performance is achieved without compromising the mechanical aspect of the material.

1.2 Research objectives

1. To impart organosolubility and diminish crystallinity in starch by chemically modifying it with phthaloylation process.

2. To fabricate the gels based on the blend of phthaloyl starch (PhSt) and hydroxyethyl cellulose (HEC) with optimum rheological, electrochemical and photovoltaic performances.
3. To study the effects of cation size of the iodide salt on the gel properties and identify the best composition for optimum QSDSSC application.
4. To investigate the effects of ionic liquid inclusion on the gel properties and identify the best composition for optimum QSDSSC application.

1.3 Scope of research work

The literature review on chemical modifications of starch, progress on polymer electrolytes and evolution of dye-sensitized solar cells are reviewed in Chapter 2. Chapter 3 will discuss the experimental procedures for the modification and characterization of phthaloyl starch followed by fabrication and characterization of PhSt-HEC based gel polymer electrolytes (GPEs). This chapter is concluded with the fabrication of DSSCs using the fabricated electrolytes. Chapter 4 presents the results obtained from this study. This chapter is dissected into four sections. The first part discusses the synthesis, verification and properties of the modified starch. The second part includes the rheological and electrochemical properties of PhSt-HEC blend based gels and consecutively the photovoltaic performances of these electrolytes. The impact of two different types of iodide salts, with contrasting cation sizes, on the properties of the gel electrolytes are revealed in the third part of Chapter 4. The effects in terms of rheological, physical and electrochemical properties and the influence of these properties on the solar cell efficiency of the gel electrolytes are discussed in-depth in this part. The final section discusses the inclusion of ionic liquid to further enhance the photoconversion efficiency of the electrolytes. The work will be concluded in Chapter 5 which also includes suggestion for future work.

1.4 Research outline

The overall research plan can be dissected into 4 phases and the research outline is depicted in Figure 1.1.

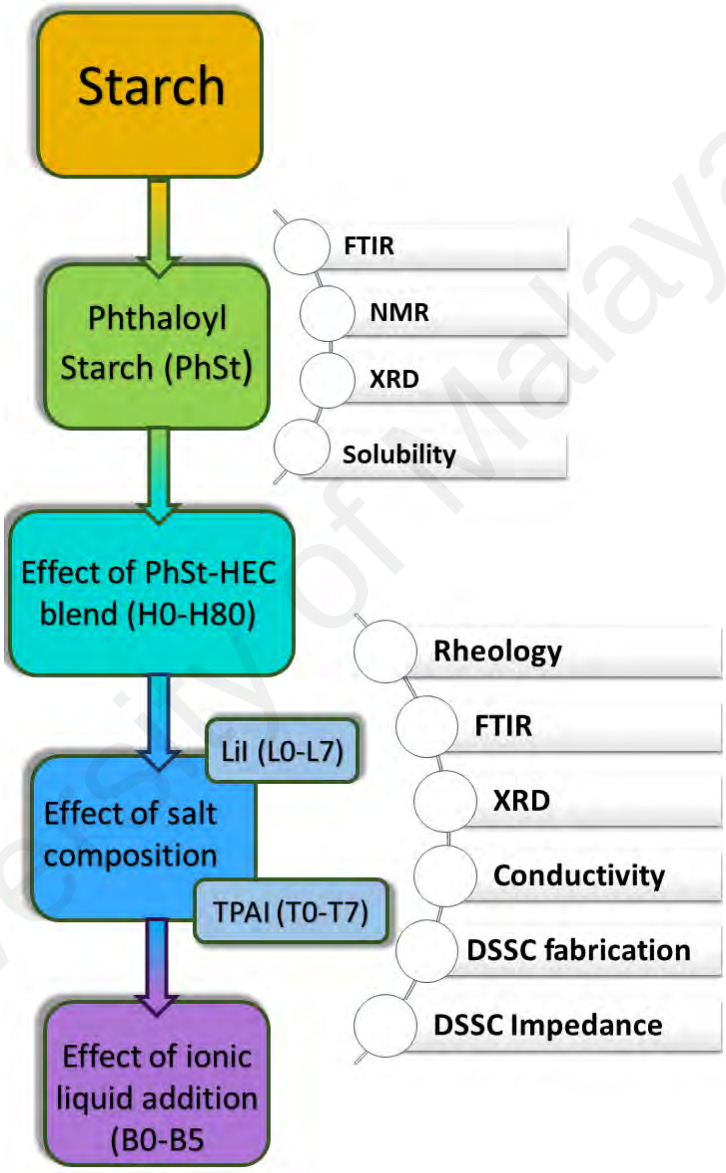

Figure 1.1: Research flowchart

CHAPTER 2: LITERATURE REVIEW

2.1 Starch

Starch is a type of polysaccharide produced by green plants as food reserves, making it the most abundant biopolymer after cellulose and chitosan. The production of starch for commercial use usually involves certain plant sources depending on geographical factors (Carvalho, 2008b). One of the criteria of starch which makes it a sustainable biochemical is the ability to find starch producing plants in wide range of climate and agricultural conditions, eg. maize in tempered and subtropical zones, cassava and banana in tropical environments, rice in inundated areas and potatoes in cold climates. Some main starch producing plant sources in Asia are presented in Figure 2.1 (Carvalho, 2008a).

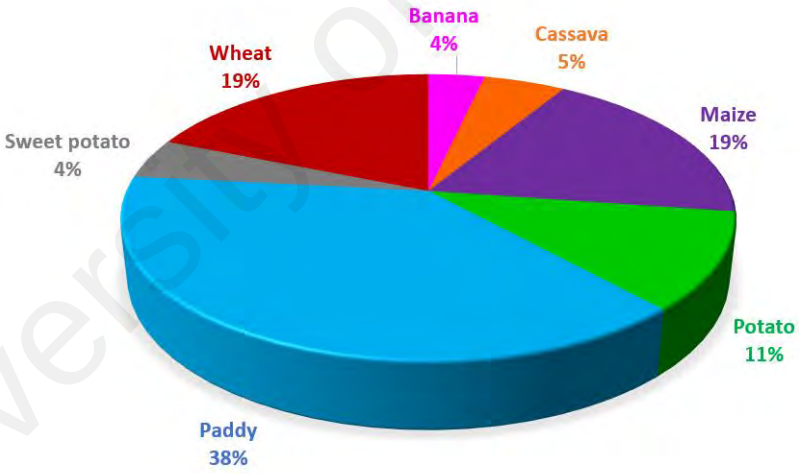

Figure 2.1: Starch producing plants sources in Asia

Chemically, starch is comprised of two types of molecules namely amylose and amylopectin (Figure 2.2). Amylose is a linear polysaccharide made up of D-glucose units joined by the α-1,4-glycosidic linkages. Amylopectin is a branched-chain polysaccharide composed of glucose units linked mainly by α-1,4-glycosidic bonds but with random α-1,6-glycosidic bonds, which accounts for the branching found in the polymer (BeMiller

& Whistler, 2009). The ratio of amylose and amylopectin in starch is dependent on the source of origin and the amylose content of starch from various plant sources are listed as following (Bates *et al.*, 1943; Fredriksson *et al.*, 1998):

i. Maize (~28%)
ii. Cassava (~16%)
iii. Potato (~20%)
iv. Wheat (~30%)
v. Banana (~11%)

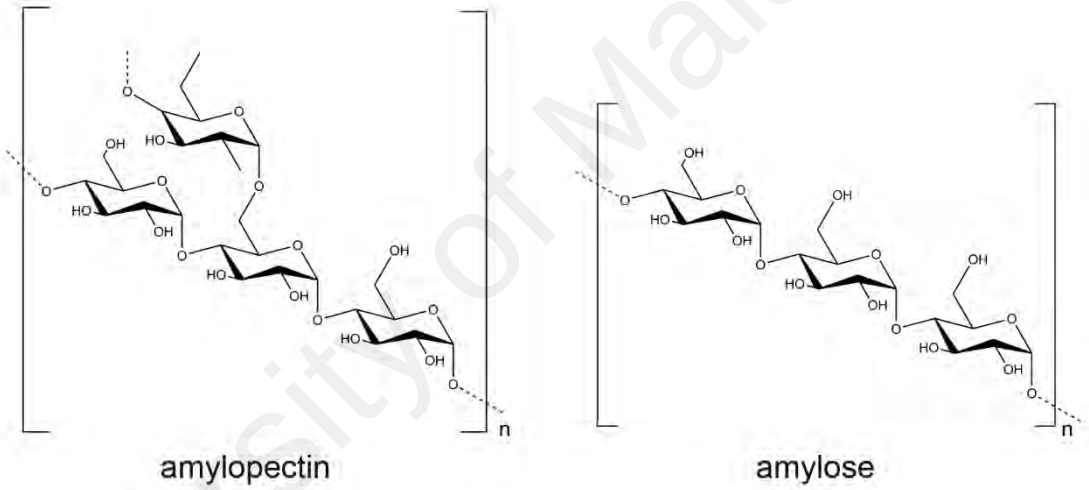

Figure 2.2: Chemical structure of amylose and amylopectin

2.1.1 Scope of starch

The traditional use of starch were initially restricted around food related industry where it was commonly used as gel former, binding agent, thickener, stabilizer and colloidal emulsifier (Schoch & Elder, 1955). Among the earliest exploitation of starch in non-food industry was as a paste or binder for sizing and printing in the textile trade (Norizuki, 1980). After the Second World War, petrochemicals took the industrial world by storm and caused material development based on natural polymers such as starch to be abandoned. However, as the impeccable status of plastics were threatened by the

environmental hazards they caused, initiatives to revive biopolymer based materials began to expand. This marked the resurgence of starch in a wide array of non-food applications (Kaur *et al.*, 2007).

One of such novel applications is in the field of pharmaceuticals where starch is widely used as pharmaceutical excipients due to its non-toxic and non-irritant properties. The role of starch in the formulation of tablets can be either be as the diluent, disintegrant, binder or lubricant (Builders & Arhewoh, 2016). Corresponding to the wide interest in starch based products in pharmaceuticals, there have been a recent trend of exploring unconventional starch sources. This enables the creation of value added products from lesser known agricultural crops. For example, a study in 2012 by Manek et al. highlights the binder properties of starch extracted from *Cyperus esculentus*, a common weed in agronomic crops found throughout USA. However, the tuber of this plant is high in starch content and this starch was used as excipient for solid dosage form. It was found that the binding efficacy of *Cyperus* starch was more effective then potato starch (Manek *et al.*, 2012).

Starch has also been considered a prospective material in packaging industry. The biodegradability, cost effectiveness and natural abundance of starch qualifies it as the apt substitute to synthetic polymers which currently dominates the packaging industry. In particular, starch emerges as an eminent candidate in food packaging considering its advantage in ensuring food safety (Lu *et al.*, 2009). In most cases, the native starch component is corroborated with appropriate additives to improve the shelf life and medical strength of the material. For instance, potassium sorbate supported in tapioca starch films helped to prevent external bacterial contamination, hence improve the film barrier properties (Flores *et al.*, 2007). From a more innovative standpoint, starch is also

capable to be transformed into foamed material by using water steam (Zhiguan *et al.*, 2013). This technique allows starch to replace polystyrene foam in packaging industry.

Another contemporary field that has steered researches of starch based applications into a whole new direction is the synthesis of starch nanocrystals. Intrinsic rigidity, special platelet like morphology and strong interfacial interactions of starch nanocrystals improve the physical properties of materials based on it (Lin *et al.*, 2011). Recent study by Bakrudeen et al., emphasized construction of starch nanocrystal based hydrogel for transdermal applications. In their study, potato based nanocrystals were successfully fabricated into drug carrying hydrogels in a transdermal patch (Bakrudeen *et al.*, 2016). Similarly, some of the recent research ventures involving starch in such contemporary applications are listed in Table 2.1.

Table 2.1: Novel applications of starch

Field	Examples	References
Pharmaceutical	Nanoparticles made from starch derivatives for transdermal drug delivery	(Santander-Ortega *et al.*, 2010)
	Tapioca starch based tablets	(Atichokudomchai & Varavinit, 2003)
	Starch based hydrogels as carriers for colon specific drug delivery systems	(El-Hag Ali & AlArifi, 2009)
Textile	Germinated maize starch in textile printing	(Teli *et al.*, 2009)
	Starch mono-phosphorylation for enhancing the stability of starch/PVA blend pastes for warp sizing	(Zhu, 2003)
Agriculture	Controlled-release fertilizer encapsulated by starch/polyvinyl alcohol coating	(Han *et al.*, 2009)
	Slow-release fertilizer encapsulated by starch-based superabsorbent polymer	(Qiao *et al.*, 2016)
Biomedical	Shape-memory starch for resorbable biomedical devices	(Beilvert *et al.*, 2014)
	Starch-based scaffolds designed for bone tissue engineering	(Salgado *et al.*, 2007)
	Scaffold development using 3D printing with a starch-based polymer	(Lam *et al.*, 2002)

Table 2.1 continued

Environmental	Starch based thin film sensors for low concentration detection of cyanide anions in water	(Isaad *et al.*, 2013)
	Use of cationic starch derivatives for the removal of anionic dyes from textile effluents	(Khalil & Aly, 2004)
Packaging	Starch-based biodegradable materials for thermoforming packaging	(Avérous *et al.*, 2001)
	Biodegradable packaging foams of starch acetate blended with corn stalk fibers	(Ganjyal *et al.*, 2004)

2.1.2 Starch as biopolymer electrolyte

In 1979, French chemist, Michel Armand's short paper opened up a new perspective in the field of solid-state ionics. Armand had suggested the use of graphite intercalation compounds for electrodes and he realized that lithium/PEO complexes could be used as solid electrolytes matching perfectly intercalation electrodes (Armand, 1994). Upon Armand's discovery, polymer electrolyte rapidly gained its position in the field of electrochemistry. The idea of having a solid polymer material exhibiting liquid-like conductivity was a very enthralling theory which promised enormous advantages over the conventional liquid electrolyte. Since then, various synthetic polymers have been experimented by electrochemists to produce an ideal polymer electrolyte whose criteria includes high electrical conductivity, corrosion resistant, minimal thickness and easy to be manufactured at large scale (Di Noto *et al.*, 2011). Concurrently, the growing awareness for environmentally responsible materials prompted the idea of biopolymer based electrolytes. A variety of biopolymers including starch, cellulose, chitosan, pectin, agarose and carrageenan have been attempted as the host in polymer electrolytes (Varshney & Gupta, 2011).

The pioneering work on starch based polymer electrolyte began around early 2000s with a simple preparation method which involved dissolution of starch and lithium salts

in aqueous system followed by solvent casting. The films produced by this technique attained an ambient temperature ionic conductivity between the ranges of 10^{-6} to 10^{-5} S cm^{-1} (Dragunski & Pawlicka, 2002). Owing to the high crystallinity of starch in its native form, the films suffered from mechanical incapability such as brittleness as well as poor ionic conductivity. Typically, to resolve such issue, small organic molecules were included into the polymer matrix to serve as a plasticizing agent. This plasticizers help in increasing the amorphous content of the polymer, lower the glass transition temperature T_g and thus improve ionic mobility. Incorporation of glycerol as the plasticizer is a common method adapted to suppress the crystallinity of starch (Marcondes *et al.*, 2010). The presence of hydroxyls in the molecule enables them to form hydrogen bonding with the hydroxyls in the starch backbone, therefore assisting in hindering inter-chain hydrogen bonding.

Glycerol plasticized starch films generally recorded ionic conductivities between 10^{-5} to 10^{-4} S cm^{-1}. In recent studies, novel plasticizers such as deep eutectic solvents and ionic liquids have been proposed to plasticize starch films and this method improved the conductivity up to 10^{-3} S cm^{-1} (Ramesh *et al.*, 2012; Selvanathan *et al.*, 2017). A detailed review of starch based polymer electrolytes are summarized in Table 2.2. Several electrochemical devices such as electric double layer capacitor (Teoh *et al.*, 2015), lithium sulfur battery (Lin *et al.*, 2016) and dye-sensitized solar cells (Nagaraj *et al.*, 2017) based on starch containing polymer electrolytes have also been studied in literature. The results of these studies have shown that starch is highly prospective to be employed as polymer electrolyte material.

However, the plasticization of starch using chemicals such as glycerol cannot be deemed as the best way to tackle its crystallinity issue. Presence of these plasticizers often increase the hygroscopic nature of the electrolyte and this may affect the physical stability

and shelf life of the material. In fact, a few studies have been especially dedicated to comprehend the effect of water absorption in electrolytes fabricated from starch (Ma *et al.*, 2007; Mattos *et al.*, 2007). The high hydrophilicity of pristine starch also prevents it from being dissolved in most of the organic solvents. This property limits the preparation of starch electrolyte to only solid films. Hence, some essential modifications need to be carried out to alter the flaws of the agropolymer to better fit into the character of an electrolyte.

Table 2.2: Starch based polymer electrolyte

Electrolyte system (Polymer-Salt-Additive)	Ionic conductivity at room temperature (S cm^{-1})	References
Starch- NH_4NO_3	2.83×10^{-5}	(Khiar & Arof, 2010)
Starch-Chitosan-$LiClO_4$	3.70×10^{-4}	(Sudhakar & Selvakumar, 2012)
Starch-NH_4I	2.40×10^{-4}	(Kumar *et al.*, 2012)
Starch-LiTFSI-DES	1.03×10^{-3}	(Ramesh *et al.*, 2012)
Starch-LiI-Glycerol	9.56×10^{-4}	(Shukur *et al.*, 2013)
Starch-LiI-MPII-TiO_2	3.63×10^{-4}	(Khanmirzaei & Ramesh, 2014)
Starch-$LiPF_6$-$BmImPF_6$	1.47×10^{-4}	(Liew & Ramesh, 2015)
Starch-NaI-MPII	1.20×10^{-3}	(Khanmirzaei *et al.*, 2015b)
Phthaloyl starch-DES	2.96×10^{-3}	(Selvanathan *et al.*, 2017)

2.1.3 Modification of starch

Despite all its virtues, the exploitation of starch in versatile applications is often inhibited by two main drawbacks of starch molecules; hydrophilicity and poor mechanical property. However, this can be easily tackled with the ability to chemically modify starch to tailor the material in accordance to certain pre-requisite properties. Commonly, the means of starch modification can be categorized as chemical, physical, enzymatical and genetical (Kaur *et al.*, 2012).

The six main chemical modifications often employed for starch are oxidation, etherification, esterification, cationization, cross-linking and grafting with other polymers (Masina *et al.*, 2017). Among these, esterification, particularly, has been proved to be one of the simple and robust methods to alter the hydrophilicity and crystallinity of starch. Examples of esterified starch for particular applications have been listed in Table 2.3.

Table 2.3: Examples of starch esterification in literature

Starch type	Acetylating agent	Highlights	Reference
Maize	Octenyl succinic anhydride	Derivative showed better emulsion and digestion properties	(Miao *et al.*, 2014)
Potato	Hexamethylene diisocyanate	Improved hydrophobicity and moldability were shown by derivative	(Wilpiszewska & Spychaj, 2007)
Potato	Disodium hydrogen phosphate	Electrorheological property was affected by the content of phosphate groups	(Sung *et al.*, 2005)
Maize	Propionic anhydride	The derivative was applied as hot melt adhesives	(Zhang *et al.*, 2014b)
Maize	Acetic anhydride	The ester was prepared via microwave-assisted method	(Biswas *et al.*, 2008)
Maize	Benzoyl chloride	Derivative exhibited lower activation energies of thermal degradation	(Stojanović *et al.*, 2005b)
Potato	Vinyl laurate	Supercritical carbon dioxide was used as the solvent	(Muljana *et al.*, 2010)
Potato	Oleic acid	The reaction was catalyzed by lipase biocatalyst	(Zarski *et al.*, 2016)
Potato	Ferulic acid chloride	Derivative were found to exhibit free radical scavenging activity	(Mathew & Abraham, 2007)
Maize and potato	Long chain fatty acid chlorides	The modified starch was able to form nanoparticles via dialysis method	(Namazi *et al.*, 2011)
Maize	Dodecenyl succinic anhydride	Reduced moisture sensitivity and surface hydrophilic character was exhibited in derivative based films	(Zhou *et al.*, 2009)

Esterification of starch usually involves substitution of the hydroxyl groups to alkyl or aryl derivatives. The groups substituted are usually larger in size with more expansive

electron clouds as compared to the hydroxyls. The steric hindrance imposed by the new group forces individual chains to repel each other as the modified starch derivatives attempt to exist in the lowest, more stable, energy state (Wiberg & Rablen, 1993). In the case where an aryl derivative is introduced into the polymer chain, hydrophobicity of starch is expected to be enhanced and this in turn will enable their dissolution in organic solvents.

The choice of substituents in chemical modification of starch often serves as the deciding factor in determining the scope of its application. A simple example will be the use of starch as emulsifiers in food products. For starch to perform as an effective emulsifier, it is often modified with octenyl succinic anhydride (OSA) to synthesize starch derivative with both hydrophilic and hydrophobic bifunctional groups (Tesch *et al.*, 2002). This chemical alteration allows starch to adsorb to the surface of oil and water, creating a stable emulsion. It was evident that addition of bulky group such as OSA creates steric hindrance, alters hydrogen bonding and lowers gelatinization temperature, all of which help to intensify the viscosity of starch (Hui *et al.*, 2009).

In some cases, the incorporation of a new functional group onto the backbone of starch can give rise to novel properties that are absent in native starch molecules. Tan et al., discovered that 1,2,3-triazolium functionalized starch derivative possesses antifungal properties which is very useful for biomedical applications. The imparted antifungal character is an impact of electrostatic interaction of positively charged moieties of the cationic molecules and negatively charged components of microbial cell membrane. This interaction amends permeation property of the membrane inducing osmotic imbalance and finally causing hydrolysis of the peptidoglycans in the microbial cell wall (Tan *et al.*, 2017).

Along with the substituent type, degree of substitution could also contribute to the efficiency of starch derivative in the targeted applications. Chen at al. had studied the possibility of using resistant starch acetate for oral colon targeting drug delivery system. They elucidated that if the polysaccharide can avoid digestion in the upper gastrointestinal tract and is only susceptible to enzymatic degradation upon arriving in the colon, then it can be used as carrier for colon targeting drug delivery system. In their work, it was proposed that one of the methods to control the rate of enzymatic degradation is by altering the degree of substitution of starch acetate. By increasing acetylation, enzymatic degradation was considerably retarded. Acetylation also accelerated starch swelling ratio when degree of substitution was lower than 2.04 (Chen *et al.*, 2007).

2.1.4 Starch blends

Besides chemical modifications, another simple and robust technique commonly adapted to alter the physicochemical properties of starch is by blending it with other polymers. In terms of processing, starch blends can be achieved by two methods namely melting processing and dispersion processing. In melting processing, starch is first gelatinized by extrusion followed by addition of the second polymer and further processing in a twin-screw extruder. On the other hand, dispersion processing is a much simpler technique as starch and the other components of the blend is dispersed in a common solvent system. The impact of physically mixing the polymers can result in an additive effect, in which the properties of the blend originates from each individual components, or non-additive effect, which provokes novel properties that are absent in either of the native components of the blend (Jasmien *et al.*, 2015).

Huo et.al prepared starch film incorporated with chitosan microcapsules for a novel drug delivery system. Upon addition of chitosan into starch matrix, the thermostability and mechanical property of the blend film were found to be far superior to the neat ones.

With higher chitosan content, the hydrophobicity of the film improved, resulting in a sustained drug release. Furthermore, the drug releasing mechanism of the film also demonstrated pH sensitivity, an interesting feature that is advantageous for targeted drug delivery applications (Huo *et al.*, 2016).

The blend of thermoplastic starch (TPS) with polycaprolactone (PCL) processed by melt mixing was investigated by Ninago et al. The resulting blend exhibited higher opacity and ultraviolet (UV) absorption capacity, both being inherent qualities of PCL. Addition of PCL positively favored water vapor barrier capacity of the blend films without compromising the thermal stability (Ninago *et al.*, 2015).

In a recent study by Ghanbari et al., the addition of cellulose nanofibers into thermoplastic starch resulted in films with improved mechanical properties as indicated by dynamic mechanical thermal analysis (DMTA). Moisture absorption of the composite films declined greatly in comparison to neat starch films (Ghanbari *et al.*, 2018).

2.2 Cellulose derivative as blending agent

In accordance to the current pursuit for sustainable materials, polymer electrolytes fabricated from natural polymers, in particular, cellulose derivatives have obtained special focus recently. Cellulose derivatives are often incorporated into a synthetic polymer system with the purpose of improving the mechanical properties of the materials while at the same time reducing its ecological footprint. Sato et al. found that combining cyanoethylated cellulose, which has a rigid backbone, with crosslinkable methacrylate monomers produces GPE of considerable mechanical strength even at cellulose concentration of 7 wt.%. The interaction between the highly-polar polymer matrixes that included a cellulose derivative with the liquid electrolyte aided in retarding electrolyte evaporation in the gel (Sato *et al.*, 2005). A similar approach has been done by Nirmale et al. who fabricated GPE based on photo-induced in-situ polymerization of

PEG-methacrylates along with cellulose triacetate (TCA). The presence of TCA improved ionic conductivity, owing to its ether and carbonyl functional groups (Nirmale *et al.*, 2017).

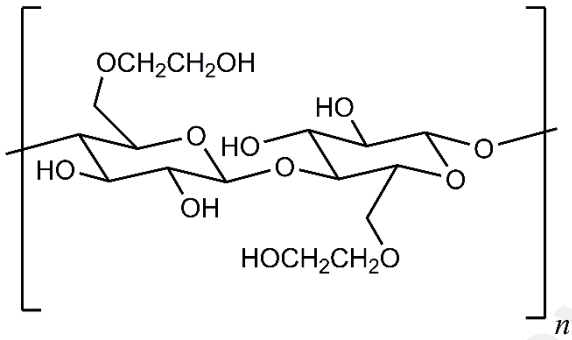

Figure 2.3: Structure of HEC

One of the most effective cellulose derivatives used to alter rheological properties is hydroxyethyl cellulose (HEC) which is widely recognized as a gelling and thickening agent in cosmetics, pharmaceutical and paint industry (Mudgil *et al.*, 2014). As shown in Figure 2.3, HEC comprises of cellulose chain with hydroxyethyl groups in place of the hydroxyls. Recent literatures have highlighted the prospects of HEC as polymer electrolyte material with good thermal stability and favorable electrochemical performance (Chong *et al.*, 2017; Gupta & Varshney, 2017; Sudhakar *et al.*, 2015) . According to Zhang et al., a dense HEC membrane sandwiched between two porous PVDF layers helps to avoid micro short-circuits to a large extent which is crucial to improve the safety of the electrochemical device (Zhang *et al.*, 2017). The attachment of hydroxyethyl group onto the cellulose backbone in HEC imparts organosolubility. This enables the incorporation of various organic solvents for the fabrication of GPE based on the biopolymer. For instance, Li et al. prepared gel membrane by soaking the HEC membrane in organic electrolyte consisting of LiPF6 solution in ethylene carbonate/dimethyl carbonate/ethylmethyl carbonate (Li *et al.*, 2015). The electrolyte showed uptake of organic liquid electrolyte up to 78.3 wt.% and good electrochemical

performance including high ionic conductivity at room temperature and a high lithium ion transference number.

2.3 Solar cell

Solar cell is an electrochemical device that performs the conversion of light energy into electrical energy. The operation of solar cell lies on the basis that light is composed of elementary particles called photons. Each photon carries a characteristic energy depending on its frequency. When photons with sufficient energy hits a material, electrons are ejected out of it. A photovoltaic device captures this electrons and directs them to flow around an electric circuit, hence generating efficiency (Reinders *et al.*, 2017).

In general, solar cells can be categorized into three main types. The traditional crystalline silicon based devices are regarded as the first generation solar cells and most of the commercialized solar panels found in the market belong to this category. The fabrication of this solar cells solar cells are performed by sandwiching n-type and p-type silicon forming the p-n junction, the most essential component of the photovoltaic efficiency and stability (Ikhmayies, 2018). Single junction silicon devices have a theoretical maximum efficiency of 30 %. The commercial domestic solar panels of this category often manage to record an efficiency of about 15 %. However, this classical solid-state junction devices requires highly pure materials and thus is very cost intensive to produce.

In order to address the high production costs imposed by first generation solar cells, novel thin film based solar cells known as second generation solar cells were introduced. A thin-film solar cell is fabricated by depositing layer of photovoltaic material on a substrate. Some of the most successful materials used in thin films are amorphous silicon, cadmium telluride and copper indium gallium selenide (Deb, 1996). These materials can

be deposited on any substrates including glass, metals and polymers (Lee & Ebong, 2017). Thus, the production cost can be reduced as compared to its predecessor. The variety of substrate materials employed in this technology, allow fabrication of thin, light and flexible solar devices (Han *et al.*, 2017). The conflict with the second generation solar cell arises from its poor efficiencies, making it difficult to be commercialized.

The instigation of a third generation solar cell is an attempt to reconcile the best features from the first two generations; high efficiency and low cost of production. In this technology, more focus was directed towards exploring charge transfer and charge collection processes in order to design the most efficient method for energy capture (Conibeer, 2007). Among the innovative technologies introduced in this generation includes organic solar cells (Yeh & Yeh, 2013), perovskite solar cell (Assadi *et al.*, 2018), dye-sensitized solar cell (Hagfeldt *et al.*, 2010), quantum dot solar cells (Kamat, 2013) and concentrator photovoltaic (Pérez-Higueras *et al.*, 2011).

2.4 Dye-sensitized solar cell

Dye-sensitized solar cell (DSSC) is a third generation photovoltaic device, developed first by O'Regan and Gratzel in 1991. The conceptualization of DSSC draws inspiration from photosynthesis in which chlorophyll only plays a role in light harvesting but does not participate in charge transfer (O'Regan & Grätzel, 1991). Similarly, in DSSC, charge generation takes place at semiconductor-dye interface while charge transport is performed by the semiconductor and electrolyte. This feature is what differentiates DSSC from conventional photovoltaic where the semiconductor undertakes both processes (Grätzel, 2003). By assigning the processes to different components, the necessity to use a material with both superior light harvesting property and carrier transport property can be avoided. This greatly favors DSSC in terms of ease and cost of fabrication. The technology also provides a lot of room for improvisation as the spectral properties optimization can be

performed by altering the dye molecule, while charge transport properties can be improved by optimizing the semiconductor and the electrolyte composition (Nazeeruddin *et al.*, 2011).

2.4.1 Working principle

The architecture of DSSC comprises a photoanode made from semiconductor with a layer dye molecules adsorbed on its surface, a counter electrode and a layer of electrolyte sandwiched between the two electrodes (Figure 2.4). The electrolyte consists of a redox couple traditionally being the iodide/triiodide couple.

$$S_{adsorbed} + hv \rightarrow {S^*}_{adsorbed} \quad (2.1)$$

$${S^*}_{adsorbed} \rightarrow {S^+}_{adsorbed} + {e^-}_{injected} \quad (2.2)$$

$$I_3^- + 2e^- \rightarrow 3I^- \quad (2.3)$$

$${S^+}_{adsorbed} + \frac{3}{2}I^- \rightarrow S_{adsorbed} + \frac{1}{2}I_3^- \quad (2.4)$$

Upon illumination, the dye molecules absorb the incident photons and this promotes the electrons of the dye from the highest occupied molecular orbital (HOMO) to the lowest unoccupied molecular orbital (LUMO) (Equation 2.1). The photo-excited electrons then enter the conduction band of the semiconductor, leaving the dye molecules in an oxidized state (Equation 2.2). The injected electrons then maneuver through the TiO_2 layer and enter the external load, subsequently reaching the counter electrode. At the cathode, the electrons reduce triiodide into iodide ions which then travel towards the photoanode (Equation 2.3). At the photoanode-dye interface, the iodide ions are reduced to triiodide species, hence releasing electrons which are returned to the oxidized dye molecule (Equation 2.4). With the regeneration of the dye molecules, the circuit is completed. Besides the mechanism explained above, there are a number of recombination

reactions that may take place within the cell. The photo-injected electrons may recombine to the oxidized dye molecules or the oxidized species of the redox couple.

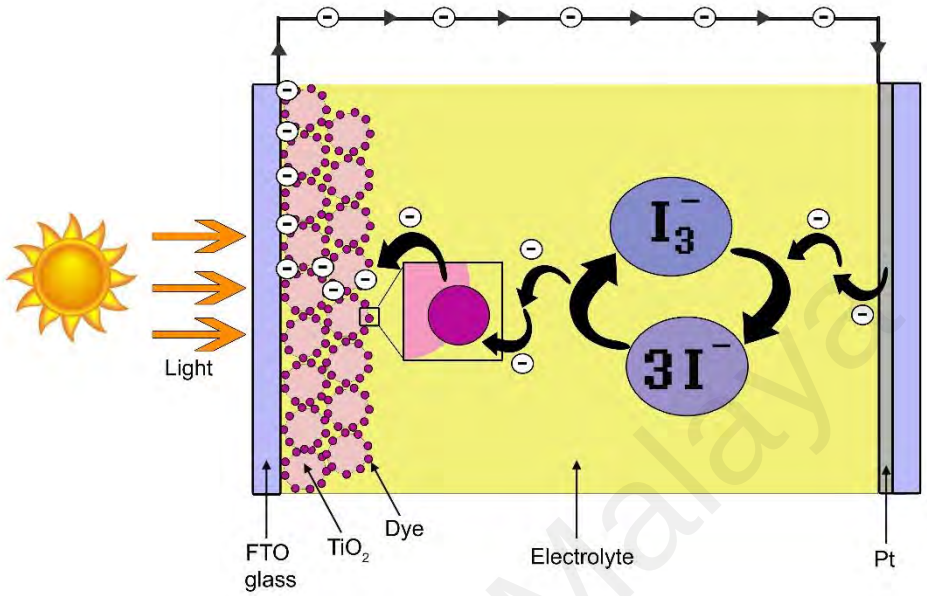

Figure 2.4: Schematic representation of DSSC

2.4.2 Components

2.4.2.1 Photoanode

Generally in DSSC, the photoanode is composed of a layer of semiconducting oxide film deposited onto the conducting substrate (Figure 2.4). The choice of semiconductor oxides depends on three main criteria, namely (Grätzel, 2003):

i. The conduction band of semiconductor oxides should be lower than the LUMO of the dye.

ii. The effective surface area of the semiconductor should be able to afford sufficient dye adsorption.

iii. The semiconductor should support fast electron transport and suppress electron recombination processes.

Some of the oxides that have been experimented as photoelectrodes are TiO_2, ZnO, SnO_2 and chalcogenides. Among all these materials, TiO_2 prevails the others in terms of

cost effectiveness, chemical stability and non-toxicity (Sharma *et al.*, 2017). The fabrication of TiO_2 based photoanode is also a rather robust method which often involves coating of the TiO_2 colloidal solution or paste on a conducting substrate followed by sintering at 450-500 °C.

TiO_2 can be found in nature as rutile, anatase and brookite. The brookite phase is the least preferred form as it is thermodynamically unstable (Kandiel *et al.*, 2013). On the other hand, intensity-modulated photocurrent spectroscopy shows that the electron transport in rutile layer is slower than in anatase layer due to the inter-particle connectivity with particle packing density (Sreekala *et al.*, 2013). A study by Park in 2010 also revealed that the surface area of the rutile film is approximately 25 % lower than that of the anatase film, hence affecting the amount of dye adsorbed on both films (Park, 2010). Due to these reasons, the anatase phase remains the most widely used form of TiO_2 for photoanode preparation.

The mesoporous structure of the TiO_2 layer is another crucial aspect which helps to provide a folded surface for dye adsorption, hence enhancing light harvesting efficiency (Sharma *et al.*, 2017). In fact, the mesoporous assembly of TiO_2 mimics the stacked structure of thylakoid vesicles in green leaves which improves light capturing efficiency of chlorophyll (Ruban, 2009). A porous semiconductor film is also necessary to enable the electrolyte to penetrate the film efficiently to suppress the rate-determining step via diffusion of redox ions into the film. In literature, it was found that the porosity of TiO_2 colloidal solution or paste can be manipulated through the sintering process by the addition of polymers such as polyethylene glycol (PEG) and ethyl cellulose (EC) (Hočevar *et al.*, 2013; Zama *et al.*, 2017).

One of the factors that affects the efficiency of a DSSC is the electron recombination process that occurs between the conducting substrate-electrolyte interfaces. Due to the

porous nature of the semiconductor layer, the conducting substrate cannot be entirely insulated from the electrolyte. This issue can be resolved by employing a thin dense blocking layer between the substrate and mesoporous TiO_2 layer. Some of the materials which have demonstrated to be effective blocking layers are TiO_2 (Manthina & Agrios, 2016), ZnO (Guo *et al.*, 2005; Liu *et al.*, 2011), Au (Chang *et al.*, 2011), Nb_2O_5 (Xia *et al.*, 2007) and graphene oxide (Kim *et al.*, 2009). The deposition of these materials on the working electrode can be done via various techniques such as spin coating (Lee *et al.*, 2012), dip coating (Yu *et al.*, 2009), chemical vapor deposition (Thelakkat *et al.*, 2002), sputtering (Waita *et al.*, 2009) and spray pyrolysis (Peng *et al.*, 2004). It is important to ensure that the thickness of blocking layer does not exceed certain values (typically 300 nm) in order to prevent the layer from acting as a charge trap site (Kim *et al.*, 2011).

2.4.2.2 Dye

As dictated by the name itself, dye is a salient component in DSSC. The choice of dye strongly influences the open circuit voltage value, governed by the oxidation potential of the sensitizer and the short circuit current, which corresponds to the absorption properties of the dye. Some of the prerequisites that determine the performance of dye are (Nazeeruddin *et al.*, 2011):

i. It should exhibit intense absorption in the visible region (400-700 nm).

ii. It must bear certain attachment groups such as carboxylate or phosphonate to enable grafting onto the surface of semiconductor oxide layer.

iii. The energy level of the LUMO should be in proximity with the conduction band of the semiconductor in order to reduce energy losses upon electron transfer.

iv. It should have a relatively high redox potential to allow regeneration from its oxidized state by electron donation from the redox couple in electrolyte.

v. The dye must be stable for about 108 turnover cycles which guarantees long term usability of the dye.

The types of dye employed in DSSC can be dissected into two categories; inorganic dye and organic dye. Inorganic dyes are commonly composed of transition-metal complexes such as ruthenium (Qin & Peng, 2012), copper (Dragonetti *et al.*, 2018) and zinc (Milan *et al.*, 2017) based compounds. Intricate processes for synthesis of metal complex sensitizers alongside the environmental burden imposed by these complexes triggered the need to explore a more cost and nature friendly alternative. This induced the introduction of organic dyes which can be easily extracted from flowers, roots and leaves of various plants (Richhariya *et al.*, 2017). Some the extensively studied pigment groups with examples of their respective plant sources are (Hug *et al.*, 2014; Khan *et al.*, 2017; Shalini *et al.*, 2015):

i. Chlorophyll (e.g., arugula, parsley, spinach, henna)

ii. Anthocyanin (e.g., rose, lily, pomegranate, red cabbage)

iii. Xanthophyll (e.g., marigold, yellow rose)

iv. Betacyanin (e.g., cherry, grapes, raspberry, bougainvillea)

v. Carotenoid (e.g., capsicum, walnuts, turmeric)

However, till date, the best performing solar cells with long term stability has been achieved by the polypyridyl complexes of ruthenium. For a long period of time, cis-bis(isothiocyanato)bis(2,2′-bipyridyl-4,4′-dicarboxylato)ruthenium(II) complex, also

known as N3 dye (Figure 2.5), continues to be the paragon of sensitizing agent in DSSC (Nazeeruddin *et al.*, 1993). The carboxylate group on the 4,4′-dicarboxy-2,2′-bipyridine ligand enables attachment of the dye molecule on the semiconductor layer through bidentate coordination and ester linkages. The thiocyanate group, on the other hand, improves absorption of visible light.

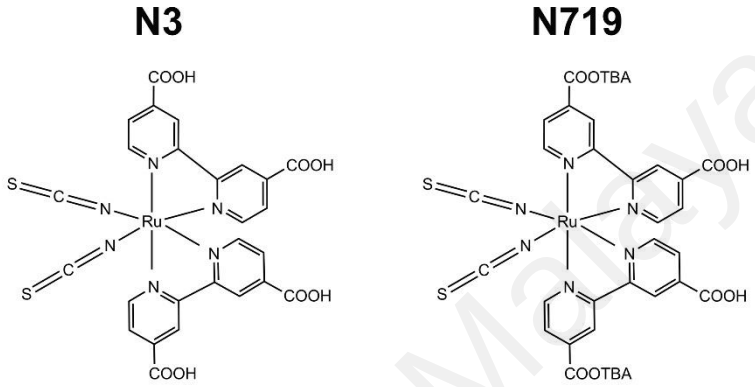

Figure 2.5: Chemical structures of ruthenium based dyes

The success of N3 dye as an efficient sensitizer motivated scientists to improvise the dye structure to further boost its efficiency. The conduction band of TiO_2 is known to have a Nernstian dependence on pH and due to this, the protonation state of the dye is expected to influence the energy level of the semiconductor's conduction band (Tachibana *et al.*, 2000; Yan & Hupp, 1997). A fully protonated sensitizer, as in the case of N3, will charge the semiconductor layer positively via adsorption. Such imparted positivity of the surface will assist in adsorption of anionic ruthenium complex and accommodate electron transfer from the HOMO of the dye to the conduction band of TiO_2. This series of event will impact positively on the photocurrent values of the cell. However, at the same time, the surface protonation induces positive shift of the conduction band edge (Nazeeruddin *et al.*, 2011). In conclusion, a fully protonated dye will result in high J_{SC} and low V_{OC}. The converse is true for a non-protonated dye. The ideal solution for this dilemma was found to be a dye structure of only two protonated

form with the other two protons being substituted by tetrabutylammonium cation (Figure 2.5). This dye structure was later named N719.

2.4.2.3 Counter electrode

The role of a counter electrode (CE) in a DSSC is to receive electrons from the external circuit and electrocatalyzes the reduction of the redox species in electrolyte. Some of advantageous properties for CE materials are (Cruz *et al.*, 2012):

i. low electrical resistance
ii. high electrocatalytic activity towards redox species
iii. chemical stability
iv. transparency

Till date, the conventional type of CE employed in most DSSC is platinum electrode which is usually fabricated by coating a thin layer of platinum on the surface of a conducting glass (Kim *et al.*, 2006). Although the productivity of these platinum electrodes have remained unsurpassed, the scarcity of the noble metal and the consecutive cost factor demands development of novel counter electrodes utilizing low-cost and abundant materials (Veerappan *et al.*, 2012; Xu *et al.*, 2011). Some of the initiatives in this direction is the possibility of replacing platinum with carbonaceous materials. This includes studies based on carbon black (Kang *et al.*, 2016; Liu *et al.*, 2017), activated carbon (Arbab *et al.*, 2016), graphene (Wang & Hu, 2012) and multi-walled carbon nanotubes (Yeh *et al.*, 2014; Zheng *et al.*, 2015) based counter electrodes.

2.4.2.4 Electrolyte

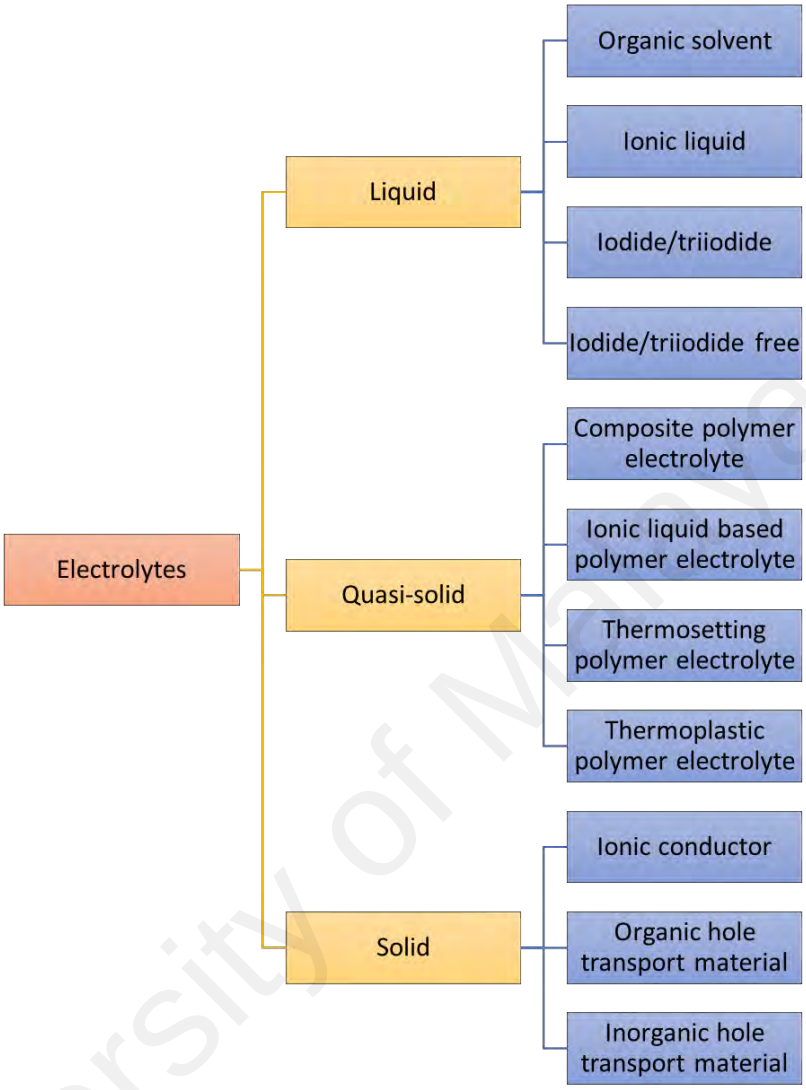

Figure 2.6: Classification of electrolytes in solar cell

As it is the case in any electrochemical device, electrolytes are one of the essential components in DSSC. Being mainly responsible for the internal charge transport between the electrodes in order to continually replenish the dye, electrolytes can directly influence photocurrent density (J_{SC}), photovoltage (V_{OC}), and fill factor (FF) of a cell. Some of the crucial prerequisites of an electrolyte in DSSC are (Ardo & Meyer, 2009; Yu *et al.*, 2011):

i. provide the potential barrier for photovoltaic conversion

ii. rapid transport of charges to prevail the possibilities of recombination reactions

iii. good interfacial contact between the mesoporous semiconductor and CE

iv. sustained chemical, thermal, optical, electrochemical and mechanical stability

v. does not exhibit strong absorption in the visible light range to avoid competition with the dye molecule.

Typically, the characterization of the types of electrolytes can be done with respect to their physical states which, as summarized in Figure 2.6, comprises of solid, liquid and quasi-solid electrolytes (Wu *et al.*, 2015).

During the inceptive stages of DSSC, organic solvents consisting of iodide/triiodide redox couple were the initial choices of electrolyte used and this liquid electrolyte attained a maximum efficiency of 7.9 % (O'Regan & Grätzel, 1991). Till date, liquid electrolytes remain the most extensive and successful type of electrolytes with a record breaking efficiency of 13 % when applied in traditional DSSC (Mathew *et al.*, 2014). The solvents used in liquid electrolytes need to comply with certain conditions such as melting point below −20 °C and boiling point above 100 °C, high dielectric constant and low viscosity (Yu *et al.*, 2011). So far, there are two categories of solvents which are in close agreement to these requirements, namely polar organic solvents and ionic liquids.

Amongst the various polar organic solvents experimented, acetonitrile received particular attention owing to its excellent chemical stability (Hagfeldt & Grätzel, 2000). A study by Hauch et al. pointed out that, upon determination of diffusion constant of triiodide in different solvents and cations, acetonitrile and Li^+ combination achieved the

best diffusion constant (Hauch & Georg, 2001). Some of the highest efficiencies in traditional DSSC were also attained with acetonitrile based electrolytes (Joly *et al.*, 2014). However, the low boiling point of acetonitrile (82 °C) restrains its usage in commercial solar cells.

Interestingly, water was also proposed as one of the prospective solvents in liquid electrolytes (Desilvestro *et al.*, 1985; Kalyanasundaram *et al.*, 1987; Liska *et al.*, 1988). For instance, in 2010, Gratzel et al. studied water based electrolytes using hydrophobic dyes and recorded an efficiency of 2.4 %, which remain the highest value obtained for a pure aqueous solvent (Law *et al.*, 2010). The major bottleneck for such aqueous based electrolyte is the oxidation of iodide (I^-) to iodate (IO_3^-) in the presence of water, which inherently reduces the I_3^- ions leading to instability in cell performance (Tributsch, 2004). The selection of water as the electrolyte medium also greatly restricts the options of dyes that can be applied, provided that most of these sensitizers are susceptible to hydrolysis (Hagfeldt *et al.*, 2010). Therefore, until these issues remain unsolved, application of aqueous based electrolytes will not be a feasible option.

Ionic liquid (IL) has been recently established as the new age solvent and highly acclaimed for its superior properties such as multiple solvation interactions with both organic as well as inorganic compounds, high chemical and thermal stability, high ion conductivity and wide electrochemical window (Jayakumar *et al.*, 2015). This new age solvent has also been nicknamed as the "designer solvent" owing to its ability to alter cation and anion combination adapting to the required application. Role of IL as electrolytes in DSSC can be in two forms. Firstly, IL can be used as the solvent medium of liquid electrolytes and secondly, it can be source of charge carriers, just like the conventional inorganic salts, in quasi-solid DSSC (Wu *et al.*, 2015). The latter form will be elaborated in following sections.

One of the preliminary studies involving IL electrolytes is by Papageorgiou et al. who fabricated methyl-hexyl-imidazolium iodide based DSSC. This cells particularly exhibited outstanding stability with an estimated sensitizer turnover in excess of 50 million (Papageorgiou *et al.*, 1996). The encouraging results have motivated various researchers to explore different types of IL as electrolytes in DSSC and it was found that imidazolium iodide based IL produced the best performance (Chen *et al.*, 2013). In addition to that, low vapor pressure of these IL is deemed to be an added perk for the solvent as this may translate into lower chances of evaporation and leakages (Bier & Dietrich, 2010). However, despite all the merits, high viscosity and thus low ionic mobility persists to be the major disadvantages of IL based DSSC (Zistler *et al.*, 2006). This is often tackled by introducing a low viscous co-solvent into the system and this auxiliary solvent can either be some organic solvents (Shi *et al.*, 2008) or other low viscosity IL itself (Fan *et al.*, 2010; Ito *et al.*, 2006). With greater understanding of the intrinsic behaviors of IL in the future, more effective means can be introduced to materialize the idea of efficient solvent-free liquid electrolytes for DSSC.

2.5 Quasi-solid Dye-sensitized Solar Cell

2.5.1 Introduction

Despite remarkable efficiencies attained upon using liquid electrolytes, the application of these electrolytes in commercialized DSSC was deterred by practical flaws such as mechanical instability, leakage, volatilization of solvent, and photodegradation of the dye (Nazeeruddin *et al.*, 2005). On the other hand, the credentials of a completely solid electrolyte do not live up to the required performance often due to poor contact between electrodes (Wu *et al.*, 2008). The trade-off between electrochemical performance and mechanical stability of the electrolyte was achieved by introducing a new class of electrolytes, namely quasi-solid electrolyte. A quasi-solid state refers to the condition of a material which exists between solid and liquid states. This unique state allows the

electrolyte to possess both the cohesive property of solid and diffusive property of liquid (Wang *et al.*, 2003b). Based on the formation technique and physical features of the material, quasi solid electrolytes can be dissected into four main categories: composite polymer electrolyte, ionic liquid electrolyte, thermosetting electrolyte and thermoplastic electrolyte.

2.5.2 Composite polymer electrolyte

One of the methods proposed to convert liquid electrolytes into quasi-solid state is via the addition of inorganic nanoparticles or gelators and the gels produced by this method are named composite polymer electrolytes. This method is notably advantageous due to the formation of inorganic network within the electrolyte matrix, functioning as mode of transport for the ions and eventually enhancing charge transport efficiency (Huo *et al.*, 2007).

TiO_2 nanoparticles are one of the widely used organic gelators in quasi-solid electrolytes. For instance, Katsaros et al. fabricated DSSC using polymer electrolytes comprising PEO, LiI and I_2 incorporated with TiO_2 which displayed an efficiency of 4.2 % (Katsaros *et al.*, 2002). The arrangement of TiO_2 within the polymer chains was as such that a stable three-dimensional network with interstitial gap was created, enabling swift movement of the redox ions. Similarly, PVDF-HFP based electrolyte gelated with TiO_2 was investigated by Huo et al., who apparently observed six fold improvement in the I_3^- diffusion coefficient (Huo *et al.*, 2007).

Wang et al. attempted to prepare composite electrolyte by including fumed SiO_2 nanoparticles into ionic liquids to produce QSDSSC yielding 7 % efficiency (Wang *et al.*, 2003a). The high performance of the electrolyte inspired subsequent researches with SiO_2 as the inorganic gelator. One of such studies is by Yoon et al., who highlighted shape dependence of SiO_2 nanomaterials in quasi-solid electrolyte. According to this study, by

altering the shape of silica from nanospheres to nanorods, a 38 % increase in the overall efficiency was observed (Yoon *et al.*, 2014). Apart from the oxides of silicon and titanium, Al_2O_3 and ZnO nanoparticles based QSDSSC have also been experimented recently (Chi *et al.*, 2013; Singh *et al.*, 2016).

Another versatile approach to fabricate composite electrolytes is through the insertion of nanoclay minerals as the gelating agent (Ito *et al.*, 2008; Jin & Chen, 2012; Wang *et al.*, 2013a). Unique features of nanoclays such as high chemical stability, excellent swelling capability, ion exchange capacity, light scattering property, and rheological property projects them as highly prospective gelators in QSDSSC (Wu *et al.*, 2015). In a recent paper by Mhaisalkar et al., synthetic nitrate-hydrotalcite nanoclay based QSDSSC was shown to record efficiency as high as 9.6%, proving the potential of nanoclays in future works (Wang *et al.*, 2013b).

2.5.3 Thermoplastic polymer electrolyte

Typically, thermoplastic polymer electrolyte (TPPE) involves three main components namely polymer, salt and solvent. The primary function of the polymer is to serve as the matrix of the gel in order to bestow mechanical stability. Addition of inorganic salts introduces charge carriers into the matrix which elevates the ionic conductivity of the electrolyte. Most often, the major composition of the electrolyte is made of the solvent component which is regarded as packets of liquid trapped within the polymer chains. The solvent forms a crucial part of the system as it affords the space for charge carrier migration, diminishes crystallinity of the gel, decreases polymer-polymer interaction and increases the free volume and segmental mobility of the system (Wu *et al.*, 2015). The composition of the solvent system can either be any polar organic solvent solely or a mixed system with small organic molecule (called plasticizer) along with the organosolvent.

The preparation of the TPPE involves dissolution of the salt in solvent medium in order to form the electrolytic solution and into this, the polymers are added followed by sufficient amount of heating and stirring. During this process, the swelling, adsorption, inflation and entanglement of polymer chains convert the dilute electrolyte system into a gel with viscoelastic properties (Wu *et al.*, 2008). The entire gelation process is due to the establishment of various weak interactions within the electrolyte matrix including hydrogen bonds, van der Waals and electrostatic interaction (Nogueira *et al.*, 2004). Since these interactions are highly temperature-dependent, the physical state of the gels (from viscous to dilute condition) can be governed by altering its temperature. Hence, giving rise to the name "thermoplastic gels" which indicates the reversibility of the gels from hard to soft upon heating and vice versa with cooling (Wu *et al.*, 2007a).

The pioneer work on thermoplastic polymer electrolyte began in 1995 by Cao et al., in which PAN was incorporated with ethylene carbonate, propylene carbonate and acetonitrile and sodium iodide (Cao *et al.*, 1995). Ever since that, a plethora of studies on synthetic polymers based TPPE in QSDSSC have been carried out. Table 2.4 outlines some of these studies.

Amongst the various polymers tested, PEO and their derivatives are the most prevalently used polymer in TPPE (Su'ait *et al.*, 2015). In fact, some of the highest efficiency for TPPE based QSDSSC were obtained with PEO as the host material (Lee *et al.*, 2018). In 2009, Shi et al. reported QSDSSC fabricated from high molecular weight PEO and the cells boasted a power conversion efficiency of 10.11 % (Shi *et al.*, 2009). It is proposed that the superior performance of PEO based TPPE is credited to the presence of multiple ether and polyhydric groups throughout the polymer chains which serves as complexation sites for the cations. As the cations are engaged in an interaction with the

polymer chains, the iodide anions are more liberated to move around (Nogueira *et al.*, 2004).

Table 2.4: Examples of TPPE based QSDSSC in literature

Polymer	Electrolyte component	Dye	Efficiency, η (%)	Reference
Synthetic polymers				
PAN	EC/PC/TPAI/LiI/I_2	N719	6.40	(Wanninayake *et al.*, 2016)
PMMA	EC/PC/ TPAI/KI/I_2	N719	3.99	(Dissanayake *et al.*, 2014)
PVA	EC/PC/DMSO/ TPAI/KI/I_2	N3	4.59	(Arof *et al.*, 2014)
PVDF-HFP	MPN/TBP/ KI/I_2	N719	4.75	(Huang *et al.*, 2011)
PVP	Methanol/KI/ I_2	N719	3.74	(Chalkias *et al.*, 2018)
PEO	Acetonitrile/ LiI/KI/ I_2	N719	5.80	(Agarwala *et al.*, 2011)
PEG	PC/KI/ I_2	N719	7.22	(Wu *et al.*, 2007a)
Natural polymers				
Phthaloyl chitosan	EC/DMF/ TPAI/I_2	N3	6.36	(Yusuf *et al.*, 2017)
Hydroxypropyl cellulose	EC/PC/MPII/ NaI/ I_2	N719	5.79	(Khanmirzaei *et al.*, 2015a)
Cyanoethylated hydroxypropyl cellulose	MPN/MHII/ TBP/NaI/ I_2	N719	7.55	(Huang *et al.*, 2012)
Agarose	NMP/ NaI/ I_2	N/A	4.14	(Yang *et al.*, 2011)
Polymer blends				
PEO/PMMA	EC/PC/DMC/ TBP/LiI/ I_2	N719	4.90	(Aram *et al.*, 2015)
PVDF-HFP/PAN-VA	Acetonitrile/ LiI/KI/ I_2	N719	6.30	(Venkatesan *et al.*, 2014)
Phthaloyl chitosan/PEO	EC/DMF/TPAI/BMII/ I_2	N3	9.61	(Buraidah *et al.*, 2017)

Besides the addition of a single polymer component as the gelating agent, utilization of polymer blends is also a useful procedure adapted to achieve TPPE with desirable properties. By blending PVDF into PEO-$LiClO_4$ electrolyte, Jacob et al. had shown that the ionic conductivity can be improved by two orders of magnitude (Jacob *et al.*, 1997). In a recent study Hsu et al. demonstrated the difference in photovoltaic performances of DSSC composed of graphene oxide nanosheet-polyaniline (GOS-PANI)

nanohybrid/PEO blend gel electrolytes (Hsu *et al.*, 2014). In their study it was evident that due to the improvement in ionic conductivity and electrochemical catalytic activity of the gel electrolyte, higher efficiency was observed for the DSSCs based on the blend in comparison to pristine PEO electrolyte-based DSSC sample.

2.5.4 Thermosetting polymer electrolyte

Essentially, the preparation of a thermosetting polymer electrolyte (TSPE) is similar to TPPE except for the fact that, gelation process is an effect of crosslinking reaction with formations of permanent covalent bonds (Li *et al.*, 2006; Liska *et al.*, 1988). The gels produced by this technique often comprises a three-dimensional network within which the solvent is entrapped. The term "thermosetting" implies the irreversible physical state of the gel with temperature (Wu *et al.*, 2007b). In most cases, the visual impression of a TSPE is very similar to solid electrolyte but the internal presence of solvent qualifies them to be quasi-solid electrolytes.

In-situ polymerization by chemical, photochemical or thermal means is one of the frequent mechanism employed for the fabrication of TSPE (Wang *et al.*, 2005a). It is believed that by carrying out the polymerization of the electrolytes after assembling between the electrodes, penetration and wetting of the mesoporous layer in photoanode can be improved (Wu *et al.*, 2015). This is also conjectured to reduce unwanted recombination reactions that may diminish cell efficiency. However, the designing of polymerization for QSDSSC can be slightly tricky as there are certain restrictions that need to be imposed. For example, the polymerization should occur without an initiator and complete without a by-product, as both these components may affect photovoltaic properties of the cell (Murai *et al.*, 2002). Also, the temperature at which polymerization takes place has to be ensured not to exceed the decomposition temperature of dye molecules.

TSPE fabricated from thermally polymerized poly(ethylene oxide-co-propylene oxide) trimethacrylate is one the studies in which enhanced open circuit voltage due to suppressed recombination was reported (Komiya *et al.*, 2004). Three polymerizable reactive groups in the oligomer enabled the formation of a three-dimensional polymer network, capable of containing a larger amount of solvent due to larger free volume. Another innovative approach was adapted by Winther-Jensen et al. who combined photocatalysis and photoinduced polymerization (Winther-Jensen *et al.*, 2008). In their work, a novel method of using TiO_2 nanoparticles as both photo-initiator and co-gelator in a charge transfer polymerization reaction was presented.

2.5.5 Ionic liquid polymer electrolyte

As discussed earlier, IL has been used as solvent in liquid electrolyte DSSC. However, the versatile nature of IL also permits it to be used as the charge carrier component in electrolytes. When iodide based IL is employed in polymer electrolytes as the source of ions, it is called ionic liquid polymer electrolytes (Gorlov & Kloo, 2008).

IL is a widely known ingredient added in TPPE to improve the photovoltaic properties of the gels due to its higher dielectric constant and plasticizing effect. Particularly, imidazolium iodides have been used often in QSDSSC. An important aspect that requires scrutiny when selecting IL as an additive is the alkyl-substituents on the imidazolium cations (Zakeeruddin & Grätzel, 2009). Since these substituents regulate the van der Waals interactions among cations and Coulombic interactions with the anion, the physical properties of the IL are hugely affected (Hwang *et al.*, 2013). As the chain length increases, the room temperature viscosity of the IL increases as an implication of greater van der Waals interactions. Conversely, the shortening of the chain translates into higher lattice energy and increases possibility for solidification of the salt at ambient temperature. In a comparative study of PVDF-HFP containing imidazolium ionic liquids

of different carbon chain lengths by Suryanaryanan et al., it was noted that the cell efficiency was mainly controlled by photocurrent density values as photovoltage remain unaffected by different alkyl chains (Suryanarayanan *et al.*, 2007). Although the ionic conductivities decreased, the electron lifetime improved with increasing chain length. Aggregation of imidazolium cations on the photoanode increases in the presence of longer chains, leading to a higher diffusion coefficient of electrons injected in photoanode.

CHAPTER 3: RESEARCH METHODOLOGY

3.1 Chemicals

Table 3.1 lists the chemicals and the corresponding suppliers used throughout this work. The chemicals have been used as received without further purification.

Table 3.1: List of chemicals and suppliers

Chemical / material	Details
Starch	Omya Hamburg
Hydroxyethyl cellulose	Sigma Aldrich
Phthalic Anhydride	Merck
Isopropanol	Sigma-Aldrich
N,N-dimethylformamide	Merck
Tetrapropylammonium iodide	Fischer Scientific
Lithium Iodide	Fisher Scientific
1-methylimidazole	Sigma-Aldrich
1-iodobutane	Sigma-Aldrich
Cyclohexane	Sigma-Aldrich

3.2 Synthesis of phthaloyl starch

For phthaloylation of starch, the synthesis was carried out according to the procedure of Khan et al. (Khan *et al.*, 1997). 10 g of starch were suspended into a flask containing 60 mL of DMF and heated up to 80 °C. The mixture was maintained at the temperature for 30 min under stirring. 18.5 g of phthalic anhydride and 8 g of pyridine were then added to the mixture, which was kept under constant stirring for 4 h at 80 °C. The phthaloylated starch product was then retrieved by precipitation with isopropanol and dried in vacuum until constant weight. The molar ratio of phthalic anhydride to anhydroglucose unit was kept at 2:1.

3.3 Characterization of phthaloyl starch

3.3.1 Nuclear Magnetic Resonance (NMR)

NMR spectroscopy is an analytical technique that aids in interpreting the molecular structure of the sample. By deciphering the spectral peaks, the arrangement of carbon-hydrogen framework within the structure can be further validated.

Proton nuclear magnetic resonance was taken at 399.65 MHz with JNM–GSX270 Fourier Transform Spectrometer. DMSO-d6 is used as the solvent with sample concentration of 20% w/v. The samples were also analyzed by solid-state ^{13}C NMR (JNM–ECX500) in a range of 0–200 ppm with 1024 scans under cross polarization/magic angle spin (CP-MAS) conditions. All chemical shifts are reported in parts per million (ppm).

3.3.2 Fourier Transform Infra-Red (FTIR)

FTIR spectroscopy identifies the different types of chemical bonds present in a molecule by analyzing the IR absorption spectrum over a range of frequencies. The theoretical basis behind this technique is that for any given molecular bond, there are specific frequencies at which it can vibrate, depending on the elements involved and the types of bonds between them. Therefore, FTIR spectral analysis is very useful in providing information on possible chemical interactions within system.

In particular, Attenuated Total Reflectance Fourier Transform Infra-Red (ATR-FTIR) has in recent years revolutionized semi-solid and liquid sample analyses by simplifying sample preparation methods and improving spectral reproducibility. This method functions by measuring the changes that occur in a totally internally reflected infrared beam when the beam comes into contact with a sample.

In this work, ATR-FTIR spectra were recorded with a Spotlight 400 spectrometer (Perkin Elmer, UK). The acquisition parameters were done with a total of 32 accumulations at 2 cm^{-1} resolution with a spectral range from 650–4000 cm^{-1}. For FTIR deconvolution analysis, multiple peak fitting procedure was performed using Origin Pro 9.1 software with second–order derivatives to determine the hidden peaks. A Gaussian model was used in which the coefficient of determination, R^2 values were always within ±0.99.

3.3.3 Solubility test

Solubility test was carried out to identify the best solvent system for gel formation. Approximately 50 mg of PhSt was put into the test tubes and tested for its solubility in various solvents at room temperature. For comparison, solubility of native starch in the various solvents was also carried out. The solubility was then observed visually.

3.3.4 Degree of substitution

About 0.5 g of the phthaloyl starch sample was dissolved in 20 cm^3 of 0.2 M NaOH and 50 cm^3 of distilled water was added (Stojanović *et al.*, 2005a). The solution was transferred to a 100 cm^3 volumetric flask, which was then filled up to the mark with distilled water. 25 cm^3 of the solution was transferred to an Erlenmeyer flask and diluted by addition of 50 cm^3 of distilled water. The excess of NaOH was back-titrated with standard 0.05 M HCl using phenolphthalein as the indicator. The titration was repeated three times and the average value of the HCl volume was used for the calculations. A blank was also titrated. The amount of COOH, n_{COOH} is equated to:

$$n_{COOH} = (V_b\text{-}V) \times C_{HCl} \times 4 \quad (3.1)$$

where V (in cm^3) is the volume of HCl used for the titration of the blank; V_b (in cm^3) is volume of HCl used for titration of the sample; C_{HCl} (in mol/dm^3) is the HCl concentration and 4 is the ratio of the total solution volume (100 cm^3) and the volume taken for titration

(25 cm^3). The procedure was repeated three times for each sample and the average value of the n_{COOH} was taken for the DS calculation. The DS was calculated from the following equation:

$$DS = (162 \times n_{COOH})/(m\text{-}149 \times n_{COOH}) \quad (3.2)$$

where 162 g/mol is the molar mass of an anhydroglucose unit (AGU); n_{COOH} (in mol) is the amount of COOH, 149 g/mol is the net increase in the mass of an AGU for each phthaloyl group substituted, and m (in g) is the mass of the dry sample.

3.3.5 X-Ray Diffraction (XRD) analysis

Crystallinity is a state of molecular structure referring to a long range periodic geometric pattern of atomic spacings (Crompton, 1993). In semicrystalline polymers, some of the macro-molecules are arranged in crystalline regions while the matrix is amorphous. The term amorphous describe polymers totally lacking in long-range spatial order. One of the simplest methods to monitor the pattern in crystallinity of polymers is via X-ray diffraction studies.

In this work, the XRD analysis was recorded at room temperature using an Empyrean diffractometer (PANalytical, Netherlands) at 2θ angles between 10º and 60º with a step size of 0.026º, using Cu/Kα1 irradiation. The powder samples were adhered onto an air-tight sample holder consisting of a coin cell assembly coated with Mylar film whereas gel samples were uniformly applied on the surface of the sample holder.

The degree of crystallinity was calculated according to the peak-height method using HighScore Plus v3.0.4 produced by PANalytical. In this approach, X-ray diffraction pattern was obtained after removing the linear background. Crystallinity (%) was then calculated as the intensity ratio of the crystalline diffraction peaks and of the sum of all measured intensity (Equation 3.3).

$$\text{Crystallinity (\%)} = 100 \times \Sigma I_c / (\Sigma I_{total} - \Sigma I_{background}) \quad (3.3)$$

where I_c denotes crystalline peak intensity, I_{total} denotes total peak intensity and $I_{background}$ signifies background intensity.

3.4 Preparation of gel polymer electrolyte

3.4.1 Variation of PhSt and HEC content

The electrolyte fabrication in this study is divided into two phases. In the first part, GPE comprising of phthaloyl starch and HEC of various weight ratios as listed in Table 3.2 were prepared.

Table 3.2: Designation of PhSt-HEC based gels

Designation	Phthaloyl starch		Hydroxyethyl cellulose	
	mass (g)	wt.%	mass (g)	wt.%
H0	0.40	100	0.00	0
H10	0.36	90	0.04	10
H20	0.32	80	0.08	20
H30	0.28	70	0.12	30
H40	0.24	60	0.16	40
H50	0.20	50	0.20	50
H60	0.16	40	0.24	60
H70	0.12	30	0.28	70
H80	0.08	20	0.32	80

The wt.% of PhSt and HEC were calculated as per the following equation:

$$\text{wt.\% of HEC} = \frac{x}{\text{Total mass of PhSt+HEC}} \times 100\% \quad (3.4)$$

where *x* corresponds to the mass of HEC. The required amounts of the polymers were added into DMF followed by gentle stirring at 70 °C for 6 h. In all samples, the solvent to polymer weight ratio was fixed at 1:3. The resulting gels were then subjected to conductivity and rheological analyses.

For the second part of the study which involves electrolyte preparation for QSDSSC fabrication, blank gels with optimum polymer composition (H20-H60) was chosen and a fixed amount of 5 wt.% of TPAI was added. The salt was dissolved in the solvent, followed by addition of polymers as explained above. Once the gel is formed, I_2 (10 wt.% of salt) is added at 40 °C and stirred for 1 h. These samples were designated as HT series (HT20-HT60).

3.4.2 Variation of LiI and TPAI content

From the results in previous section, the GPE with the highest efficiency (H30) was used as the polymer host. Different amounts of LiI and TPAI were added respectively to the gel. The photographs of these gels are attached in Appendix A. Addition of wt.% of the salts was done according to the following equation :

$$\text{wt.\% of salt} = \frac{x}{x + \text{Total mass of (PhSt+HEC+DMF)}} \times 100\% \quad (3.5)$$

where x is the mass of salt. The detailed composition of the gels fabricated are listed in Table 3.3.

Table 3.3: Designation of gels with different salt amounts

Designation	Mass of PhSt (g)	Mass of HEC (g)	Mass of DMF (g)	Mass of salt (g)	wt.% of salt (%)	Mass of I_2 (g)
LiI series						
L0	0.28	0.12	1.20	0.00	0.0	0.000
L1	0.28	0.12	1.20	0.04	2.5	0.008
L2	0.28	0.12	1.20	0.08	5.0	0.016
L3	0.28	0.12	1.20	0.13	7.5	0.025
L4	0.28	0.12	1.20	0.18	10.0	0.034
L5	0.28	0.12	1.20	0.23	12.5	0.043
L6	0.28	0.12	1.20	0.28	15.0	0.054
L7	0.28	0.12	1.20	0.34	17.5	0.064
TPAI series						
T0	0.28	0.12	1.20	0.00	0.0	0.000
T1	0.28	0.12	1.20	0.04	2.5	0.003
T2	0.28	0.12	1.20	0.08	5.0	0.007
T3	0.28	0.12	1.20	0.13	7.5	0.011

Table 3.3 continued

T4	0.28	0.12	1.20	0.18	10.0	0.014
T5	0.28	0.12	1.20	0.23	12.5	0.019
T6	0.28	0.12	1.20	0.28	15.0	0.023
T7	0.28	0.12	1.20	0.34	17.5	0.028

3.4.3 Variation of BMII content

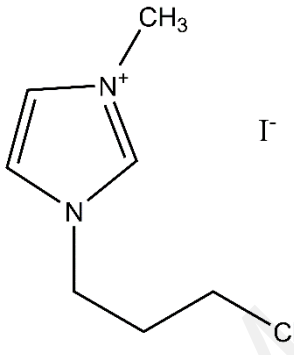

Figure 3.1: Structure of BMII

1-butyl-3-methylimidazolium iodide (BMII), shown in Figure 3.1, was synthesized by reacting equimolar amounts of 1-methylimidazole and 1-iodobutane dissolved in cyclohexane at 70 °C under nitrogen for 24 h. The resultant product was washed with n-hexane to remove the unreacted material. The product was dried in vacuum at 60 °C until constant weight. Purity of the samples was validated by ^{1}H NMR, (ppm, $CDCl_3$, 400 MHz): 9.16 (s, 1H, –NCH=N^+–), 7.72 (dd, 2H, –N–CH=CH–N^+–), 4.21 (t, 2H, –CH_2–N–), 3.88 (s, 3H, =N–CH3), 1.78 (m, 2H, –CH_2–CH_2–CH_2–), 1.29 (m, 2H, –CH_2–CH_2–CH_3), 0.91 (t, 3H, –CH_2–CH_2–CH_3), as attached in Appendix B.

Different weight percentages of 1-butyl-3-methylimidazolium iodide (BMII), as tabulated in Table 3.4, were added to the most efficient salt composition from previous section, T5 (designated as B0 in this series). The calculation of wt.% of BMII was performed according to the following equation:

$$\text{wt.\% of BMII} = \frac{x}{x + \text{Total mass of (PhSt+HEC+DMF+TPAI)}} \times 100\% \quad (3.6)$$

where x is the mass of BMII.

Table 3.4: Designation of gels with different BMII contents

Designation	Mass of PhSt (g)	Mass of HEC (g)	Mass of DMF (g)	Mass of TPAI (g)	BMII		Mass of I_2 (g)
					Mass (g)	wt.%	
B0	0.28	0.12	1.20	0.23	0.00	0.0	0.019
B1	0.28	0.12	1.20	0.23	0.04	2.0	0.022
B2	0.28	0.12	1.20	0.23	0.08	4.0	0.026
B3	0.28	0.12	1.20	0.23	0.12	6.0	0.030
B4	0.28	0.12	1.20	0.23	0.16	8.0	0.034
B5	0.28	0.12	1.20	0.23	0.20	10.0	0.038

3.5 Dye-sensitized solar cell fabrication

3.5.1 Preparation of dye solution

0.03 mol dm^{-3} dye solution was prepared by dissolving 10 mg of Ruthenizer 535 also known as N3 dye in 5 mL of ethanol. The solution was then stirred until homogenous.

3.5.2 Preparation of counter electrode

The platinum counter electrode used in this work was prepared by coating Fluorine Tin Oxide (FTO) glasses (from *Solaronix* SA) with Platisol T solution (from *Solaronix* SA) followed by sintering at 450 °C for 40 min.

3.5.3 Preparation of photoanode

The fabrication of mesoporous TiO_2 layered photoanode was done according to the procedure reported by Bandara et al. (Bandara *et al.*, 2013). FTO glasses that were used as the substrates, were rinsed with distilled water and ethanol before use. The glass substrate was first coated with a TiO_2 based blocking layer. To do this, 0.5 g of P90 Degussa TiO_2 powder was ground in a mortar with 2 mL of pH 1 nitric acid for 30 min. The resulting slurry was spin-coated on the FTO glass at 2350 rpm for 60 s. After air drying for 30 min, it was sintered at 450 °C for 30 min.

For the second layer, the TiO_2 colloidal suspension was prepared by grinding 0.5 g of P25 Degussa TiO_2 powder with 2 mL of pH 1 HNO_3. 0.25 g of poly(ethylene glycol), PEG 4000 and two drops of Triton X-100 was further added to attain optimal viscosity and adhesiveness of the slurry. The TiO_2 colloidal suspension was casted on the FTO glass by the doctor blade technique. The TiO_2 electrode was sintered in the furnace at 450 ^oC for 45 min. Sintering of the oxide layers at 450 ^oC gives the film two important properties: the individual particles come into close contact so that the conductance and charge collection properties are improved; and the aerial oxidation at elevated temperatures removes organic matter from the mesoporous film that could act as potential trap sites (Friedrich, 2011). The photoanode was then soaked in ethanolic N719 dye solution for 24 h. The complete procedure for photoanode preparation is summarized in the Figure 3.2.

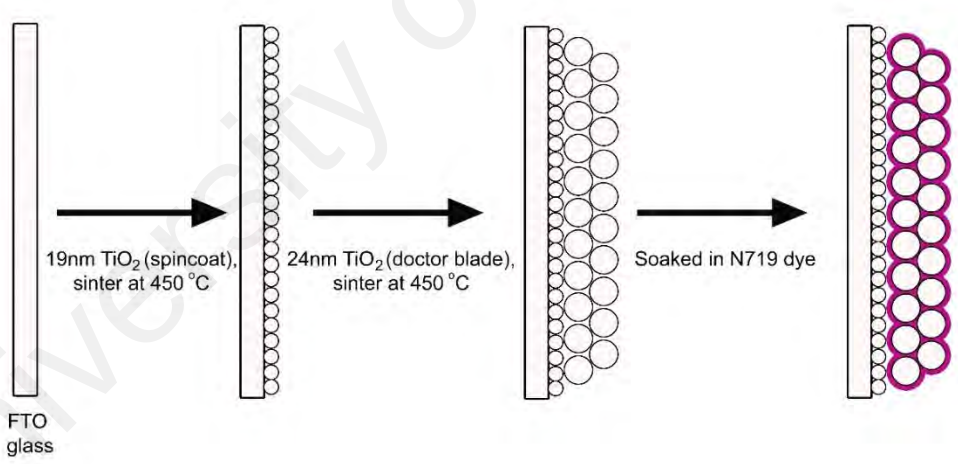

Figure 3.2: Preparation of photoanode

3.6 Characterization of gel polymer electrolyte

3.6.1 Rheological studies

Rheology is defined as the study of deformation and flow of matter. In rheological experiments, a material is subjected to shear forces and theoretically, the response the material may be in terms of the flow of ideal viscous liquid or the deformation of ideal

elastic solid (Mezger, 2006). However, in practice, the behavior of most real materials lie between the two extremes and these materials which exhibit viscous and elastic character simultaneously are termed as viscoelastic material. For most practical applications, it is very vital to gauge the balance between the solid and liquid characters of a material, and rheological characterization can be very beneficial to achieve this.

All rheological tests were performed using an Anton Paar Physica MCR 301 rheometer with a parallel-plate geometry (2.5 cm diameter). Amplitude sweep tests of the gel samples were studied by recording the variations in storage modulus, G′ (signifying solid properties) and loss modulus, G″(signifying solid properties) as a function of strain ranging from 0.1 to 250 % at an angular frequency of 10 $rads^{-1}$. The frequency sweep studies were carried out in the frequency range between 0.01 and 200 Hz with the strain kept constant at 1 %. The temperature dependent rheological properties of the samples were done by scanning from 10 to 100 °C at rate of 5 °C/min with strain and frequency of 0.01 % and 1 Hz respectively.

For the tack test study, the experiments were done at three intervals. First, the fresh sample was placed on the bottom plate and the top plate was lowered to a measuring gap of 0.25 mm. The sample was then subjected to short shearing for 1 s with a shear speed of 1000 s^{-1}. Finally, the top plate was removed vertically at a constant velocity of 5 m s^{-1} and the normal force experienced by the top plate was recorded. As the top plate is removed, the sample pulls on the measuring system and therefore the measured normal force values are negative. A schematic representation of the tack test study is presented in Figure 3.3. Operation of the rheometer and analysis of the rheological parameters were carried out using the Rheoplus/32 V3.60 software.

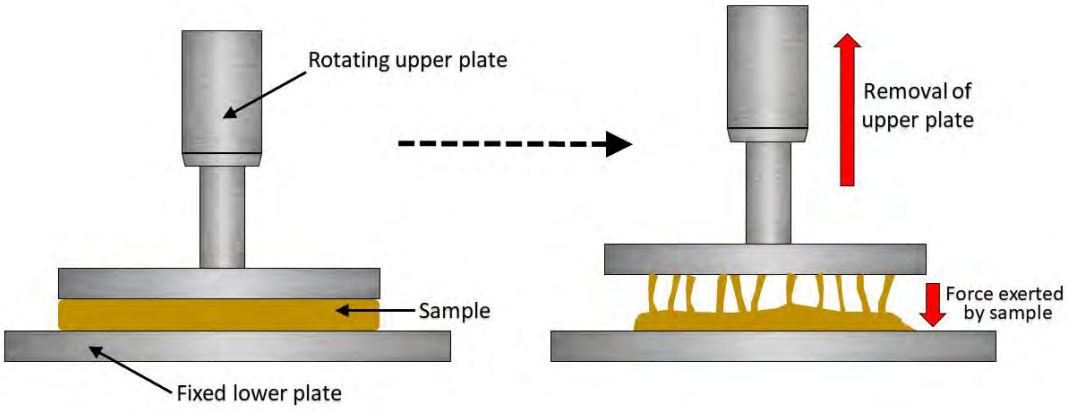

Figure 3.3: Graphical representation of tack test

3.6.2 Electrochemical impedance spectroscopy (EIS)

In order to measure the ionic conductivities of the gels, the EIS technique was adapted where impedance values were recorded using HIOKI 3531 Z HiTester in the frequency range between 50 Hz and 200 kHz. The samples were sandwiched between two stainless steel disc electrodes. The impedance data were presented in Nyquist plots, which showed the imaginary part, Z_i of impedance, against its real part of the cell, Z_r. The ionic conductivity (σ) of the GPEs can be calculated by using the bulk resistance, R_B values and following Equation 3.2.

$$\sigma = \frac{t}{R_B \times A} \tag{3.7}$$

where t is the thickness of the electrolyte, R_B is the bulk resistance and A is the film-electrode contact area.

Equivalent circuit fitting was performed on the impedance data of the samples to extract information on the R_B of the quasi-solid electrolyte system. Equivalent circuit modelling allows the system to be represented by the combination of electrical components which best fits the experimental values. The Nyquist plots for all the samples in this study display a straight line which intersects the horizontal axis and tilts to an angle

less than 90°. This type of plot is typical for system with ionic current conduction (Rajendran *et al.*, 2007) and is best represented by a circuit comprising resistance, R (point of intersection with the horizontal axis) in series with constant phase element (CPE) (Vondrák *et al.*, 2005). Equations 3.8 and 3.9 show the real and imaginary components of impedance, Z_r and Z_i associated to the equivalent circuit proposed:

$$Z_r = R + \frac{\cos\frac{\pi p}{2}}{C\omega^p} \tag{3.8}$$

$$Z_i = R + \frac{\sin\frac{\pi p}{2}}{C\omega^p} \tag{3.9}$$

where ω is the angular frequency, R and C denote resistance and capacitance while p is the parameter related to the tilted angle of the spike.

3.6.3 DSSC characterization

The performance of the QSDSSCs was studied using an Autolab instrument under solar simulator (Oriel LCS-100) with light intensity calibrated to 100 mW cm^{-2}. The area of the tested DSSC was 0.196 cm^2. The photographs of the fabricated DSSC are attached in Figure 3.4 and Appendix C.

Figure 3.5 shows a typical photocurrent density-voltage (J-V) curve obtained from the DSSC measurements. The performance of a cell is evaluated in terms efficiency, η with equates to:

$$\eta = \frac{P_{out}}{P_{in}} \times 100 = \frac{J_{SC} \times V_{OC} \times FF}{P_{in}} \times 100 \tag{3.10}$$

where η is the solar cell efficiency whereas P_{out} and P_{in} are the output and incident light powers respectively. J_{SC} is short circuit photocurrent, V_{OC} is open circuit voltage and FF is the fill factor. These three main parameters determines the extent of the solar cell performance. J_{SC} is governed by the light harvesting efficiency of the dye, its capacity to inject electrons into the TiO_2 conduction band and the ability of the semiconductor to

transport them to the collecting electrode (Raga *et al.*, 2012). On the other hand, V_{OC} is the difference of the Fermi level of electrons in the TiO_2 and the redox potential of the electrolyte (Wang *et al.*, 2006). Fill factor is a parameter that indicates the quality of solar cell and it can be calculated using the following equation:

$$FF = \frac{J_{max} \times V_{max}}{J_{SC} \times V_{OC}} \tag{3.11}$$

where J_{max} and V_{max} are the maximum current density and voltage. Graphically, fill factor represents the squareness of the J-V curve and correlates to the area of the largest rectangle that fits the J-V curve.

Figure 3.4: Setup of DSSC characterization

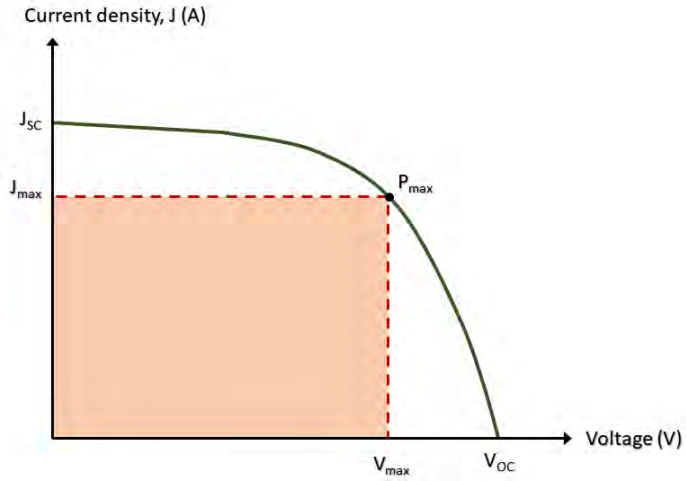

Figure 3.5: Typical current-voltage curve of DSSC

Additionally, the DSSCs were tested with electrochemical impedance spectroscopy (EIS) using a potentiostat–galvanostat device (Metrohm Autolab PGSTAT128N, FRA32 M). The impedance of the cells were measured by applying a bias at the open-circuit voltage, V_{OC} of the cell and the readings were taken within a frequency range of 10 mHz to 100 kHz with an a.c. amplitude of 10 mV.

CHAPTER 4: RESULTS AND DISCUSSION

4.1 Phthloylation of starch

The starch molecules were chemically modified by substituting the hydroxyl groups with phthaloyl groups. The attachment of the bulky phthaloyl group is essential to amend the hydrophilic nature of starch in order to allow homogenous dissolution of the starch derivative in organic solvent. The presence of the phthaloyl group which contains chemically reactive functional groups, such as ester carbonyl, acid carbonyl and aromatic ring, is expected to improve the polyfunctionality of the polymer, thus providing larger number of sites for ion migration.

4.1.1 FTIR

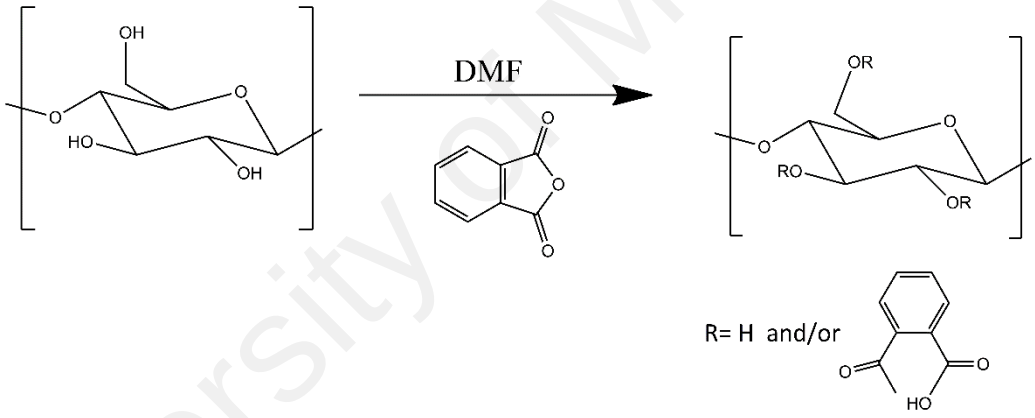

Figure 4.1: Reaction scheme of phthaloylation of starch

As shown in Figure 4.1, the starch molecules were chemically modified by substituting the hydroxyl groups with phthaloyl groups. The attachment of the bulky phthaloyl group is essential to amend the hydrophilic nature of starch in order to allow homogenous dissolution of the starch derivative in organic solvents. The presence of the phthaloyl group which contains chemically reactive functional groups, such as ester carbonyl, acid carbonyl and aromatic ring, is expected to improve the polyfunctionality of the polymer, thus providing larger number of sites for ion migration.

Figure 4.2 depicts the comparison of FTIR spectra between starch and PhSt. The introduction of phthaloyl group into the starch molecule was confirmed by the appearance of new peaks in the FTIR spectrum in addition to the typical peaks of pristine starch including O-H stretching (3315 cm^{-1}), C-H (2927 cm^{-1}) and C-O stretching (1000-1100 cm^{-1}) (Chauhan *et al.*, 2015; Lopez *et al.*, 2014). The spectrum of phthaloyl starch exhibited new characteristic absorption peak at 1715 cm^{-1}, corresponding to the phthalate group and this is in agreement with previous literature (Kondaveeti S. *et al.*, 2015; Liu *et al.*, 2007). The absorption peaks observed at 1601 cm^{-1} and 747 cm^{-1} can be attributed to the aromatic ring present in the phthaloyl group.

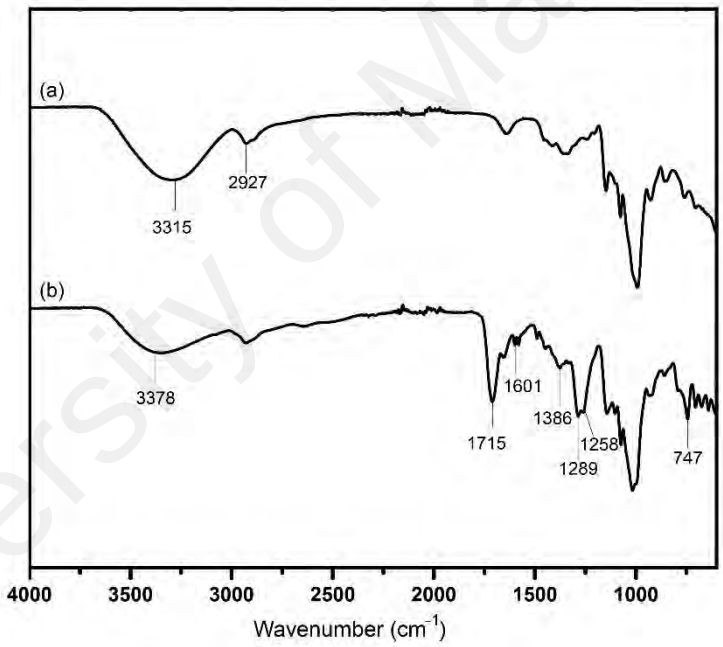

Figure 4.2: FTIR spectra of (a) starch and (b) phthaloyl starch

Besides that, additional peaks identified in the fingerprint regions, at 1289 cm^{-1} are assigned to the esteric C-O stretch. The peak corresponding to the hydroxyl groups was also found to shift from 3315 cm^{-1} in pure starch to 3378 cm^{-1} in the esterified starch. The intensity of the hydroxyl peak was also found to be lower in phthaloyl starch and this is expected as a portion of the hydroxyl groups of the starch have now been substituted into the phthalate ester group. The shift in the OH absorbance peak frequency can be explained

in terms of the extent of hydrogen bonding. Free hydroxyls on the starch polymer chains tend to have higher frequencies compared to associated hydroxyls (hydroxyls attached to other hydroxyls by hydrogen bonds) (Liang & Ludescher, 2015). Thus the shift towards a higher frequency in the esterified starch suggests the disruption of intermolecular hydrogen bonding due the presence of the bulky phthaloyl group.

4.1.2 ^{1}H NMR analysis

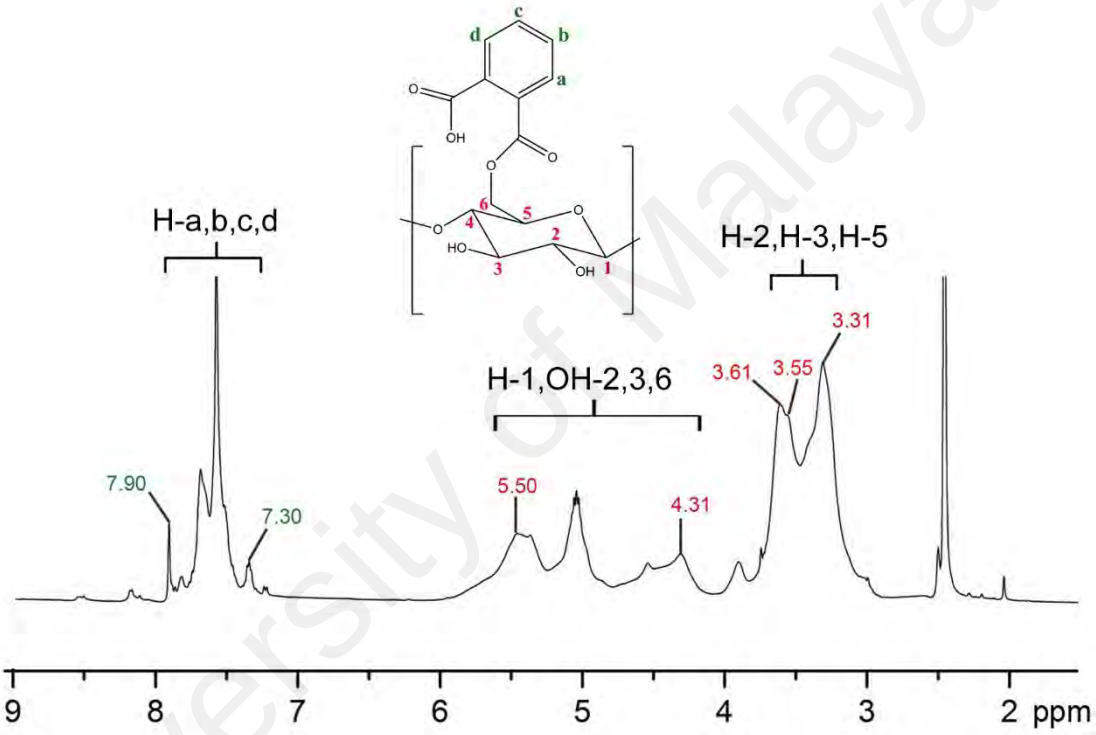

Figure 4.3: ^{1}H NMR spectra of phthaloyl starch

The ^{1}H NMR spectra of the synthesized phthaloyl starch further verifies the phthaloylation reaction (Figure 4.3). The spectral lines present between 3.00 and 5.50 ppm which correspond to the protons of the anhydroglucose units shows that the backbone of the starch molecule remained largely intact during the esterification process. Chemical signals of the protons at 3.31, 3.61 and 3.55 ppm are assigned to H-2, H-3, and H-5 respectively. The shifts of H-1 and OH-2, 3, 6 are assigned to peaks between 4.31 and 5.50 ppm (Namazi *et al.*, 2011). The attachment of the phthaloyl group to the starch

molecule was confirmed by the presence of spectral lines between 7.30-7.90 ppm which is characteristic to aromatic ring protons (Kondaveeti S. *et al.*, 2015). The peak corresponding to carboxylic acid proton is absent in the spectra and this is expected to be due to the lability of these protons which allows their exchange with the DMSO deuterium. Hence, to further verify the structure, the sample was subjected to ^{13}C NMR analysis.

4.1.3 ^{13}C NMR analysis

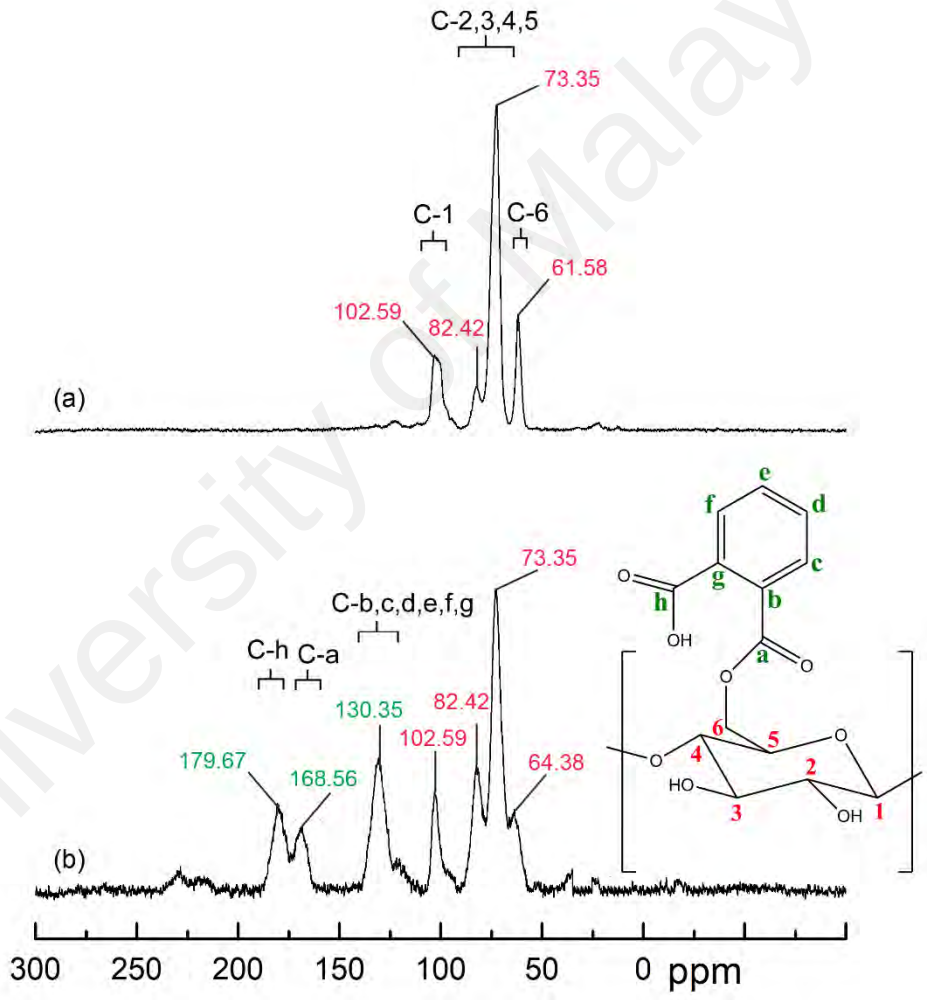

Figure 4.4: ^{13}C NMR spectra of (a) starch and (b) phthaloyl starch

In the ^{13}C NMR spectrum of starch (Figure 4.4), signals attributed to anomeric carbon (C-1) appeared at 102.59 ppm. The peak at 61.58 ppm corresponds to the primary carbon whereas the peaks at 73.35 ppm and 82.42 ppm are due to C-2, C-3, C-5 and C-4 carbons

in the polymer backbone (Mathew & Abraham, 2007). Similar peak assignments were found in ^{13}C NMR spectrum of PhSt, however, the C-6 peak appeared slightly shifted downfield at 64.38 ppm. This observation indicates the esterification took place predominantly at the hydroxyl of C-6 in starch. In addition to these native starch peaks, three new signals were also detected in PhSt. The peak at 130.35 ppm, 168.56 ppm and 179.67 ppm can assigned to the aromatic carbons, ester carbonyl and carboxylic acid carbonyl of the phthaloyl group (Hu *et al.*, 2013; Kondaveeti *et al.*, 2013). The presence of these additional peaks verifies the derivatization of starch into PhSt.

4.1.4 XRD analysis

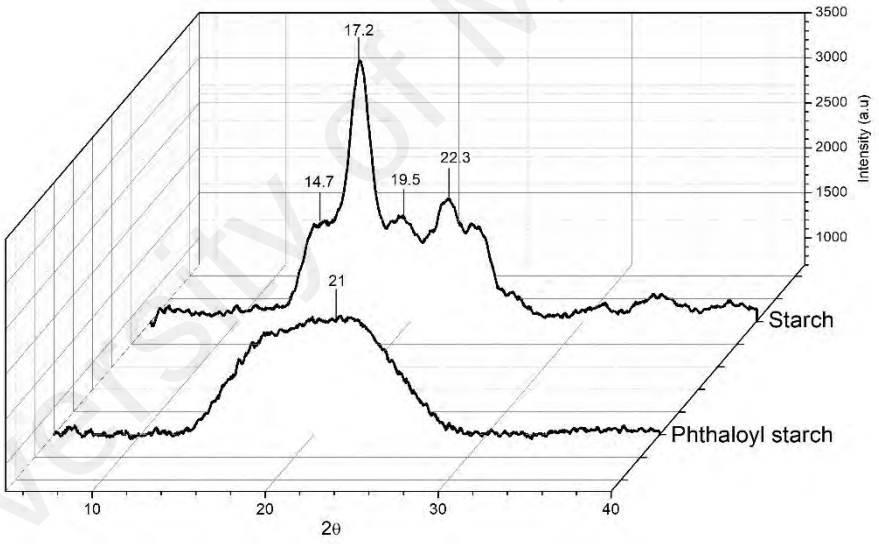

Figure 4.5: XRD diffractograms of starch and phthaloyl starch

As depicted in Figure 4.5, the XRD diffractograms of native potato starch exhibit a typical B-type crystalline structure (Mathew & Abraham, 2007), with a strong diffraction peak at around 2θ of 17.2° and smaller peaks at 14.7°,19.5° and 22.3°. Instead, the phthaloyl starch diffractogram shows a broad peak centered around 21°. Upon esterification, the phthaloyl groups substitute some of the hydroxyl groups on starch. The

presence of the bulky phthaloyl group impedes the formation of intermolecular hydrogen bonds and this in turn results in the destruction of the ordered crystalline structure.

4.1.5 Degree of substitution

The degree of substitution of the phthaloyl starch, calculated via the back-titration method, was determined to be 0.8. This value specifies that on average, there are eight groups of substituted phthaloyl per 10 anhydroglucose unit. As depicted in Figure 4.1, the highest possibility of substitution of the phthaloyl group is at the hydroxyl in position C-6 because of its higher chemical reactivity. This was also supported by the 13C NMR spectral analysis which showed significant peak shifts for C-6.

4.1.6 Solubility

Table 4.1 shows the solubility of starch and phthaloyl starch in various solvents at room temperature. When native starch is suspended in water at ambient temperature, it swells. Upon heating, the starch granules continue to swell further until it rupture and release amylose and amylopectin to form a solution consisting of complex colloidal suspension (Koganti *et al.*, 2011). The dissolution of starch in water is due to its ability to form networks with water molecules via hydrogen bonding. However, being hydrophilic in nature, starch is insoluble in organic solvents. In this work, it was evident that upon phthaloylation, the starch derivative was soluble in organic solvents such as DMF, DMSO and DMA. The attachment of phthaloyl group to the starch backbone introduces hydrophobic moieties which enables the dissolution of phthaloyl starch in organic solvent. However, as suggested by degree of substitution value, not all of the hydroxyl groups have been substituted by the hydrophobic reagent. The presence of unsubstituted hydroxyls throughout the backbone allows phthaloyl starch to be still soluble in water (Shogren & Biswas, 2006).

Table 4.1: Solubility of phthaloyl starch in various solvents

Solvent	Solubility of Starch	Solubility of PhSt
Water	✓ (complete dissolution upon heating)	✓
Dimethyl formamide (DMF)	×	✓
Dimethyl sulfoxide (DMSO)	×	✓
Dimethyl acetamide (DMA)	×	✓
Pyridine	×	✓
Acetonitrile	×	×
Ethanol	×	×
Cyclohexane	×	×
Chloroform	×	×
Acetone	×	×

✓ : Soluble × : Insoluble

4.2 EFFECT OF POLYMER BLEND COMPOSITION ON GPE

4.2.1 Preparation of PhSt-HEC based blank gels

Figure 4.6: Photograph of HEC-PhSt-DMF gels

The first part of this study intends to explore the rheological and electrical properties of gels with different proportions of polymer blends in order to select the best composition for QSDSSC fabrication. To serve this purpose, different compositions of PhSt and HEC were added as the polymer host in the gels and in all the samples, the polymer component was always fixed to comprise 25 wt.% of the electrolyte. As shown in Figure 4.6, clear and homogeneous samples were obtained up to 80 wt.% of HEC, beyond which homogeneity was unattainable. It is also interesting to observe the transformation in the

texture of the gels; from a viscous liquid to a sticky gel and finally a rubbery lump; with gradual addition of HEC.

4.2.1.1 Rheological properties

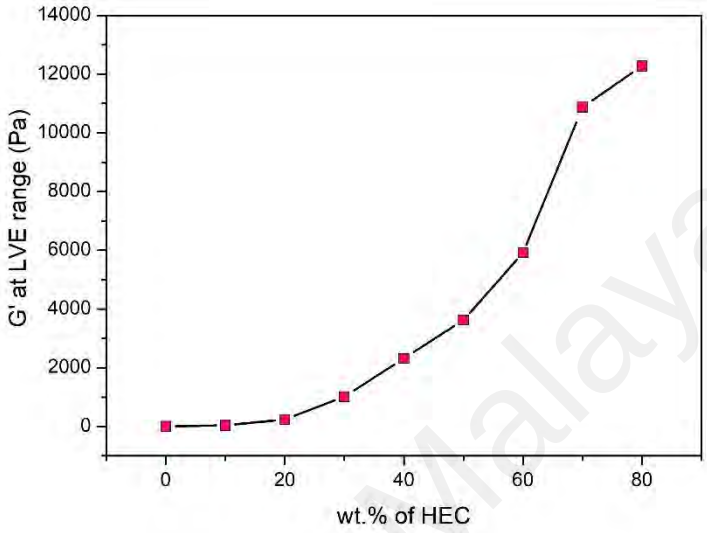

Figure 4.7: Storage modulus at LVE range for PhSt-HEC-DMF gels

The rheological properties of the gels in the first system were studied by the means of two analyses, namely amplitude sweep tests and tack tests. Amplitude sweep tests (AST) were performed to gauge the viscoelastic properties of the gels. Typically in AST,the evolution of storage modulus, G' and loss modulus, G'' is monitored as the function of strain. The complete figures of amplitude sweep curves for PhSt-HEC-DMF gels are attached in Appendix D. Figure 4.7 depicts the trend of G' values at linear viscoelastic (LVE) region for samples with different HEC contents. As expected, by increasing the HEC content in the polymer blends, G' value increases profoundly, especially from 20 wt.% HEC onwards. This verifies the transformation of the gel electrolytes from soft, viscous material to stiff, elastic gel. The stiffness imparted to the gels upon addition of HEC is attributed to the intrinsic rigidity of cellulose chains. The β-1,4 glycosidic linkages found in cellulose compels the polymer to arrange itself in long, straight chains

which increases the possibility for intermolecular hydrogen bonding. This arrangement assists in imposing rigidity to the gels (Backinowski *et al.*, 2013).

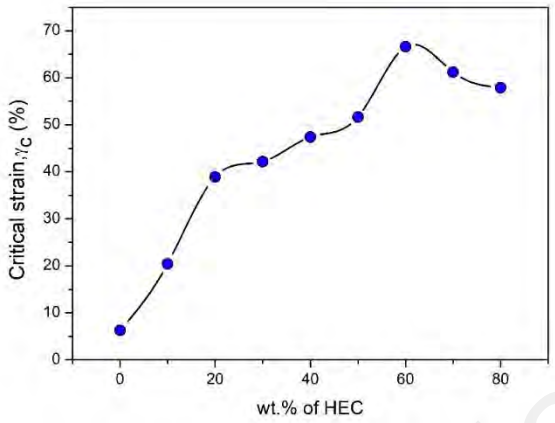

Figure 4.8: Critical strain values for PhSt-HEC-DMF gels

Besides the rigidity of the gels, AST also provides information on the strength of the gels. This aspect can be observed by studying the critical strain, γ_c beyond which the storage modulus declines indicating a disruption in the network structure. Gels with higher values of critical strain are inferred to be stronger. Figure 4.8 shows that the polymer gel strength increases with addition of HEC, where significant improvement is detected with addition of 20 wt.% HEC onwards. The improvement in the strength of the gels is hypothesized to be the effect of entanglement between the different polymer chains. The presence of large phthaloyl groups inhibits entanglement of PhSt chains. Thus, compositions with higher PhSt content exhibited poor gel strength. From 20 wt.% HEC onwards, there are sufficient cellulose chains in the gel matrix to promote HEC-PhSt chain entanglement. The interaction between the two polysaccharides results in a more compact gel structure which is less susceptible to deformation. Beyond 60 wt.% HEC, the critical strain values declined slightly suggesting a dip in the gel strength. When the concentration of HEC in the gels reaches a maximum amount, it allows the cellulose chains to form more extensive hydrogen bonding as there is now lesser amount of starch

chains available to disrupt the cellulose-cellulose interaction. These arrangement disfavors chain entanglement and makes the gel slightly weaker.

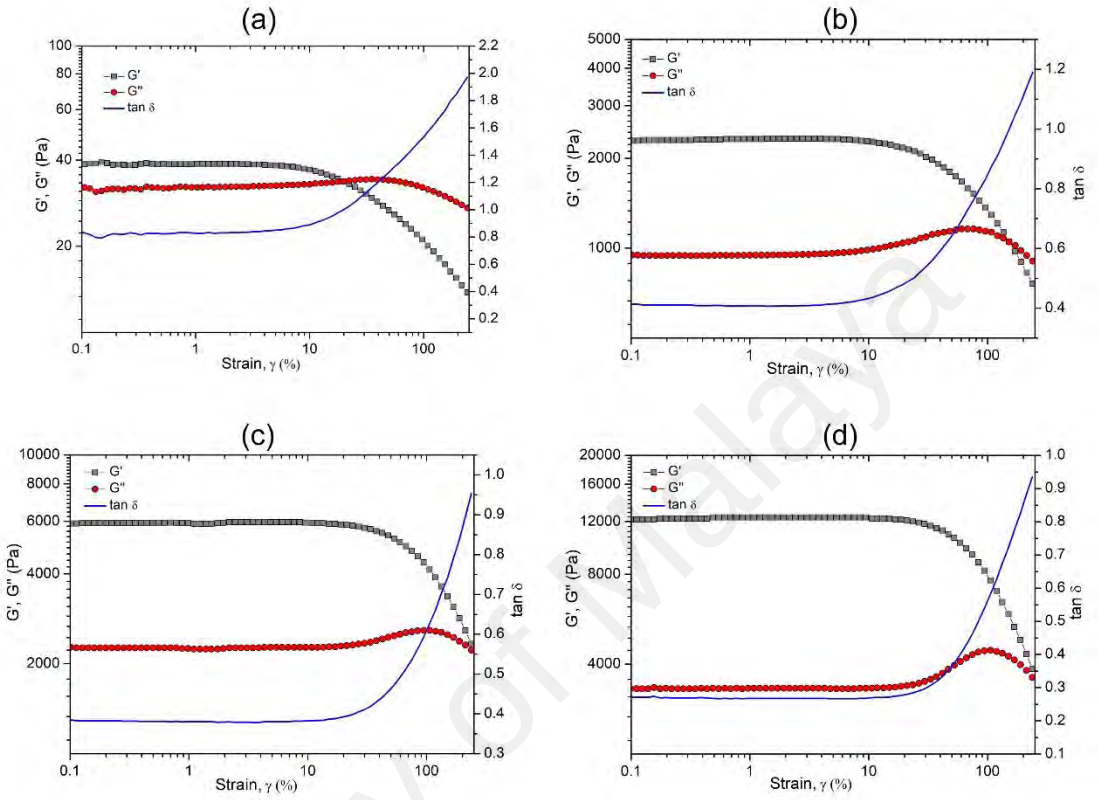

Figure 4.9: Amplitude sweep curves of (a) H10, (b) H40, (c) H60 and (d) H80

The loss factor, tan δ which equates to the ratio of G" to G' is an important parameter in AST as it defines the balance between the solid and liquid character in a viscoelastic material. The shift in tan δ value with increasing imposed deformation provides information on the behavior of microstructures within the gel matrix. The presence of microstructures signifies the existence of forces between the molecules and particles in the gel. Thus when a certain amount of external force larger than the intermolecular forces is applied, these microstructures collapse. When tan δ < 1, it denotes that the external force is smaller than internal forces. In this state, the gels exhibit quasi-elastic behavior in which the material is capable of storing energy and thus microstructurally regenerate to its initial conformation. Whereas when tan δ > 1, the applied force prevails leading to

irreversible microstructural collapse and the gels display viscous, liquid-like character (Mezger, 2006; Stoppe & Horn, 2017). Prevalently, the sustainance of tan δ value below 1 even at higher strain magnitude reflects the strength of the gels. As shown in Figure 4.9, for H10 tan δ exceeds unity at strain magnitude about 10%. However, with the addition of HEC beyond 20 wt.%, tan δ value below 1 sustains up to 100% strain. Therefore it can be concluded that the incorporation of HEC as part of the polymer host improves both rigidity and strength of the gels.

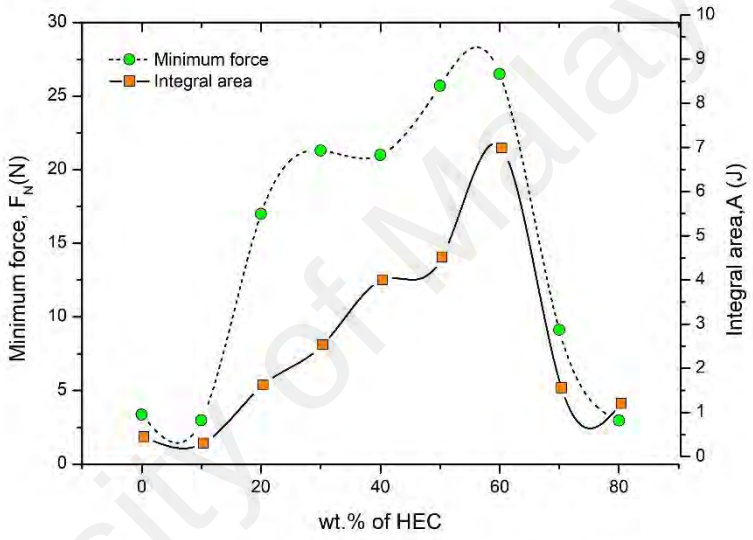

Figure 4.10: Tack test parameters of PhSt-HEC-DMF gels

Adhesiveness is the property of materials that are capable of forming an attachment with the substrate upon contact. This property is very vital for electrolytes in QSDSSC as it helps to establish effective contact between the electrodes and the electrolyte. The samples were subjected to tack test, a useful technique to explore the cohesive and adhesive forces of the gels. The tack test curves for PhSt-HEC-DMF gels are attached in Appendix E. In tack test, the parameter of concern is the minimum normal force, which denotes the tackiness of the samples and the area under the curve, which signifies the cohesive and adhesive strengths of the material. The trend of minimum force for the different polymer compositions is presented in Figure 4.10 and it is apparent that

appreciable tackiness can only be observed beyond 20 wt.% of HEC. The upward trend in minimum force value continues up to 60 wt.% of HEC, above which it begins to drop. The integral area under the curve value also follows the same trend as the minimum force indicating that the tack value is essentially governed by adhesive and cohesive forces.

Good adhesion in polymeric material is usually achieved by the synergistic combination of liquid-like features to form good molecular contact under applied pressure (adhesive strength) and solid-like property to resist applied stress once the inter-surface contact has been formed (cohesive strength) (Grillet *et al.*, 2012). Therefore, the tack property of the sample is dependent on the ratio of its viscous and elastic components and this can be monitored using the values of tan δ at the LVE range. A gel exhibits stickiness only when the tan δ is in a medium range. Based on information from AST (Figure 4.9), PhSt rich gels shows high tan δ (favors liquid character) whereas HEC rich samples shows low tan δ (promotes solid character). Thus, an optimum adhesion is achieved by the combination of both polysaccharides as in the case of H60. As the content of HEC exceeds 60 wt.%, the minimum force drops significantly. These gels have very high G' values and their poor adhesive property is an implication of the materials inability to initially deform to make good contact as well as dissipate energy via viscous contribution.

A frequency sweep study is very useful in determining the response of the polymer chains in the gel to an external force with respect to time scale. The frequency dependence of the elastic and viscous moduli are presented in Figure 4.11. Similar trend in the evolution of the moduli with increasing frequency can be seen in all the samples. At low frequency, the G' values reaches a plateau typically known as equilibrium modulus of the gel. This plateau behavior can only be attributed to chemical crosslinks in the gel because the lifetime of physical entanglements is shorter than the rate of deformation, thus they cannot contribute to a sustained elastic energy (Grillet *et al.*, 2012). At higher frequencies,

polymer chains do not have sufficient time to rearrange. The longer lifetime of physical entanglements compared to oscillation frequency enables the solvent and polymer entanglements to contribute to the elastic and viscous moduli (Patel *et al.*, 1992). In addition, the frequency sweep curves provide information on the relationship between G' and G" values with increasing amount of HEC in the gels. As it is evident in Figure 4.11 (a), for H20 the G' curve is only slightly above G" throughout the oscillation frequencies. For H30 (Figure 4.11(b)), the separation between G' and G" is seen to be better than H20. Following similar trend, H50 and H70 (Figure 4.11 (c) and (d)), exhibit G' curves much higher and well separated from G" curves. These observation again consolidates the fact that at H20 and H30, the solid and liquid characters of the gels are almost equally balanced. However, from H50 onwards, the solid character clearly prevails than its liquid counterpart.

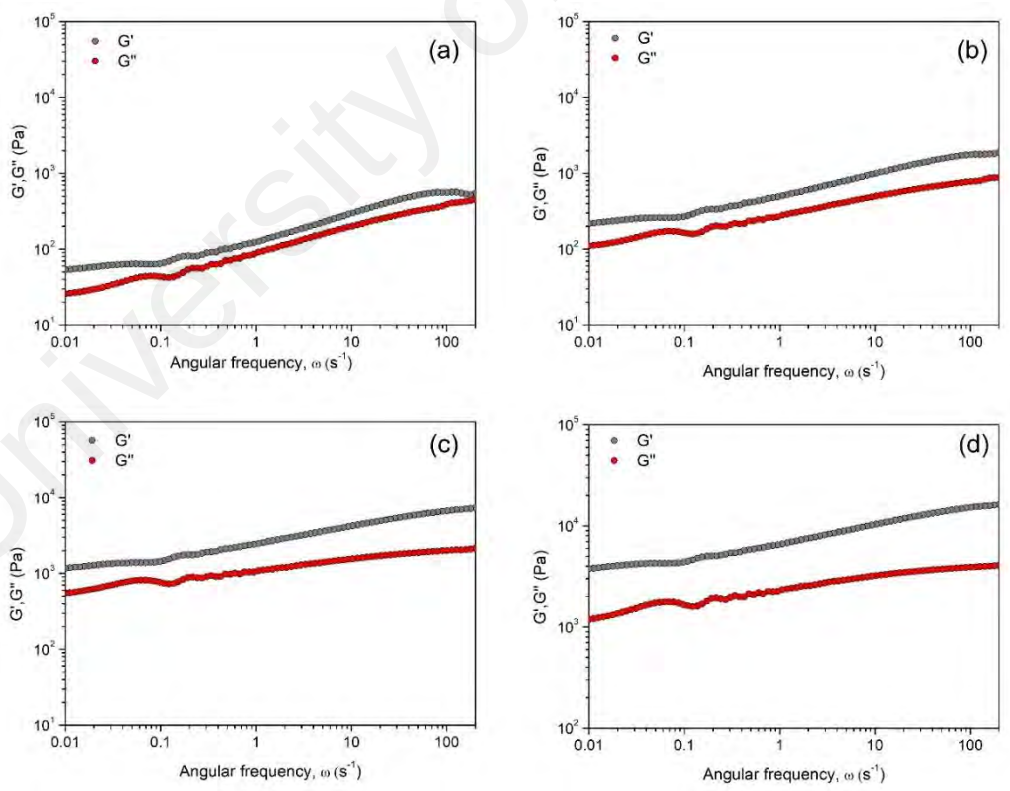

Figure 4.11: Frequency sweep curves of (a) H20, (b) H30, (c) H50 and (d) H70

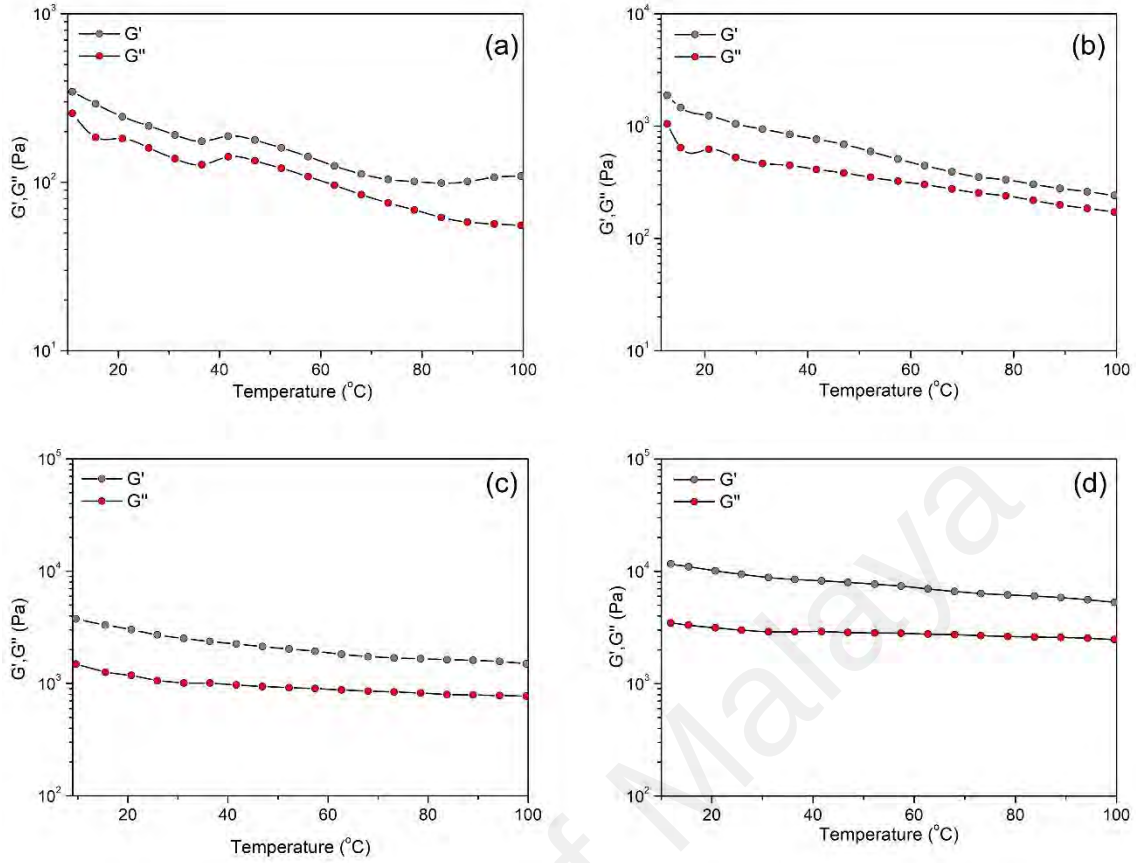

Figure 4.12: Temperature dependent moduli of (a) H20, (b) H30, (c) H50 and (d) H70

Figure 4.12 depicts the dynamics of the G' and G" values as a function of temperature. For all the samples, the G' values were higher than G" and there were no crossover between the moduli throughout the entire temperature spectrum. The presence of a crossover of the moduli with G" exceeding G' values indicates that the stiffness of the material has been compromised upon heating which resulted in the flowing of the gel. The absence of such crossover at all temperature verifies that the gel structure were not disrupted even at post ambient temperature and is an important aspect for the practical application of the gels in solar cells. The dependence of the moduli on temperature is observed to be varied with different contents of HEC in the gel. In samples with lower HEC, i.e. H20 and H30, the G' values showed a more evident decrease in value as

temperature increases. However, in HEC rich samples, the moduli values are less affected by the increase in temperature. Both the trends are related to the stiffness of the gel. With higher HEC content, the gel is stiffer and less affected by the increment in temperature. Similar to frequency dependent studies, the temperature dependent moduli also show better separation between G' and G" curves with increasing HEC content. Thus, it can be concluded that the addition of HEC into the blend improves thermal stability of the gels in general.

4.2.1.2 FTIR analysis

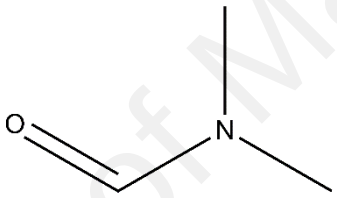

Figure 4.13: Structure of DMF

The possible chemical interactions between polymers and solvent were studied via FTIR analysis. Owing to the fact that a 1:4 polymer to solvent ratio was used in the electrolyte preparation, the peaks attributed to PhSt and HEC are mostly overshadowed by the intense peaks of the solvent, DMF. Figure 4.14 shows the peaks for C=O stretch, N-(CH_3) deformation and CH_3 rocking mode of DMF molecules (Figure 4.13) are clearly observed at 1663 cm^{-1}, 1384 cm^{-1} and 1093 cm^{-1} respectively. The strongest absorption peak in the samples is the one attributed to the most polar group present; C=O stretch of DMF. This band exhibited a downshift from 1663 cm^{-1} in native DMF to 1648 cm^{-1} in the polymer gels.

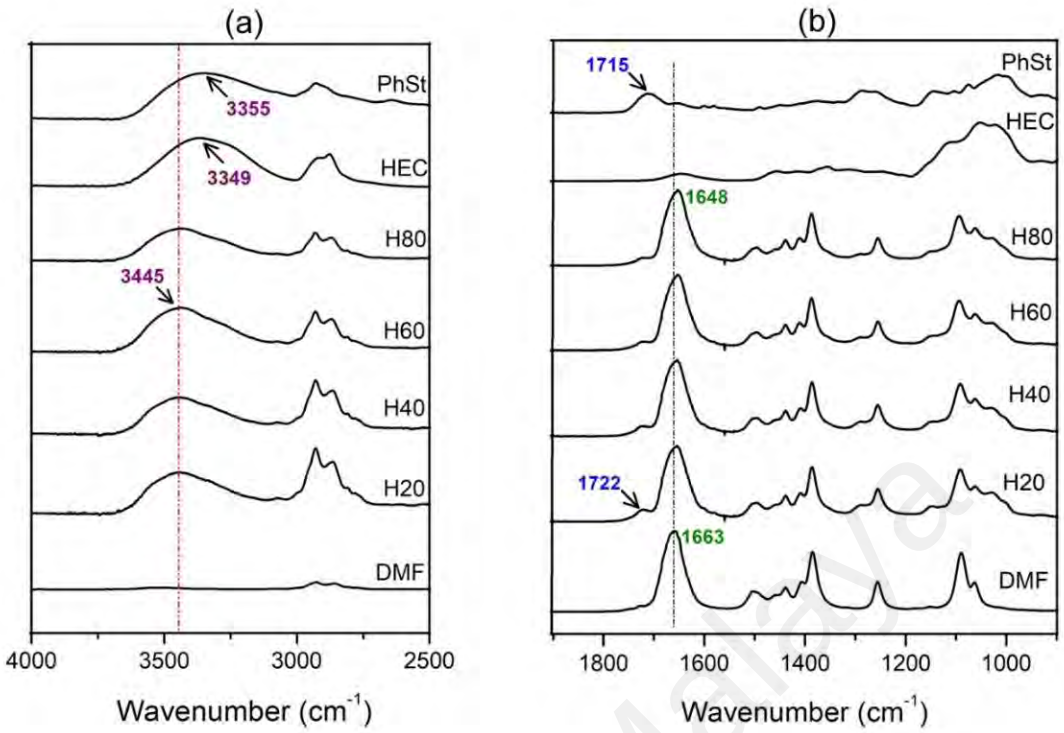

Figure 4.14: FTIR spectra of PhSt-HEC-DMF gels

The shift to a lower frequency indicates hydrogen bonding interaction between carbonyls in DMF and hydroxyls of the polymers. Being a polar aprotic solvent, DMF does not have an acidic hydrogens and hence, incapable of forming hydrogen bonds with themselves. This enables the oxygen and nitrogen atoms to be available with polymer chains. As shown in Figure 4.14, the position of hydroxyl absorption peaks of PhSt and HEC are at 3355 cm^{-1} and 3349 cm^{-1} respectively. However, in the polymer gels, this values significantly shifts to a much higher wavenumber of 3445 cm^{-1}. The upward shift of hydroxyls in polysaccharides can be perceived as an impact of lower extent of inter-chain hydrogen bonding. The presence of DMF molecules throughout the gel matrix disfavors polymer-polymer interaction and instead fosters polymer-solvent interaction.

4.2.1.3 Crystallinity

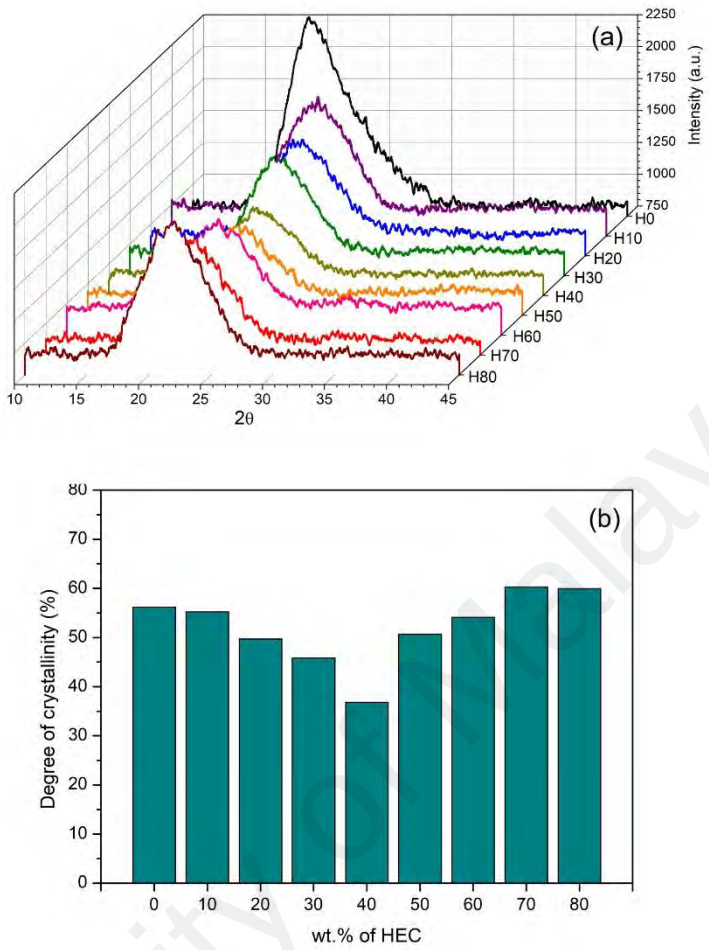

Figure 4.15: XRD diffractograms of HEC-PhSt-DMF gels

Figure 4.15 presents the XRD diffractograms of PhSt-HEC gels. A continuous decline in the intensity of the peaks centered at around 22° with addition of HEC up to 40 % is clearly observed. Similar trend is also observed in the values of degree of crystallinity. The decline in crystallinity is deduced to be the impact of inter-polymer hydrogen bonding between HEC and PhSt. The interaction between both the polymers restricts the molecular chain segment movements and restrain the crystallization process of HEC and PhSt individually (Zhong *et al.*, 2011). Similar observations have been reported in different polysaccharides blends such as starch-chitosan systems (Liu *et al.*, 2013; Xu *et al.*, 2005). However, beyond 40 wt.% HEC, the crystallinity increases again and this maybe an implication of the higher amount of cellulose chains which have the tendency

to arrange in a more rigid fashion. In fact, this was also corroborated by the increment of the storage modulus of these gels as discussed in Figure 4.7. The increasing stiffness of the gels with more than 40 wt.% HEC is in correlation with the increment of degree of crystallinity of the gels, both phenomena attributed to the rigid arrangement of cellulose chains.

4.2.1.4 Ionic conductivity

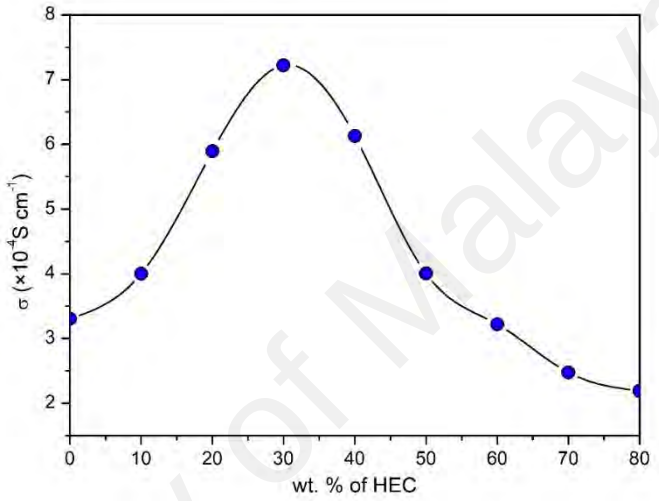

Figure 4.16: Conductivity of HEC-PhSt-DMF gels at 30°C

Figure 4.16 reveals that the ionic conductivity, σ of the gels increases with increasing amount of HEC gradually attaining an optimum value with 30 wt.% HEC. The ionic conductivity in this system is governed by two factors namely crystallinity and stiffness of the gels. Conductivity of polymer electrolytes is enhanced within a system with higher amorphous phase, in which the polymer chains could maneuver to create dynamic, disarranged domain that facilitates ions migration. On the other hand, with increasing stiffness of the gels, the movement of electrolytic solution within the polymer matrix is expected to be restricted hence curtailing overall conductivity. Amplitude sweep studies suggests a continuous upward trend in rigidity of the gels from H0 to H80. However, from XRD analysis, it is evident that up to 40 wt.%, addition of HEC helps to diminish crystallinity. Therefore, the σ values from H0 to H40 is the product of these two

antagonistic effects. The highest σ is attained in H30 which indicates that this gel composition contains a good share of both amorphous and less rigid environment. Whereas in H40, the decline in crystallinity could not compensate for the detrimental effects of the gel rigidity, leading to a drop in σ. The monotonous decline in σ from H50 onwards is the combined result of high crystallinity and gel rigidity.

4.2.2 Fabrication of quasi-solid electrolyte based on PhSt-HEC blends

Rheological analysis indicates that the gels possess good mechanical stability with inclusion of 20 wt.% HEC onwards. From tack test, it can be concluded that gels with HEC more than 60 wt.% does not manifest good adhesive property. The detrimental effect of addition of HEC beyond 60 wt.% is also supported by XRD and EIS analysis in which samples H70 onwards exhibited high crystallinity and poor ionic conductivity.

Figure 4.17: Photograph of HEC-PhSt-5 wt.% TPAI gels

Thus for the next phase of the study which involves QSDSSC fabrication, samples H20-H60 were chosen and fixed amount of TPAI and I_2 were added (Figure 4.17). The impact of the rheological characters of these gels on the electrochemical and photovoltaic properties were discussed in detail in this section.

4.2.2.1 Electrochemical property

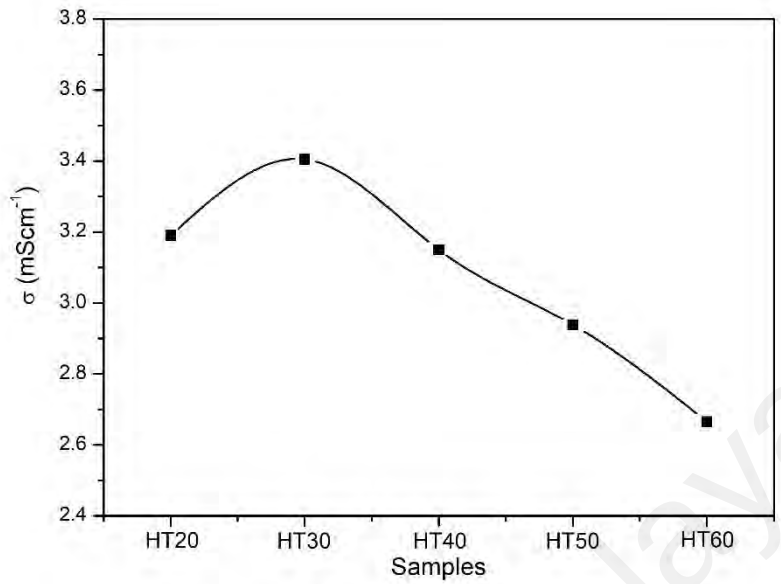

Figure 4.18: Ionic conductivity of HEC-PhSt quasi-solid electrolytes at 30°C

As shown in Figure 4.18, the conductivity of the polymer-salt series shows similar variation as the blank series (Figure 4.16) where σ increases up to 30 wt.% of HEC and drops beyond that (Figure 4.18). In order to further understand ion transfer in the electrolytes, temperature dependent conductivity studies were performed. The electrolytes exhibit Arrhenius behavior at elevated temperature and therefore its activation energy (E_a) was calculated from the slope of the Arrhenius plots (Figure 4.19 (a)). As highlighted in Figure 4.19 (b), the E_a decreased slightly with addition of HEC up to 40 wt.% and this suggests improved ion transition in gels with these compositions. The increment in E_a values above HT40 can be attributed to higher crystallinity and solid-like character of the gels which retards ionic motion. In general, the activation energy for all the samples only varies in a narrow range. Gel structure of the electrolytes occurs by the confinement of the electrolytic solution within the polymer chain backbone and the E_a value is mainly governed by the electrolytic solution (Dissanayake *et al.*, 2014; Petrowsky

& Frech, 2008). Since the composition of the electrolytic solution has been kept constant in this study, thus the E_a values do not show any drastic changes.

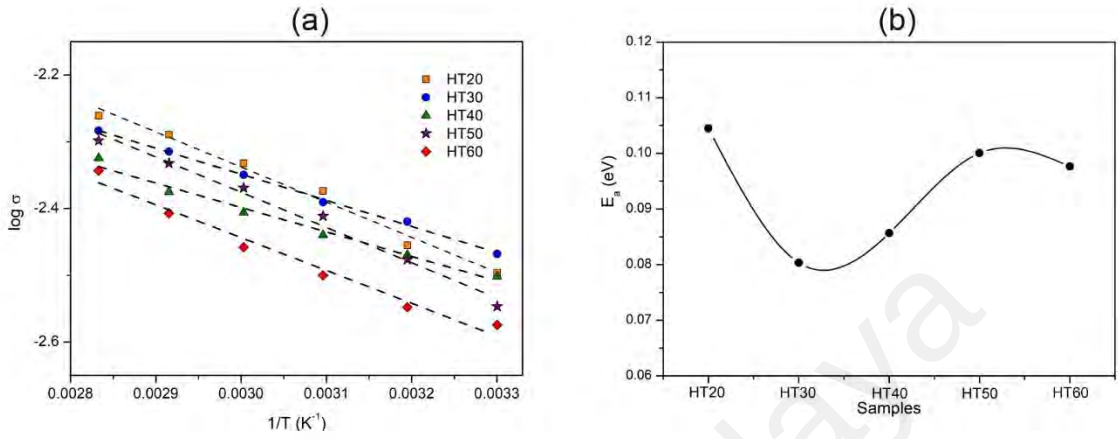

Figure 4.19: (a) Arrhenius plots and (b) activation energies of HEC-PhSt quasi-solid electrolytes

4.2.2.2 Photovoltaic performance

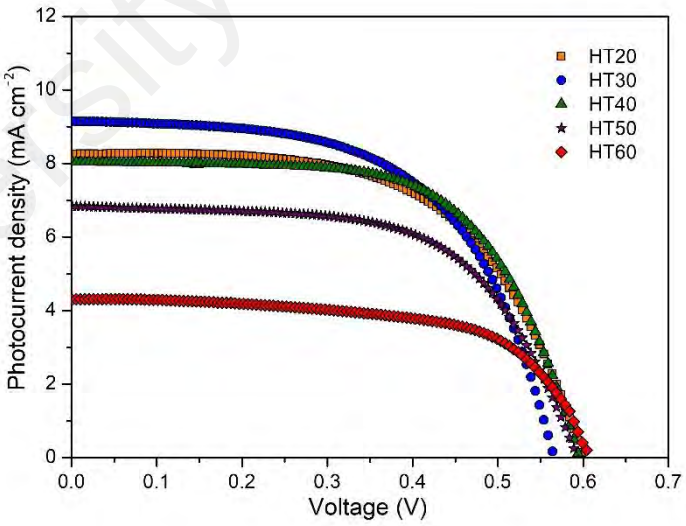

Figure 4.20: J-V curves of HEC-PhSt quasi-solid electrolytes

Figure 4.20 shows the J-V curves of the QSDSSC fabricated using electrolytes HT20 to HT60. The corresponding J-V parameters of these cells are given in Table 4.2. The

energy conversion efficiency, η increased with inclusion of HEC, attaining the highest value of 3.02 % for HT30, followed by a decline with subsequent HEC addition.

Table 4.2: J-V parameters of HEC-PhSt quasi-solid electrolytes

Sample	σ ($\times 10^{-3}$ S cm^{-1})	η (%)	J_{SC} (mA cm^{-2})	V_{OC} (V)	FF
HT20	3.19	2.85	8.56	0.60	0.56
HT30	3.41	3.02	9.02	0.57	0.60
HT40	3.15	2.88	8.09	0.59	0.60
HT50	2.94	2.43	6.47	0.60	0.62
HT60	2.66	1.82	4.37	0.59	0.70

The trend in efficiencies is mainly in accordance with the current density, J_{SC} values which also tallies with the ionic conductivities of the electrolytes. Despite lower σ, HT40 showed similar efficiency compared to HT20. This finding is associated with the adhesive nature of the gel (Figure 4.10) which improves electrode-electrolyte contact and assists in penetration of the electrolytes into the mesoporous TiO_2 layer. The fill factor values increase with higher amount of HEC in the gel composition. This is seen to be a reflection of the improved mechanical stability of the gel which positively favors the fill factor of the QSDSSC.

4.2.2.3 Impedance study of DSSC

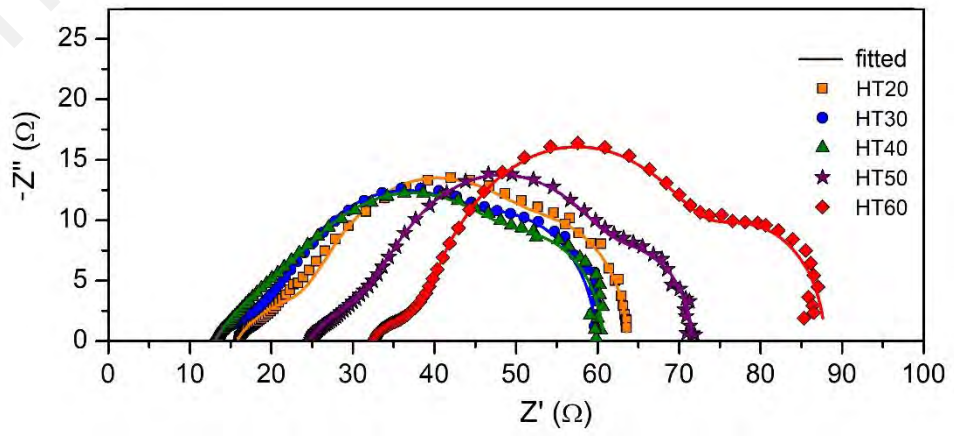

Figure 4.21: Nyquist plots of QSDSSC fabricated using PhSt-HEC based electrolytes

For a detailed comprehension of the effect of gel electrolytes on interfacial charge transport, EIS was performed. As shown in Figure 4.21, the Nyquist plots of all the DSSC exhibit three semicircles. The first semicircle which appears at high frequency range (100 kHz-100 Hz) can be imputed to the impedance at the Pt counter electrode (CE)/electrolyte interface (R_{PT}). The second semicircle appearing at mid-range frequency (100 Hz-1 Hz) ascribes to impedance at TiO_2 electrode /electrolyte interface (R_{CT}). The third semicircle at low frequency range (1-0.01 Hz) is attributed to impedance due to diffusion process in the electrolyte (R_D) (Wang *et al.*, 2005b). The depiction of these three semicircles with the corresponding resistances is illustrated in Appendix F.

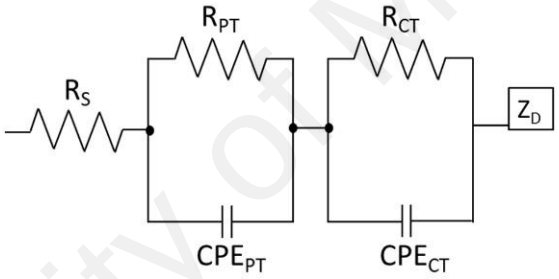

Figure 4.22: Equivalent circuit representation of QSDSSC

To derive impedance parameters of the DSSC, the Nyquist plots were fitted to the equivalent circuit in Figure 4.22 which quantifies as the following equation (Adachi *et al.*, 2006; Fabregat-Santiago *et al.*, 2011; Sarker *et al.*, 2014):

$$Z_{DSSC}=R_S+\frac{R_{PT}}{1+(j\omega)^{n_{PT}} R_{PT} CPE_{PT}}+\frac{R_{CT}}{1+(j\omega)^{n_{CT}} R_{CT} CPE_{CT}}+R_D\sqrt{\frac{D_{I_3^-}/\delta^2}{j\omega}}\tanh\sqrt{\frac{j\omega}{D_{I_3^-}/\delta^2}} \quad (4.1)$$

where R_S is the series resistance, n_{PT} is the constant phase element (CPE) indices at the counter electrode/electrolyte and n_{CT} corresponds to the photoanode/electrolyte interfaces. R_D is attributed to the resistance arising from Warburg diffusion and δ is the effective diffusion length.

Table 4.3: Equivalent circuit parameters of HEC-PhSt quasi-solid electrolytes

Sample	R_S (Ω)	R_{PT} (Ω)	R_{CT} (Ω)	R_D (Ω)	$D_{I_3^-}$ ($\times 10^{-7}$ $cm^2\ s^{-1}$)	σ ($\times 10^{-3}$ $S\ cm^{-1}$)
HT20	15.74	10.21	20.84	19.48	6.03×10^{-7}	3.19
HT30	13.43	9.16	22.59	15.72	7.23×10^{-7}	3.41
HT40	13.12	9.21	24.45	12.49	6.73×10^{-7}	3.15
HT50	24.74	8.78	27.15	16.18	4.56×10^{-7}	2.94
HT60	32.37	7.24	30.83	17.92	2.56×10^{-7}	2.66

The equivalent circuit parameters used to fit the impedance curves are listed in Table 4.3. As the Nyquist plots did not begin from 0 at real axis, the x-intercept values corresponds to the series resistance, R_S of the cell. The R_S values were rather invariable from HT20 to HT40 but drastically rose from HT50 onwards. This may be an implication of the low σ. The variation in R_{PT} values on the other hand shows slight decrease. In a typical DSSC, the reduction of triiodide ion to iodide ion takes place at the CE/electrolyte interface. The reduced R_{PT} value with increasing HEC content thus can be a result of better contact (due to better adhesion) between the electrolyte and CE which facilitates electron transfer. Inclusion of HEC was found to increase the charge recombination resistance, R_{CT}. The recombination of photoinjected electron from the semiconductor with the dye or electrolyte is more effectively suppressed by electrolytes with higher HEC content. This behavior is again attributed to the adhesive nature of these electrolytes (Figure 4.10). Similar results have been observed by Wang et al. who studied QSDSSC based on solidification of electrolyte with imidazole polymers. They reported that electrolytes with higher polymer content showed elevated R_{CT} values due to restricted recombination reaction (Wang *et al.*, 2008). The parameters related to diffusion of redox species in the electrolyte were in close dependence to ionic conductivity of the electrolytes. As expected, the drop in σ for electrolytes containing high HEC amounts resulted in an adverse effect on the triiodide diffusion demonstrated by both high R_D and

low I_3^- diffusion coefficients. The impeded motion of the ions justifies the drop in J_{SC} values from HT40 onwards.

4.3 Effect of salt composition

The choice of salt in the electrolyte composition is one of the key factors in determining the performance of electrolytes in DSSC. The effect of the type and composition of cationic species in the electrolyte has been extensively discussed in literature. In particular, the cationic species were found to play significant role in influencing electron injection efficiency, dye regeneration rate, effective diffusion coefficient and the properties of interfacial electron transfer. Therefore, the next part of the study highlights the impact of cation size on the rheological and electrochemical properties of the GPE.

4.3.1 Rheological properties

The amplitude sweep curves for PhSt-HEC-DMF gels with different amount of LiI and TPAI are attached in Appendix G and H. As depicted in Figure 4.23(a), increasing amount of LiI content from 0 to 15 wt.% resulted in an increment in the G' value. The enhanced rigidity of the gels with the addition of LiI is believed to be the consequence of active interaction between the Li^+ ions and the oxygen atoms present throughout the backbone of the polymers. The cation-polymer complexation enables a more compact packing of the polymer matrix framework which give rise to the solid character of the gels. This claim is further supported by the steady values of the critical strain of the gels which shows that the gel strength was not affected significantly upon addition of LiI from 0 to 15 wt.% . Beyond 15 wt.%, the G' value and critical strain shows a slight dip. The high concentration of salt may have triggered formation of ion aggregates, thus lowering the possibility of ion-polymer interaction.

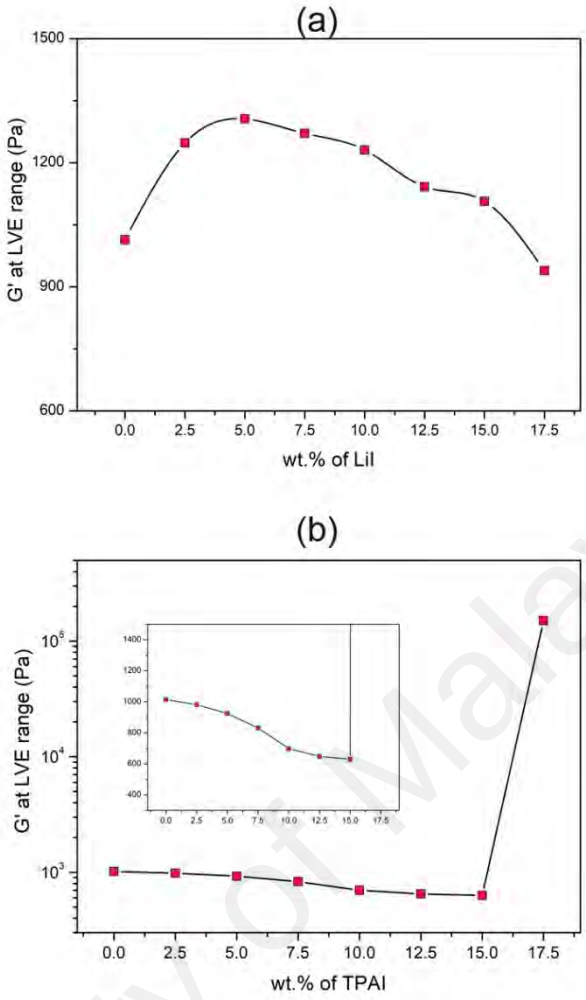

Figure 4.23: Storage modulus at LVE range of PhSt-HEC-DMF gels with (a) LiI and (b) TPAI

Figure 4.23(b) shows the variation in G' values for increasing amount of TPAI. It is very interesting to note that the effect of TPAI addition on gel rigidity was the opposite of the effect induced by LiI. Similar observation has been reported by Dintcheva et al. who studied rheological behaviour of PAN containing tetrahexyl ammonium iodide (THAI) and magnesium iodide (MgI_2) salts (Dintcheva *et al.*, 2013). They observed that PAN-EC-PC gel became more structured and rheologically stable by MgI_2 loading. Increasing amount of TPAI from 0 to 15 wt.% resulted in a significant drop of G' values and the justification for this observation relies on the nature of the cation. Lithium ions

are relatively smaller in size and thus have the ability to extensively complex with the electronegative atoms of the polymer chains (Figure 4.24(a)). Unlike the tiny lithium ions, TPA^+ is a bulky cation with limited mobility. The greater steric hindrance imposed by TPA^+ disables it from distributing itself extensively between the polymer chains (Figure 4.24(b)). In fact, the presence of these bulky cations amidst the polymer matrix is expected to prevent polymer chain entanglements. Thus, as the amount of TPA^+ is increased the rigidity of the gels continue to decline. However, upon loading of 17.5 wt.% of TPAI, the G' value at LVE range suddenly jumps to an elevated value (two order of magnitude higher). This effect is due to recrystallization of the TPAI salt and the presence of the TPAI crystals in the gels gave rise to the extremely high solid character which was translated as high G' value.

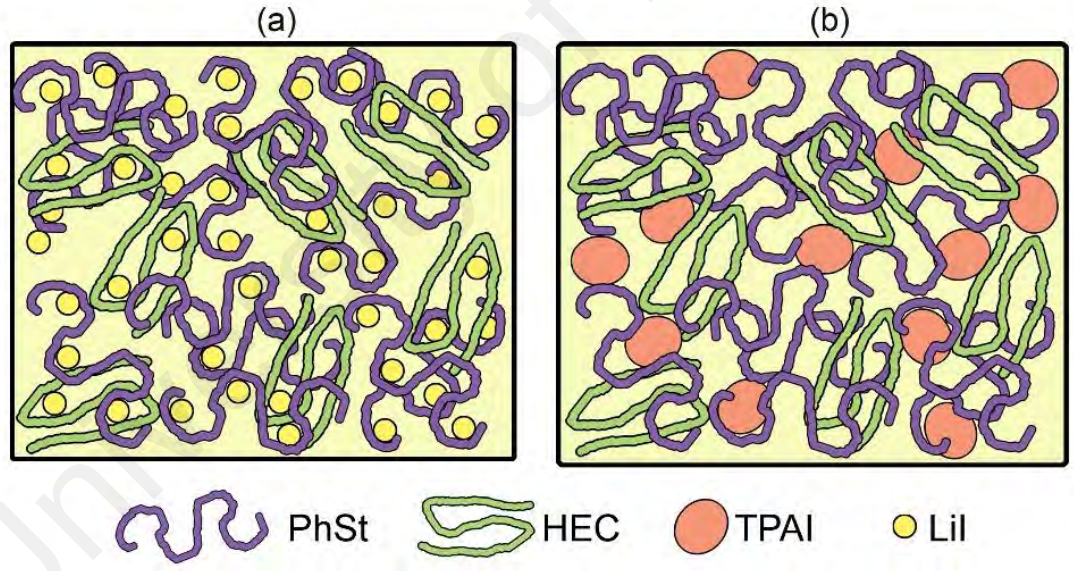

Figure 4.24: Graphical depiction of (a) Li^+ and (b) TPA^+ distribution in gel

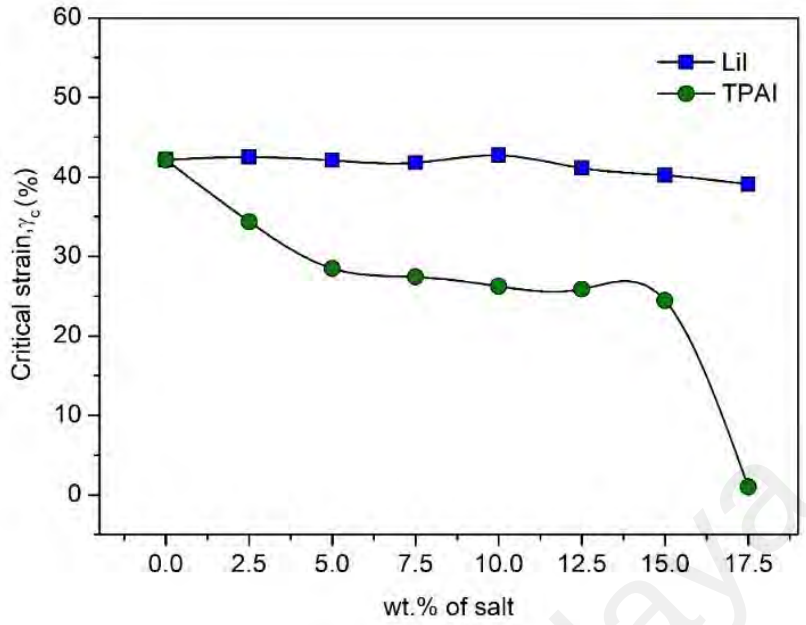

Figure 4.25: Critical strain values of PhSt-HEC-DMF with LiI and TPAI gels

As for the critical strain values which is depicted in Figure 4.25, a drastic drop was observed with initial introduction of TPAI (0 to 5.0 wt.%). Between 5.0 to 15.0 wt.%, a plateau was observed, signifying that despite the decreasing solid character, the strength of the gels remain unaffected at these concentrations. A sharp drop in critical strain value upon inclusion of 17.5 wt.% of TPAI indicates that the homogeneity of the gel is highly disrupted. There is a high possibility of salt recrystallization at this concentration which was also evident based on the unexpected high value of G' (Figure 4.23(b)).

As depicted in Figure 4.26 (a), introduction of low quantity of LiI (from 0 to 5 wt.%) impacted in improved adhesiveness signified by the higher force minimum values. The increment in integral area under the curve verifies that this is due to higher cohesive and adhesive force. Beyond 5.0 wt.% of LiI, both minimum force and integral area values begin to drop. At high LiI concentration, good adhesive property could not be imparted as effectively as at low concentration.

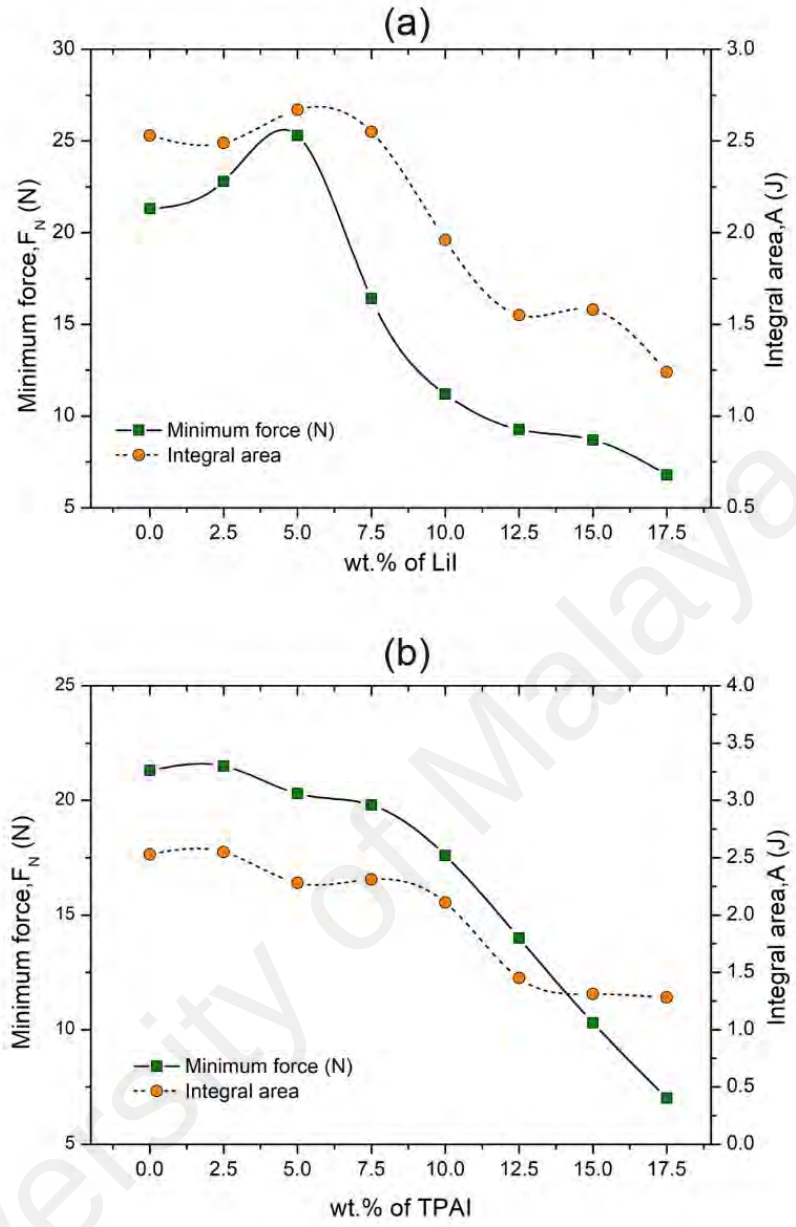

Figure 4.26: Tack test parameters of PhSt-HEC-DMF gels with (a) LiI and (b) TPAI

On the other hand, addition of TPAI into the polymer gels resulted in a continuous downward trend in both the minimum force and integral area values (Figure 4.26 (b)). The decline in adhesiveness was particularly obvious with addition of TPAI above 10 wt.%. One of the contributing factor for this can be the downward trend in the storage modulus of these gels (Figure 4.23 (b)). As discussed in section 4.2.1.1, adhesiveness is the product of balanced solid and liquid character of the gels. Thus, when the solid

character continuously decline with addition of TPAI, this influences tan δ values which in turn affects tackiness.

4.3.2 FTIR analysis

Figure 4.27 depicts the trend in FTIR peaks for PhSt-HEC-DMF based gels with varying amounts of LiI and TPAI respectively. Significant peak shifts could not be observed in all the electrolytes. Since the electrolytes consist of multiple components, the FTIR peaks observed are often a depiction of various overlapping peaks and thus, simple peak shift observations may not be useful here. In such case, FTIR deconvolutions can be performed to reveal the presence of hidden peaks which correspond to certain molecular interactions.

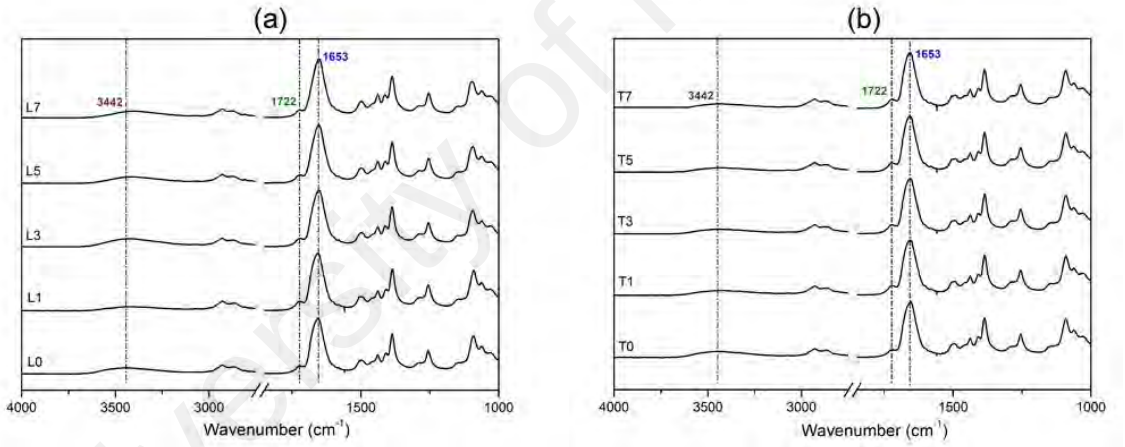

Figure 4.27: FTIR spectra of PhSt-HEC-DMF gels with (a) LiI and (b) TPAI

In this work, the peaks of L3 and T3 which are taken as representative of each electrolyte series, have been deconvoluted and analyzed. The chemical interactions within the electrolyte matrix were identified by analyzing the FTIR spectra in three main sections, namely the ether stretching region (950-1150 cm^{-1}), amide stretching region (1200-1550 cm^{-1}) and carbonyl stretching region (1550-1750 cm^{-1}) which were found to be particularly subjected to variations.

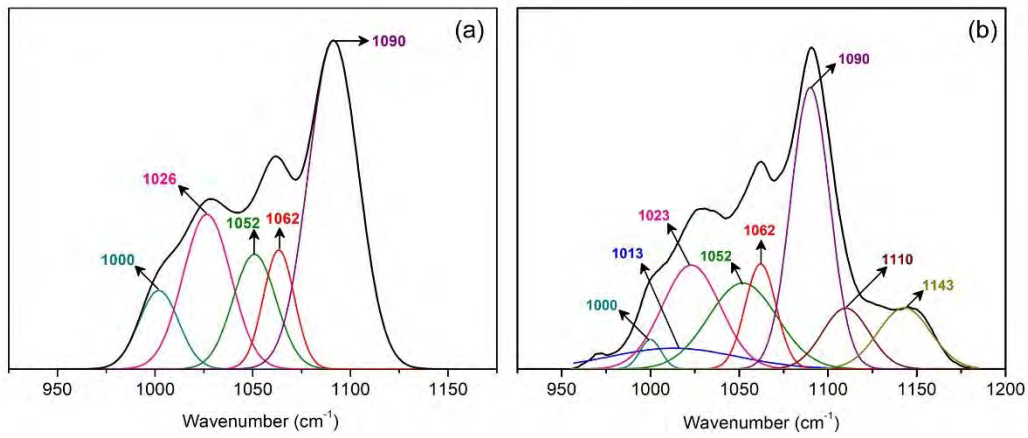

Figure 4.28: Deconvoluted FTIR spectra of PhSt-HEC-DMF with (a) LiI and (b) TPAI gels in ether region

Within the range of 950-1150 cm^{-1} (Figure 4.28), the contribution of the CH_3 rocking mode of DMF at 1062 cm^{-1} and 1090 cm^{-1} are predominant in both L3 and T3 (Zhang *et al.*, 2014a). The peaks at 1052 cm^{-1} and 1026 cm^{-1} which attribute to the ether stretching in HEC and PhSt were also evident. In T3, additional peaks at 1000 cm^{-1}, 1013 cm^{-1}, 1110 cm^{-1} and 1143 cm^{-1} which correspond to interactions between ions and C-O groups were observed whereas in L3 only one additional peak at 1000 cm^{-1} was present.

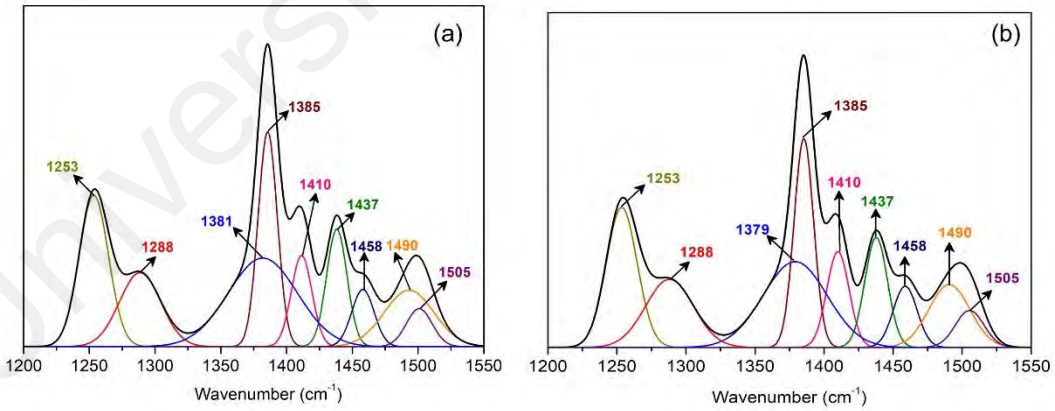

Figure 4.29: Deconvoluted FTIR spectra of PhSt-HEC-DMF with (a) LiI and (b) TPAI gels in amide region

In the amide stretching region (Figure 4.29), the peaks of both L3 and T3 resolve into nine individual peaks, most of which originate from DMF. The C-N stretching mode at 1505 cm^{-1}, CH_3 asymmetric deformation mode at 1437 cm^{-1}, CH_3 umbrella mode at 1410

cm^{-1}, N-C-H bending mode at 1385 cm^{-1} and C-N asymmetric stretching at 1253 cm^{-1} can be clearly spotted (Jacob & Arof, 2000; Ståkhandske *et al.*, 1997). The peak 1288 cm^{-1}, on the other hand, corresponds to esteric C-O stretch.

Besides this, three additional peaks were observed at 1379 cm^{-1}, 1458 cm^{-1} and 1490 cm^{-1} which are presumed to be downshifted peaks of N-C-H bending mode and C-N stretching respectively. The coordination of cations to the lone pair of the nitrogen accounts for the manifestation of these peaks at lower wavenumber (Bar & Basak, 2014).

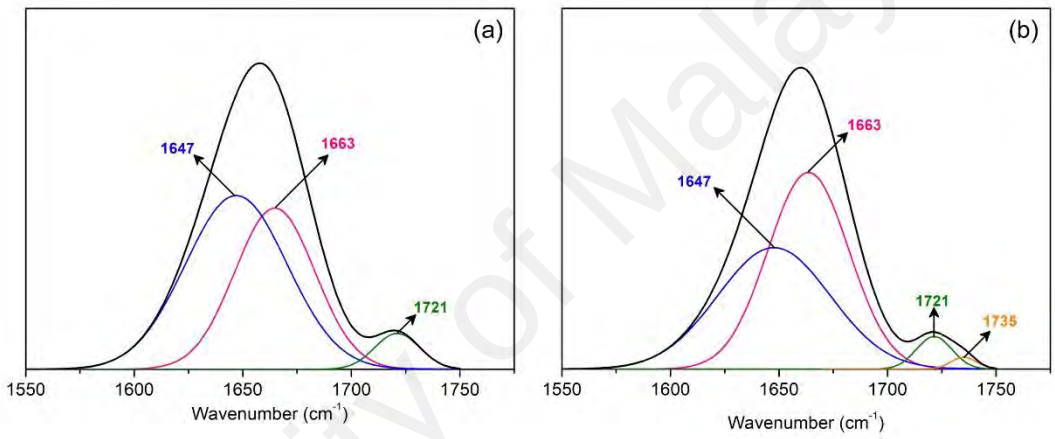

Figure 4.30: Deconvoluted FTIR spectra of PhSt-HEC-DMF with (a) LiI and (b) TPAI gels in carbonyl region

As for the range of wavenumber between 1550-1750 cm^{-1} (Figure 4.30), the region is overshadowed by two main peaks at 1663 cm^{-1} and 1721 cm^{-1} attributed to C=O stretching in DMF and PhSt. Additional peak at 1647 cm^{-1} presumably due to coordination of cations and the carbonyl group was also present in both L3 and T3. Interestingly, a tiny peak at 1735 cm^{-1} was existent in T3. As this peak appears at a higher wavenumber than the original carbonyl peak which is at 1721 cm^{-1}, the origin of this peak is speculated to be an interaction between the carbonyl in PhSt and anions (Bar & Basak, 2014).

4.3.3 Crystallinity

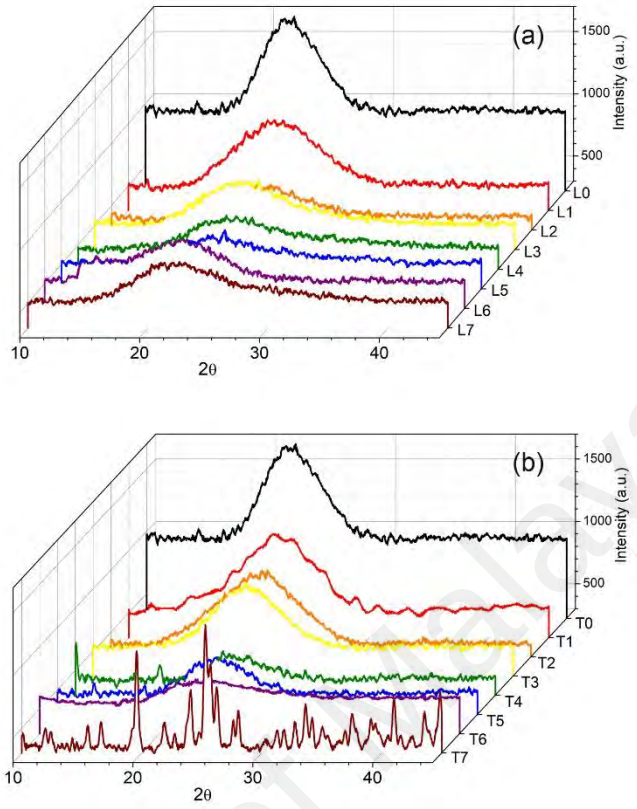

Figure 4.31: XRD diffractograms of PhSt-HEC-DMF gels with (a) LiI and (b) TPAI

Incorporation of small amount of LiI and TPAI resulted in drastic reduction of crystallinity of the polymer gels (Figure 4.31(a) and Figure 4.31(b)). Introduction of cations and anions into the polymer matrix disrupts the structural orderliness of the polymer chain arrangement. As shown in Figure 4.32, the increment of LiI content induced a gradual decline in degree of crystallinity up to 12.5 wt% of salt. This trend concurs with the observations in the rheological analysis which connoted active complexation between Li^+ and the oxygen in polymer backbone. The interaction between ion and polymer occupies the electronegative oxygen atoms throughout the polymer backbone. This in turn deters polymer-polymer H bonding which is often the main source of the crystallization in polysaccharides.

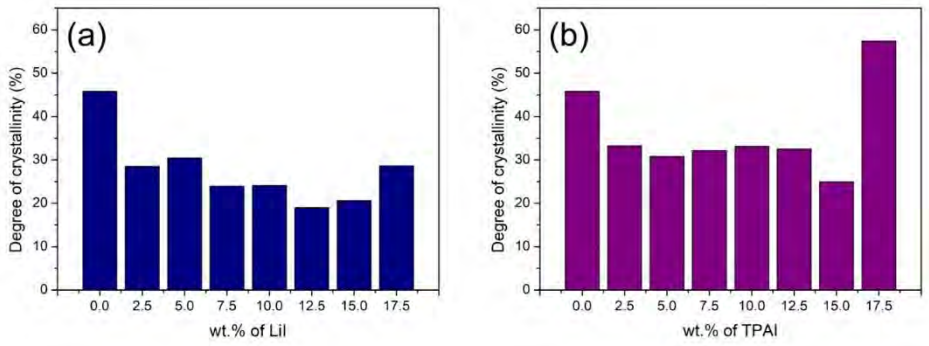

Figure 4.32: Degree of crystallinity of PhSt-HEC-DMF with (a) LiI and (b) TPAI gels

The initial incorporation of TPAI salt into the polymer gel resulted in drastic reduction of crystallinity. However from 2.5 wt.% to 12.5 wt.% of TPAI, the degree of crystallinity remained within similar values. As the bulky TPAI cations is more likely to be standard within the polymer matrix, it will not be as effective as the Li^+ ions in forming ion-polymer complexation. Hence, the addition of TPAI beyond a certain amount results in positive effects towards the crystallinity of the polymer gels. Addition of the salt beyond 12.5 wt.% causes increased crystallinity in both salt systems. For LiI series, the excessive amount of ions is expected to form ion aggregates, thus reducing the possibility of ion-polymer interaction. In the case of TPAI series, gels with salt concentration of 17.5 wt.% manifest intense sharp peaks in their XRD diffractograms which coincides with the peaks of pristine TPAI (Appendix J). This peaks establishes the recrystallizations of TPAI in those gels which was also reflected by the sudden increase in degree of crystallization at 17.5 wt.% TPAI.

4.3.4 Electrochemical properties

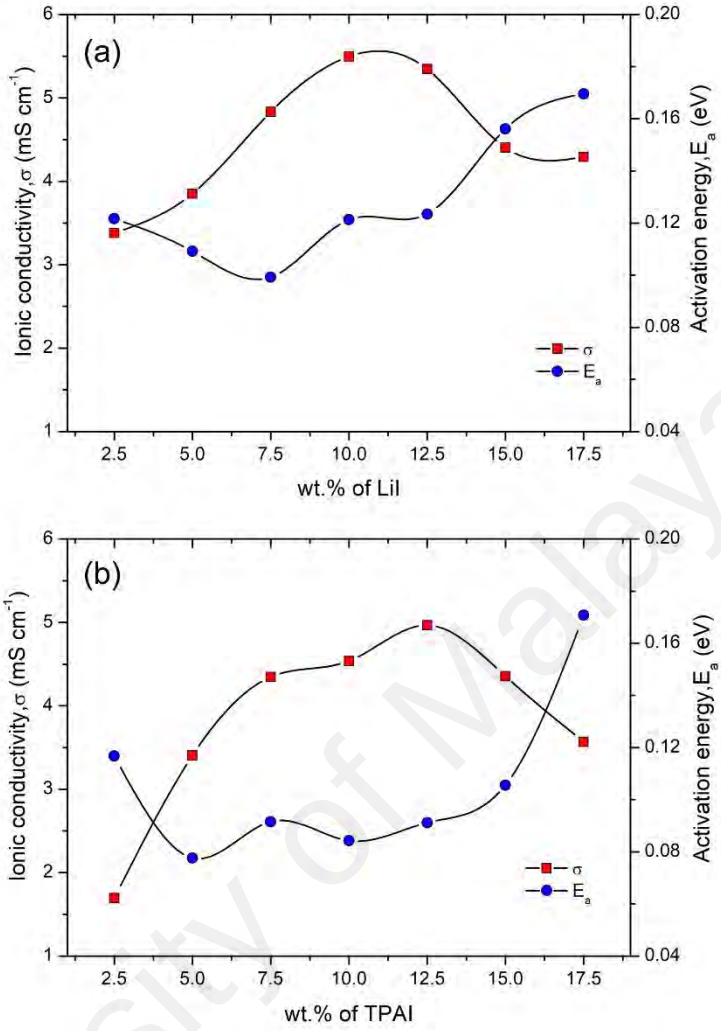

Figure 4.33: Ionic conductivity (at 30°C) and activation energy of PhSt-HEC-DMF with (a) LiI and (b) TPAI gels

Figure 4.33(a) and (b) portray the variation of ionic conductivities, σ as a function of LiI and TPAI content respectively. In the case of both the salts, the ionic conductivities increases with higher amount of salt, eventually reaching an optimum value and then drops. This pattern is typically found in most polymer electrolytes. In the LiI series, the highest σ of 5.50×10^{-3} S cm^{-1} is attained with inclusion of 10 wt.% of LiI whereas in the TPAI series, a maximum conductivity of 4.97×10^{-3} S cm^{-1} is achieved by 12.5 wt.% of TPAI. The gradual increase in σ up to an optimum salt composition is attributed to the increase in number of mobile charge carriers in the electrolytes. When the amount of salt

exceeds this optimum salt content, the excessive presence of ions tend to create steric crowding which may also result in re-association or polyionization (Echeverri *et al.*, 2012).

Unlike the discussion of the effect of HEC blend on the σ, the effect of salt composition on σ is found to be less dependent on factors affecting the polymeric structure such as crystallinity and stiffness of the gels. This can be viewed under two perspectives. Firstly, the difference in the magnitude of the storage moduli and the variation in crystallinity of the gels with addition of salt is not as prominent as observed in different PhSt-HEC compositions. Secondly, the ion-conduction in quasi-solid electrolyte, as it is the case in the current work, occurs via the local solvent channels built around the polymer gel network. Thus, the ion transfer is primarily influenced by the hopping of these ions through the solvent channels rather than segmental mobility of polymer chains. Therefore, the domination of type and amount of ions in electrolytic solution is more superior in affecting σ as compared to arrangement of polymer network.

The dominant ion conduction mechanism of polymer electrolytes can be identified by monitoring the temperature dependent conductivity behavior of the samples. If the temperature dependence of ionic conductivity obeys the Vogel-Tammah-Fulcher (VTF) equation, then ion migration is strongly governed by segmental motion of the polymer (Ratner & Shriver, 1988). On the other hand, if the temperature dependent conductivity plot complies with Arrhenian behavior, then ion transport is attributed to ion hopping via the solvent channels. PhSt-HEC based gels with varying amounts of TPAI and LiI demonstrated conformation to Arrhenius behavior. Activation energies were calculated based on the fitting of the data to Arrhenius equation (Appendix K). As evident in Figure 4.33, in both LiI and TPAI series, the E_a values oscillates within a small range of values (0.08 to 0.12 eV) for low and moderate salt concentrations. A prominent rise in E_a value

can only be observed when the LiI and TPAI salt is in high amount (beyond 15 wt.%). Recent reports have highlighted that at low and moderate salt concentrations, the E_a value is largely independent of the salt concentration (Petrowsky & Frech, 2010). This is again attributed to the ion conduction mechanism through solvent channels, thus causing the ion transport to be dominated by a single activation process which substantially depends on the solvent family.

4.3.5 Photovoltaic performance

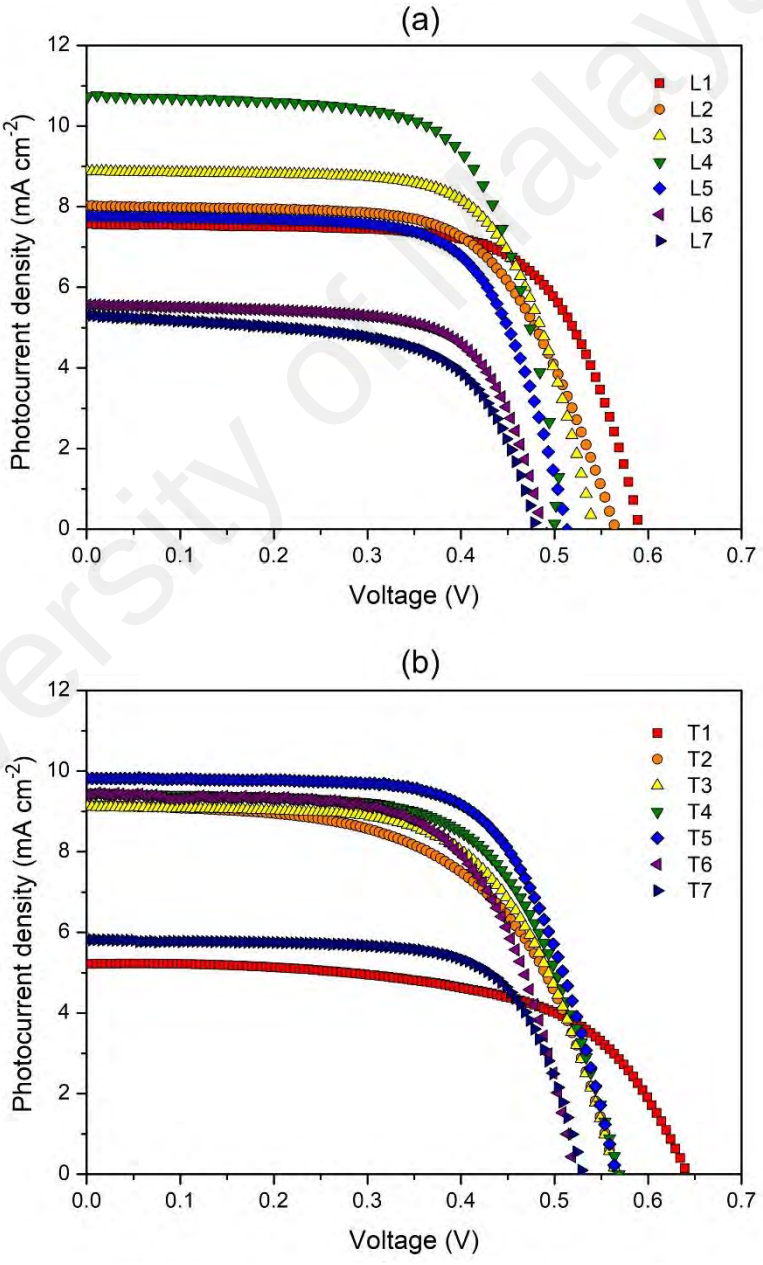

Figure 4.34: J-V curves of PhSt-HEC with (a) LiI and (b) TPAI gels

Figure 4.34 depicts the J-V curve obtained from the DSSC fabrication of the gel electrolytes. In the LiI series, a maximum value of photoconversion efficiency of 3.67% was obtained with the addition of 10.0 wt% LiI (Table 4.4). The trend in J_{SC} values showed increment up to 10.0 wt% LiI contributed by the increasing amount of iodide ions. However, beyond 10.0 wt% of LiI, the short circuit current values begin to drop and this is proposed to be the effect of higher concentration of Li^+ ions within the gel which may restrict the mobility of iodide ions. The open circuit voltage, on the other hand, exhibited a continuous downward trend as the amount of LiI increases.

Table 4.4: J-V parameters of PhSt-HEC-DMF-LiI gels

Sample	wt.% of LiI	σ ($\times 10^{-3}$ S cm^{-1})	η (%)	J_{SC} (mA cm^{-2})	V_{OC} (V)	FF
L1	2.5	3.38	3.07	7.69	0.59	0.68
L2	5.0	3.85	2.89	8.13	0.56	0.67
L3	7.5	4.83	3.29	8.85	0.54	0.69
L4	10.0	5.50	3.67	10.68	0.51	0.65
L5	12.5	5.35	2.74	7.77	0.51	0.68
L6	15.0	4.40	1.87	5.78	0.48	0.67
L7	17.5	4.29	1.57	5.03	0.48	0.65

This is because, small cations such as Li^+ have the tendency to be adsorbed onto the TiO_2 layer in the photoanode and this alters the flat band potentials (Liu *et al.*, 1998). The fill factor values for all the cells in this series are very similar, lying between 64 to 64 %. Therefore, the efficiency is mainly governed by the J_{SC} and the V_{OC} values. Between 2.5 to 10.0 wt.% of LiI, there is a drastic drop in V_{OC} accompanied by a sharp increase in Jsc. Both these phenomena are related to each other, as when the flat band potential of the semiconductor is lowered, the driving force for the electron injection from dye to TiO_2 increases (Wang & Peter, 2012). The higher injection efficiency, η_{inj} will sequentially improve J_{SC} values. Therefore, in these range of LiI compositions, the tug of war between

J_{SC} and V_{OC} affected efficiency value adversely. Beyond 10 wt.% LiI, decline in both J_{SC} and V_{OC} values cumulatively lead to a sharp dip in the solar cell efficiencies.

Table 4.5: J-V parameters of PhSt-HEC-DMF-TPAI gels

Sample	wt.% of TPAI	σ ($\times 10^{-3}$ S cm^{-1})	η (%)	J_{SC} (mA cm^{-2})	V_{OC} (V)	FF
T1	2.5	1.69	1.98	5.15	0.61	0.63
T2	5.0	3.41	3.02	9.02	0.57	0.60
T3	7.5	4.35	3.29	9.16	0.57	0.60
T4	10.0	4.54	3.40	9.46	0.56	0.64
T5	12.5	4.97	3.94	10.11	0.56	0.69
T6	15.0	4.35	3.21	8.92	0.52	0.68
T7	17.5	3.57	2.16	5.82	0.52	0.71

For the TPAI series, the highest efficiency of 3.94 % was attained upon inclusion of 12.5 wt.% of TPAI (Table 4.5). J_{SC} values increased with higher amount of TPAI up to 12.5 wt.%, more than which the values declined presumably due to ion aggregation. There was an initial drop in the V_{OC} value between 2.5 to 5.0 wt.% TPAI but from 5 wt.% onwards the values remained steady. Only when TPAI salt concentration higher than 12.5 wt.%, there was a perceptible decline of V_{OC} due to the cation adsorption. Fill factor values were found to be situated between 60 to 69 %. The overall pattern in efficiency for the TPAI series was heavily dependent on the J_{SC} values. Interestingly, the highest J_{SC} in the TPAI series was in fact lower than that in LiI series. Nevertheless, the ability of TPAI based electrolytes to sustain stable V_{OC} values yielded solar cell with better photoconversion efficiency (about 7% higher than LiI). Besides the small difference in performance, TPAI salt based gels are also generally preferred over LiI due to production sustainability. This is because, lithium salt has adverse effects in terms of long term availability and cost.

It is noteworthy to mention that the variation in J_{SC} of the TPAI series matched the trend in the ionic conductivities of these gels. However, in the LiI series, the J_{SC} values did not concur with the ionic conductivity values. These observations reflect the contribution of ionic species in the conductivity of both salt systems. When TPAI is employed as the charge carrier, the bulky TPAI is presumed to be entangled in the polymer matrix, allowing iodide ion mobility to mainly contribute to the overall ionic conductivity of the gel. Whereas, in the case of LiI, conductivity is the outcome of the motion of both Li^+ and I^- ions. Therefore, high conductivity does not necessarily translate into improved iodide ion transport.

4.3.6 Impedance study of DSSC

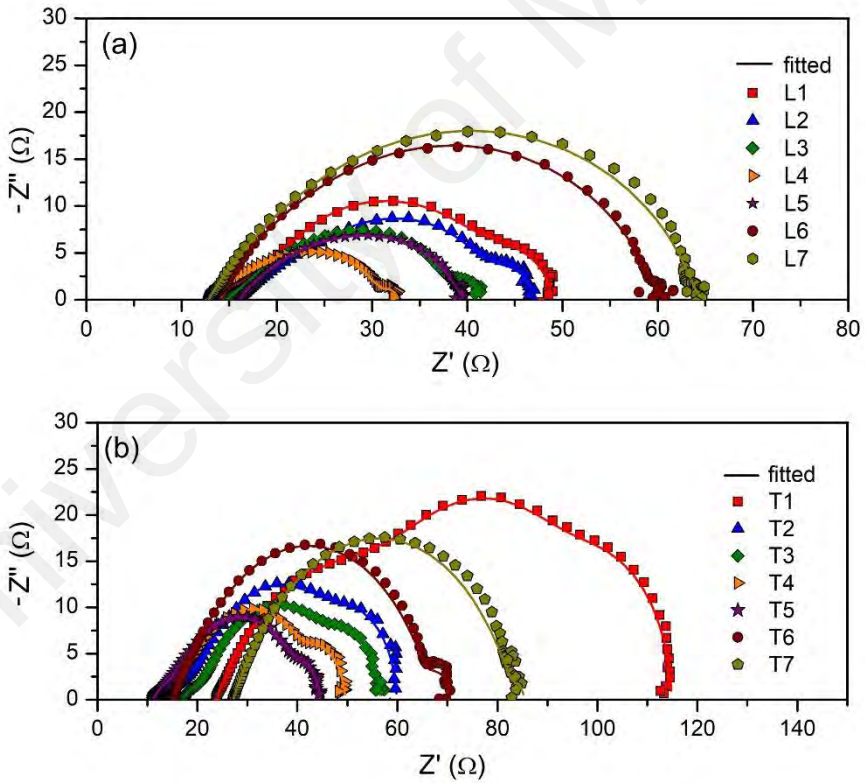

Figure 4.35: Nyquist plots of QSDSSC fabricated using (a) LiI and (b) TPAI gels

In both the series, the variation of salt content affected the impedance at each interface. As mentioned in section 4.2.2.3, the first semicircle appearing at higher frequency is attributed to the triiodide reduction at counter electrode (R_{PT})

$$I_3^- + 2e^- \rightarrow 3I^- \quad (4.2)$$

Thus a lower value of R_{PT} signifies an efficient electrocatalytic activity at the platinum electrode. As tabulated in Table 4.6, in the LiI series, the R_{PT} values between L1 to L4 were in the lower range (<10 Ω). This is seen to be repercussion of the high conductivity of these electrolytes which ensure rapid ion transport. Therefore, beyond L5, where a decline in ionic conductivity was also evident, the R_{PT} values escalate drastically. Similar observations were projected in the TPAI series, in which trends of σ and R_{PT} were inverse to each other.

Table 4.6: Equivalent circuit parameters of HEC-PhSt with LiI and TPAI gels

Designation	R_S (Ω)	R_{PT} (Ω)	R_{CT} (Ω)	R_D (Ω)	$\mathbf{D}_{I_3^-}$ ($\times 10^{-7}$ $cm^2\ s^{-1}$)	σ ($\times 10^{-3}$ $S\ cm^{-1}$)
LiI series						
L1	13.92	8.17	18.58	8.29	6.71	3.38
L2	15.91	8.12	17.62	5.48	6.46	3.85
L3	14.78	5.88	17.58	3.26	7.73	4.83
L4	12.68	6.36	11.97	1.89	8.76	5.50
L5	16.11	12.07	11.23	-	-	5.35
L6	13.21	32.90	12.95	-	-	4.40
L7	12.81	39.80	10.42	-	-	4.29
TPAI series						
T1	23.79	24.15	41.82	25.12	6.58	1.69
T2	13.43	9.16	22.59	15.72	7.23	3.41
T3	17.06	6.00	22.56	11.99	7.33	4.35
T4	12.37	5.62	21.58	9.00	8.38	4.54
T5	11.10	5.11	23.05	4.49	11.30	4.97
T6	15.03	23.50	26.47	6.09	4.15	4.35
T7	27.00	39.05	20.66	-	-	3.57

The second semicircle in the Nyquist plots addresses the charge recombination reaction between the photoanode and TiO_2 as represented in the equation below.

$$I_3^- + 2e^-(CB) \rightarrow 3I^- \quad (4.3)$$

Suppressing this reaction is important to maximize overall efficiency and thus larger R_{CT} will benefit the performance of the cell. In both LiI and TPAI series, increasing the salt content resulted in reduction of R_{CT} values. This trend can be associated with the diminishing adhesive nature of the gels as highlighted in the tack test analysis (Figure 4.26). Particularly, in the LiI series, appreciable decline in the R_{CT} were only observed beyond 10 wt.%, the same region at which minimum force of tack test drastically reduced. These findings emphasize that if the electrolyte employed possess good tack behavior to optimize the contact between electrodes, then suppression of charge recombination between photanode and I_3^- occurs more effectively.

Another interesting pattern noticed between the two series was that, predominantly the R_{CT} values of TPAI series was larger than LiI. The steric hindrance imposed by TPAI limits their penetration into the sensitized photoanode (Figure 4.36). This in turn minimizes the screening effect of negative charge at the TiO_2/electrolyte interface and successively diminishes local concentration of counter anions, I_3^-. Therefore the possibility of electron recombination from TiO_2 and I_3^- in the electrolyte is lower (Kuwahara *et al.*, 2014).

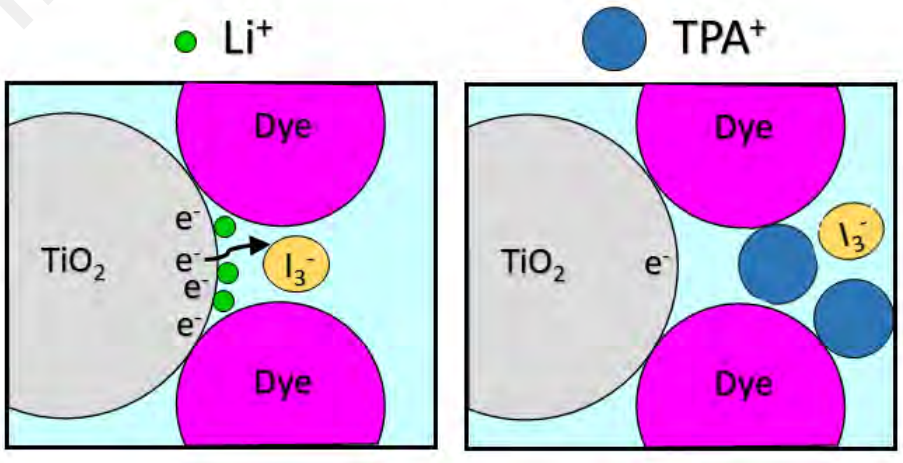

Figure 4.36: Cation interaction with photoanode surface

The third semicircle in the Nyquist plot appearing at lowest frequency domain correlates to the diffusion of the redox couple in the electrolyte. From Figure 4.35 it is apparent that for samples L5 to L7 and T7 the third semicircle is not present. It is suspected that for these samples, the impedance attributed to the Nernst diffusion process features at frequencies lower than the minimum limit of the instrument used (0.01 Hz). Nevertheless, by analyzing the electrolytes with the third semicircle, it was evident that R_D and $D_{I_3^-}$ values decreased with higher salt concentration and concurred with the conductivity values of the gels.

Overall, the sheet resistances of all the samples were found to be between 11 to 17 Ω except for T1 and T7 which showed unexceptionally high R_S values. The anomaly in the R_S values of T1 and T7 is attributed to poor ionic σ and recrystallization of salt respectively.

4.4 Effect of ionic liquid addition

From the previous section it was evident that a stable open circuit voltage can be obtained by employing TPAI as the salt. However in order to further improve the light-conversion efficiency, the short circuit current values need to be boosted. One of the efficient methods often adapted to improve J_{SC} values is by introducing ionic liquid as an auxiliary components into the system. In the next section, the effect of including 1-butyl-3-methylimidazolium iodide (BMII) into the GPEs are discussed in detail.

4.4.1 Rheological properties

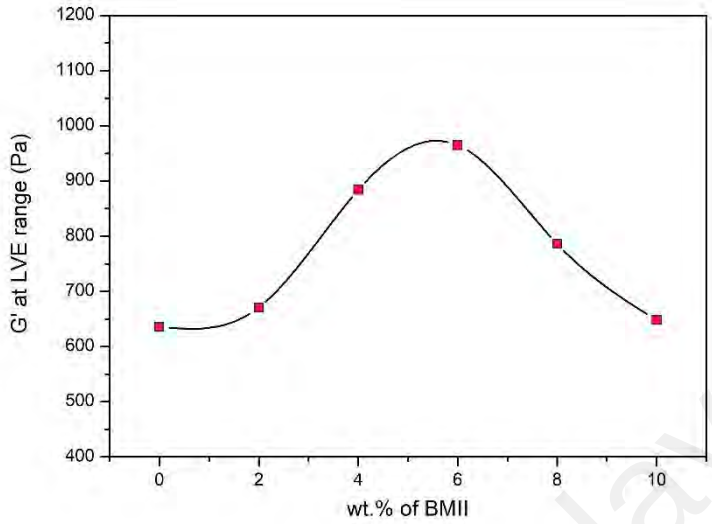

Figure 4.37: Storage modulus at LVE range of PhSt-HEC-DMF-TPAI-BMII gels

The amplitude sweep studies indicate that the storage moduli of LVE range increased with addition of ionic liquid (IL) in the system (Figure 4.37). At IL concentrations of higher than 6 wt.%, the G' values declined slightly but remained higher than gel without IL (BO). Similar pattern was realized for the critical strain values of the gels (Figure 4.38). The overall improvement in rigidity and strength of the gels upon inclusion of IL can be elucidated via two perspectives. Firstly, IL are generally known to be viscous in nature. Thus, the addition of IL inevitably increases the viscosity of the electrolytic solutions and consequently promotes the solid character of the gels. On the other hand, the presence of nitrogen atoms in the IL allows them to participate in hydrogen bonding with the polymer chains. The introduction of this new interaction contributes to the collective stiffer and stronger nature of the gels.

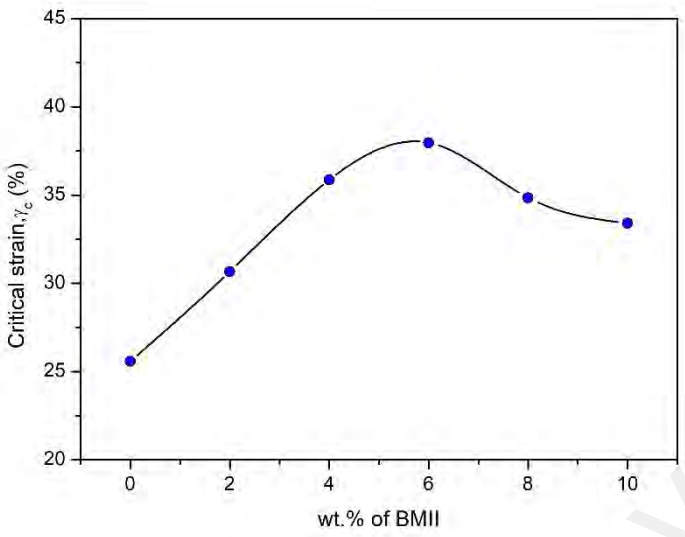

Figure 4.38: Critical strain values of PhSt-HEC-DMF-TPAI-BMII gels

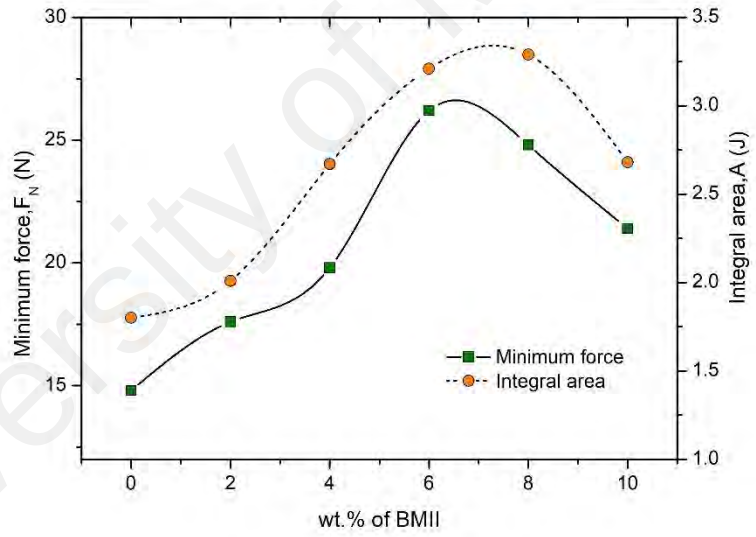

Figure 4.39: Tack test parameters of PhSt-HEC-DMF-TPAI-BMII gels

Tack test analysis also reveals that the minimum force values inflate followed by incorporation of IL, hinting improved gel tackiness (Figure 4.39). In particular, the integral areas which signifies summation of adhesive and cohesive forces, augment significantly with higher IL content. This findings further corroborate the existence of extensive polymer-IL interaction within the gel matrix.

4.4.2 Crystallinity

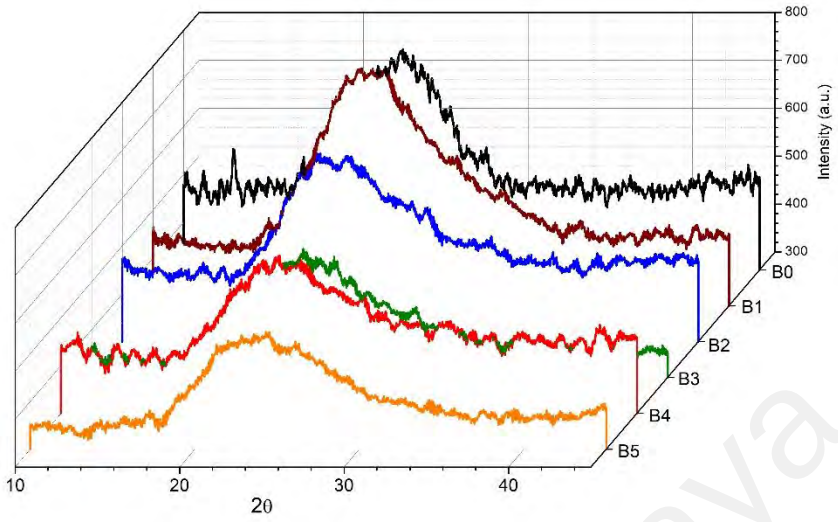

Figure 4.40: XRD diffractograms of PhSt-HEC-DMF-TPAI-BMII gels

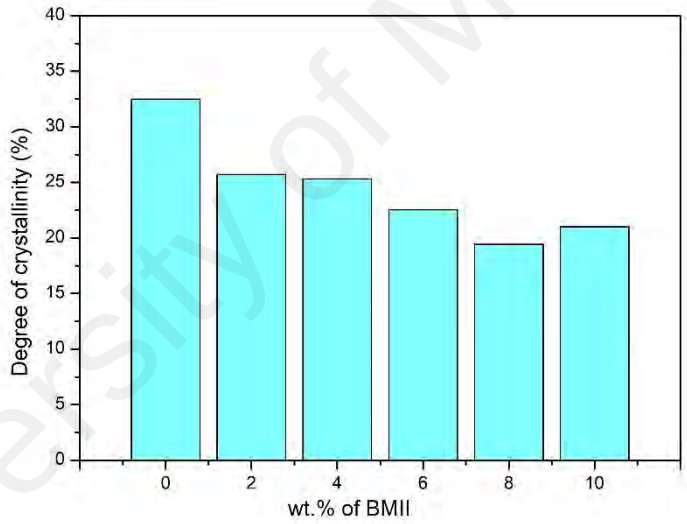

Figure 4.41: Degree of crystallinity of PhSt-HEC-DMF-TPAI-BMII gels

From XRD diffractograms in Figure 4.40, it is obvious that addition of IL has resulted the peak at 22° to decrease in intensity and increase in broadness. This became well translated in the degree of crystallinity of the gels which continued diminishing with further addition of IL (Figure 4.41). In fact, at B4, the degree of crystallinity was nearly half compared to B0. The plasticizing effect of IL in polymer gels has been previously reported in several studies. The highly mobile state of IL allows it to be interactive with the polymer chains and eventually depriving possibilities of polymer-polymer H-bonding.

4.4.3 Electrochemical properties

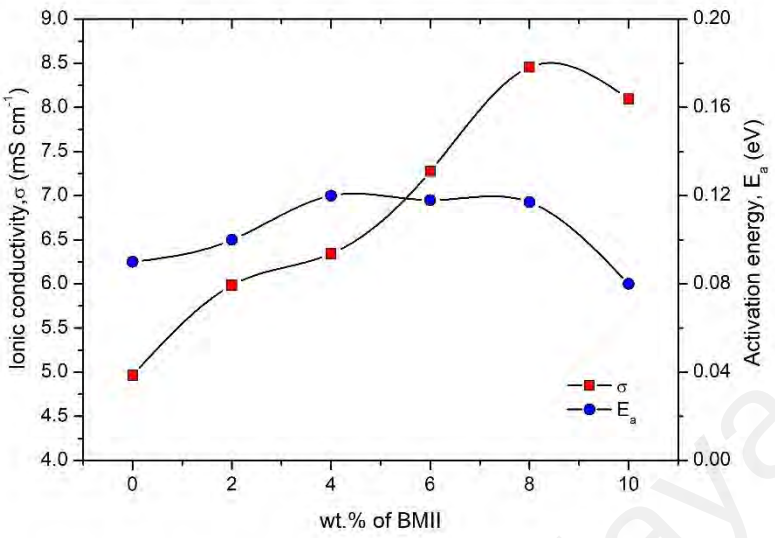

Figure 4.42: Ionic conductivity (at 30°C) and activation energy of PhSt-HEC-DMF-TPAI-BMII gels

One of the prominent features of IL which makes it a precious additives in electrolytes, is the ability to improve electrical performances. This is also evident in this study, as inclusion of BMII has remarkably enhanced the ionic conductivities of the gels (Figure 4.42). Being ions in the form of liquids, adding IL is expected to increase the number charge carriers with high mobility, hence favoring higher ionic conductivities of the gels. Beyond 8 wt.% of IL, the conductivity declined slightly and this can be attributed to the formation of neutral pairs owing to overcrowding of ions in the system. Temperature dependent conductivity studies of the gels revealed Arrhenian behavior (Appendix N). The activation energies exhibited slight decline with gradual addition of BMII up to 10 wt.%, indicating the existence of less tortuous pathway for ion mobility as an impact of ionic liquid incorporation.

4.4.4 Photovoltaic performance

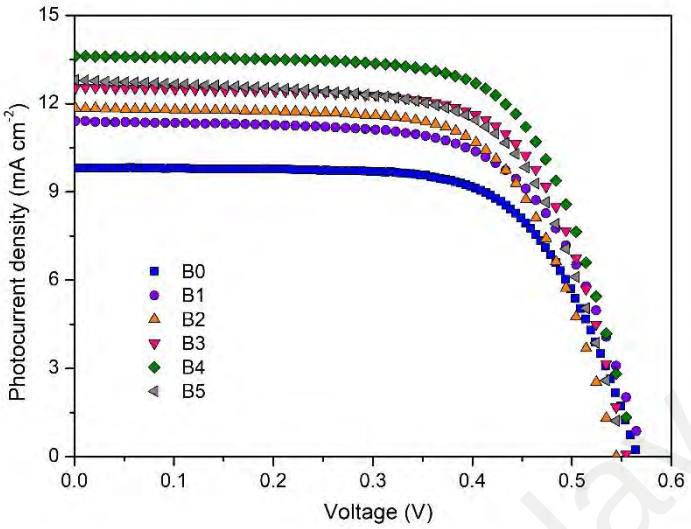

Figure 4.43: J-V curves of QSDSSC based on PhSt-HEC-DMF-TPAI-BMII gels

Table 4.7: J-V parameters of PhSt-HEC-DMF-TPAI-BMII gels

Sample	σ ($\times 10^{-3}$ S cm^{-1})	η (%)	J_{SC} (mA cm^{-2})	V_{OC} (V)	FF
B0	4.97	3.94	10.11	0.56	0.69
B1	5.98	4.24	11.41	0.56	0.65
B2	6.34	4.34	11.92	0.56	0.65
B3	7.28	4.76	12.54	0.55	0.69
B4	8.46	5.20	13.62	0.54	0.70
B5	8.10	4.65	12.80	0.54	0.67

Figure 4.43 depicts the J-V curves of DSSC comprising IL containing gel electrolytes. The J-V parameters of samples with added IL showed substantial improvement in JSC values (Table 4.7). The escalating photocurrent was translated into a boost in efficiency where the highest efficiency of 5.20 % was attained by addition of 8 wt.% of IL. The enhancement of J_{SC} values is attributed to the improved ionic conductivity of the samples. The fill factor values of these gels also were found to be consistently above 65 % and this can be attributed to the improved tack property of the gels.

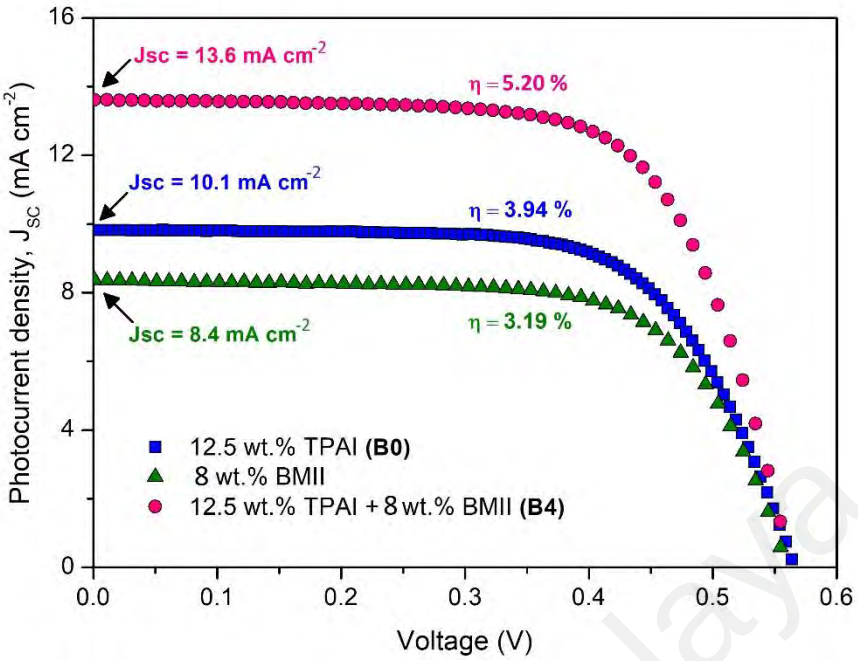

Figure 4.44: Comparison of photovoltaic performance with and without ionic liquid

To ensure that the uplift in the cell efficiency obtained by B4 is an outcome of the synergistic contribution of both TPAI and IL, a control sample which consist of 8 wt.% of IL added to blank polymer gels was prepared. The performance of polymer gels with TPAI, 8 wt.% IL and TPAI + 8wt.% IL is shown in Figure 4.44 from which it is evident that gels containing solely TPAI or BMII could not achieve the efficiency attained when both type of charge carrier are utilized.

4.4.5 Impedance study of DSSC

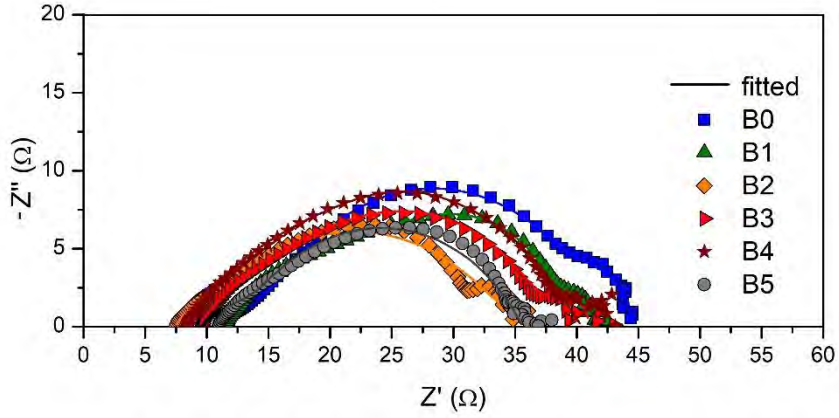

Figure 4.45: Nyquist plots of QSDSSC based on PhSt-HEC-DMF-TPAI-BMII gels

Table 4.8: Equivalent circuit parameters of PhSt-HEC-DMF-TPAI-BMII gels

Sample	R_S (Ω)	R_{PT} (Ω)	R_{CT} (Ω)	R_D (Ω)	$\mathbf{D}_{I_3^-}$ ($\times 10^{-6}$ cm^2 s^{-1})	σ ($\times 10^{-3}$ S cm^{-1})
B0	11.10	4.01	23.05	4.49	1.13	4.97
B1	11.11	3.21	23.30	3.99	1.30	5.98
B2	7.73	3.13	23.74	3.06	1.54	6.34
B3	9.21	3.02	24.76	3.06	1.59	7.28
B4	8.16	2.29	26.90	3.04	1.43	8.46
B5	10.65	2.25	22.68	3.17	1.35	8.10

The Nyquist plots of the PhSt-HEC-DMF-TPAI-BMII gels depicted triple semicircle persisting with the gels with only LiI or TPAI (Figure 4.45). As listed in Table 4.8, with gradual addition of ionic liquid, both the R_S and R_{PT} values of the cells declines slowly. These outcomes can be related to the enhanced ionic conductivity of the gels which facilitates ion transport, hence suppressing the impedance at interfaces. Similarly, when the ionic conductivity begins to decline in B5, an increase in R_S value was apparent. The effect of BMII addition is seen to influence the suppression of recombination reaction more effectively, as manifested by the inclined R_{CT} values. The bulky nature of the imidazolium cations are predicted to better shield the transport of electrons between electrolytes and semiconductor oxide layer. The trend in diffusion coefficient of I_3^- values with higher amount of BMII was rather intriguing as there was no significant increase despite the fact that J_{SC} values rose steadily. However, certain studies in literature have pointed out that, in the presence of viscous electrolytes such as ionic liquids, an alternative method for ion transport apart from the conventional diffusion mechanism may occur. This mechanism is called the Grotthus mechanism which integrates electron hopping and chemical bonds of polyiodide exchange, as illustrated below (Kawano & Watanabe, 2003; Kubo *et al.*, 2001; Usui *et al.*, 2004):

$$I_3^- + I^- \rightarrow I^- - I_2 \ldots I^- \rightarrow I^- \ldots I_2 - I^- \rightarrow I^- + I_3^- \quad (4.4)$$

Therefore, the transport of iodides via diffusion and Grotthus mechanism assist rapid ion mediated reactions to improve the overall efficiency of the cells.

CHAPTER 5: CONCLUSIONS

5.1 Conclusions

Starch was chemically modified with a simple and robust phthaloylation method by reacting starch with phthalic anhydride. The attachment of phthaloyl group to starch backbone was confirmed by FTIR and NMR studies. The effectiveness of the esterification process in suppressing the crystallinity of the starch molecules was validated by XRD analysis. The newly synthesized starch derivative was soluble in various organic solvents.

Different compositions of PhSt-HEC blends were used as the host to prepare polymers gels for QSDSSC fabrication. Starch based electrolyte have never been utilized as electrolyte in QSDSSC and this work is a pioneer attempt in this direction. Amplitude sweep studies showed that gels with good rigidity and strength properties can only be obtained with addition of 20 wt.% HEC onwards. From the tan δ values, it is evident that PhSt rich gels favored viscous character while HEC rich samples endorsed elastic character. Tack test results revealed that gels with improved adhesive property was achieved with the addition of HEC in the range of 20 to 60 wt.%. The effect of blending HEC into PhSt was also found to reduce crystallinity of the gels for blends up to 40 wt.% HEC. EIS analysis confirmed the detrimental effect of the gel rigidity which translated into poor ionic conductivity. QSDSSC were fabricated from gels with HEC between 20 to 60 wt.% and the maximum power-conversion efficiency of 3.02% was achieved with inclusion of 30 wt.% of HEC. The impact of the rheological properties of the gels on the interfacial charge transfer mechanisms in QSDSSC was demonstrated by impedance measurements of the cells. Gels with higher HEC content showed higher recombination resistance (R_{CT}) and lower counter electrode/electrolyte interfacial resistance (R_{PT}). This behavior is attributed to the adhesive properties of these gels which aids in improving electrode/electrolyte contact. However, the decline in ionic conductivity for samples with

HEC composition higher than 40 wt.% gave rise to a drop in J_{SC} values which resulted in lower efficiency.

The best polymer composition (70 % PhSt-30 % HEC) was used as the base to fabricate gel electrolytes with varying amounts of LiI and TPAI respectively to comprehend the effect of cation size on the QSDSSC performance. From amplitude sweep and tact test analyses, it was evident that the inclusion of LiI improved the rigidity and tack property of the gels. On the other hand, the converse was true for TPAI based gels which resulted in less rigid and tacky electrolytes. Crystallinity of the gels was found to decline with increasing amount of salt in both systems. The highest photoconversion efficiency of 3.94% was recorded upon addition of 12.5 wt.% TPAI. Generally, LiI based electrolytes exhibited higher J_{SC} but lower V_{OC} than TPAI based electrolytes. The good balance of high J_{SC} and V_{OC} values have enabled TPAI based electrolyte to manifest better photovoltaic performance.

The electrolyte composition with the best performance in the salt series (T5) was then further improved by addition of ionic liquid (BMII). Ionic conductivities of the gels were greatly boosted upon addition of ionic liquid and this translated into enhanced J_{SC} values. With the inclusion of 10 wt.% of BMII, the efficiency value of 5.20% was attained. To the best of our knowledge, this efficiency is the highest value in literature for DSSC based on starch based electrolytes.

5.2 Suggestion for future studies

The present work highlights the potential of starch and cellulose based gels as prospective electrolyte material in QSDSSC. However, the performance of these gels can be further improved based on the certain concepts proposed in recent literature. Among the proposed approaches are:

1. The best electrolyte system in this work can be subjected to sealing procedure followed by testing to study the stability of the cells.
2. A mixed solvent system comprising the organic solvent and plasticizer molecules such ethylene carbonate or succinonitrile is used to fabricate the gels. The presence high dielectric constant plasticizer can facilitate ionic dissociation to improve conductivity.
3. The rheological properties of starch based gels are modified by blending PhSt with other polysaccharide derivatives such guar gum and agarose.
4. Introduction of enhancers such as 4-tertbutyl pyridine (TBP) to improve the V_{OC} of the cells and in turn increase efficiency.
5. The redox couple used in the current work can be substituted to other types in order to fabricate different types of solar cells such as quantum-dot sensitized solar cell (QDDSSC).

REFERENCES

Adachi, M., Sakamoto, M., Jiu, J., Ogata, Y., & Isoda, S. (2006). Determination of Parameters of Electron Transport in Dye-Sensitized Solar Cells Using Electrochemical Impedance Spectroscopy. *The Journal of Physical Chemistry B, 110*(28), 13872-13880.

Agarwala, S., Thummalakunta, L. N. S. A., Cook, C. A., Peh, C. K. N., Wong, A. S. W., Ke, L., & Ho, G. W. (2011). Co-existence of LiI and KI in filler-free, quasi-solid-state electrolyte for efficient and stable dye-sensitized solar cell. *Journal of Power Sources, 196*(3), 1651-1656.

Aram, E., Ehsani, M., & Khonakdar, H. A. (2015). Improvement of ionic conductivity and performance of quasi-solid-state dye sensitized solar cell using PEO/PMMA gel electrolyte. *Thermochimica Acta, 615*, 61-67.

Arbab, A. A., Sun, K. C., Sahito, I. A., Memon, A. A., Choi, Y. S., & Jeong, S. H. (2016). Fabrication of textile fabric counter electrodes using activated charcoal doped multi walled carbon nanotube hybrids for dye sensitized solar cells. *Journal of Materials Chemistry A, 4*(4), 1495-1505.

Ardo, S., & Meyer, G. J. (2009). Photodriven heterogeneous charge transfer with transition-metal compounds anchored to TiO_2 semiconductor surfaces. *Chemical Society Reviews, 38*(1), 115-164.

Armand, M. (1994). The history of polymer electrolytes. *Solid State Ionics, 69*(3), 309-319.

Arof, A. K., Naeem, M., Hameed, F., Jayasundara, W. J. M. J. S. R., Careem, M. A., Teo, L. P., & Buraidah, M. H. (2014). Quasi solid state dye-sensitized solar cells based on polyvinyl alcohol (PVA) electrolytes containing I^- / I_3^- redox couple. *Optical and Quantum Electronics, 46*(1), 143-154.

Assadi, M. K., Bakhoda, S., Saidur, R., & Hanaei, H. (2018). Recent progress in perovskite solar cells. *Renewable and Sustainable Energy Reviews, 81*, 2812-2822.

Atichokudomchai, N., & Varavinit, S. (2003). Characterization and utilization of acid-modified cross-linked Tapioca starch in pharmaceutical tablets. *Carbohydrate Polymers, 53*(3), 263-270.

Avérous, L., Fringant, C., & Moro, L. (2001). Starch-Based Biodegradable Materials Suitable for Thermoforming Packaging. *Starch - Stärke, 53*(8), 368-371.

Backinowski, L. V., Tarchevsky, I. A., Chlenov, M. A., & Marchenko, G. N. (2013). *Cellulose: Biosynthesis and Structure*: Springer Berlin Heidelberg.

Bakrudeen, H. B., Sudarvizhi, C., & Reddy, B. S. R. (2016). Starch nanocrystals based hydrogel: Construction, characterizations and transdermal application. *Materials Science and Engineering: C, 68*, 880-889.

Bandara, T. M. W. J., Jayasundara, W. J. M. J. S. R., Dissanayake, M. A. K. L., Furlani, M., Albinsson, I., & Mellander, B. E. (2013). Effect of cation size on the performance of dye sensitized nanocrystalline TiO_2 solar cells based on quasi-solid state PAN electrolytes containing quaternary ammonium iodides. *Electrochimica Acta, 109*, 609-616.

Bar, N., & Basak, P. (2014). Quasi-Solid Semi-Interpenetrating Polymer Networks as Electrolytes: Part II. Assessing the Modes of Ion–Ion and Ion–Polymer Interactions Employing Mid-Fourier Transform Infrared Vibrational Spectroscopy. *The Journal of Physical Chemistry C, 118*(20), 10640-10650.

Bates, F. L., French, D., & Rundle, R. E. (1943). Amylose and Amylopectin Content of Starches Determined by their Iodine Complex Formation1. *Journal of the American Chemical Society, 65*(2), 142-148.

Beilvert, A., Chaubet, F., Chaunier, L., Guilois, S., Pavon-Djavid, G., Letourneur, D., Meddahi-Pellé, A., & Lourdin, D. (2014). Shape-memory starch for resorbable biomedical devices. *Carbohydrate Polymers, 99*, 242-248.

BeMiller, J. N., & Whistler, R. L. (2009). *Starch: Chemistry and Technology*. Amsterdam,Netherlands: Elsevier Science.

Bier, M., & Dietrich, S. (2010). Vapour pressure of ionic liquids. *Molecular Physics, 108*(2), 211-214.

Biswas, A., Shogren, R. L., Selling, G., Salch, J., Willett, J. L., & Buchanan, C. M. (2008). Rapid and environmentally friendly preparation of starch esters. *Carbohydrate Polymers, 74*(1), 137-141.

Builders, P. F., & Arhewoh, M. I. (2016). Pharmaceutical applications of native starch in conventional drug delivery. *Starch - Stärke, 68*(9-10), 864-873.

Buraidah, M. H., Shah, S., Teo, L. P., Chowdhury, F. I., Careem, M. A., Albinsson, I., Mellander, B. E., & Arof, A. K. (2017). High efficient dye sensitized solar cells using phthaloylchitosan based gel polymer electrolytes. *Electrochimica Acta, 245*, 846-853.

Cao, F., Oskam, G., & Searson, P. C. (1995). A Solid State, Dye Sensitized Photoelectrochemical Cell. *The Journal of Physical Chemistry, 99*(47), 17071-17073.

Carvalho, A. J. F. (2008a). Chapter 15 - Starch: Major Sources, Properties and Applications as Thermoplastic Materials. In M. N. Belgacem & A. Gandini (Eds.), *Monomers, Polymers and Composites from Renewable Resources* (pp. 321-342). Amsterdam: Elsevier.

Carvalho, A. J. F. (2008b). Chapter 15 - Starch: Major Sources, Properties and Applications as Thermoplastic Materials A2 - Belgacem, Mohamed Naceur. In A. Gandini (Ed.), *Monomers, Polymers and Composites from Renewable Resources* (pp. 321-342). Amsterdam: Elsevier.

Chalkias, D. A., Giannopoulos, D. I., Kollia, E., Petala, A., Kostopoulos, V., & Papanicolaou, G. C. (2018). Preparation of polyvinylpyrrolidone-based polymer electrolytes and their application by in-situ gelation in dye-sensitized solar cells. *Electrochimica Acta, 271*, 632-640.

Chang, H., Cho, K.-C., Kuo, C.-G., Kao, M.-J., Huang, K.-D., Chu, K.-H., & Lin, X.-P. (2011). Application of a Schottky barrier to dye-sensitized solar cells (DSSCs) with multilayer thin films of photoelectrodes. *Journal of Alloys and Compounds, 509*, S486-S489.

Chauhan, K., Priya, V., Singh, P., Chauhan, G. S., Kumari, S., & Singhal, R. K. (2015). A green and highly efficient sulfur functionalization of starch. *RSC Advances, 5*(64), 51762-51772.

Chen, C.-Y., Wang, M., Li, J.-Y., Pootrakulchote, N., Alibabaei, L., Ngoc-le, C.-h., Decoppet, J.-D., Tsai, J.-H., Grätzel, C., Wu, C.-G., Zakeeruddin, S. M., & Grätzel, M. (2009). Highly Efficient Light-Harvesting Ruthenium Sensitizer for Thin-Film Dye-Sensitized Solar Cells. *ACS Nano, 3*(10), 3103-3109.

Chen, L., Li, X., Li, L., & Guo, S. (2007). Acetylated starch-based biodegradable materials with potential biomedical applications as drug delivery systems. *Current Applied Physics, 7*, e90-e93.

Chen, X., Xu, D., Qiu, L., Li, S., Zhang, W., & Yan, F. (2013). Imidazolium functionalized TEMPO/iodide hybrid redox couple for highly efficient dye-sensitized solar cells. *Journal of Materials Chemistry A, 1*(31), 8759-8765.

Chi, W. S., Roh, D. K., Kim, S. J., Heo, S. Y., & Kim, J. H. (2013). Hybrid electrolytes prepared from ionic liquid-grafted alumina for high-efficiency quasi-solid-state dye-sensitized solar cells. *Nanoscale, 5*(12), 5341-5348.

Chong, M. Y., Numan, A., Liew, C.-W., Ramesh, K., & Ramesh, S. (2017). Comparison of the performance of copper oxide and yttrium oxide nanoparticle based hydroxylethyl cellulose electrolytes for supercapacitors. *Journal of Applied Polymer Science, 134*(13), doi: 10.1002/app.44636.

Conibeer, G. (2007). Third-generation photovoltaics. *Materials Today, 10*(11), 42-50.

Crompton, T. R. (1993). Degree of Crystallinity and Melting Temperature *Practical Polymer Analysis* (pp. 630-647). Boston, MA: Springer US.

Cruz, R., Pacheco Tanaka, D. A., & Mendes, A. (2012). Reduced graphene oxide films as transparent counter-electrodes for dye-sensitized solar cells. *Solar Energy, 86*(2), 716-724.

Deb, S. K. (1996). Thin-film solar cells: An overview. *Renewable Energy, 8*(1), 375-379.

Desilvestro, J., Graetzel, M., Kavan, L., Moser, J., & Augustynski, J. (1985). Highly efficient sensitization of titanium dioxide. *Journal of the American Chemical Society, 107*(10), 2988-2990.

Di Noto, V., Lavina, S., Giffin, G. A., Negro, E., & Scrosati, B. (2011). Polymer electrolytes: Present, past and future. *Electrochimica Acta, 57*(Supplement C), 4-13.

Dintcheva, N. T., Furlani, M., Jayasundara, W. J. M. J. S. R., Bandara, T. M. W. J., Mellander, B.-E., & La Mantia, F. P. (2013). Rheological behavior of PAN-based electrolytic gel containing tetrahexylammonium and magnesium iodide for photoelectrochemical applications. *Rheologica Acta, 52*(10), 881-889.

Dissanayake, M. A. K. L., Jayathissa, R., Seneviratne, V. A., Thotawatthage, C. A., Senadeera, G. K. R., & Mellander, B. E. (2014). Polymethylmethacrylate (PMMA) based quasi-solid electrolyte with binary iodide salt for efficiency enhancement in TiO2 based dye sensitized solar cells. *Solid State Ionics, 265*, 85-91.

Dragonetti, C., Magni, M., Colombo, A., Melchiorre, F., Biagini, P., & Roberto, D. (2018). Coupling of a Copper Dye with a Copper Electrolyte: A Fascinating Springboard for Sustainable Dye-Sensitized Solar Cells. *ACS Applied Energy Materials, 1*(2), 751-756.

Dragunski, D. C., & Pawlicka, A. (2002). Starch Based Solid Polymeric Electrolytes. *Molecular Crystals and Liquid Crystals, 374*(1), 561-568.

Echeverri, M., Kim, N., & Kyu, T. (2012). Ionic Conductivity in Relation to Ternary Phase Diagram of Poly(ethylene oxide), Succinonitrile, and Lithium Bis(trifluoromethane)sulfonimide Blends. *Macromolecules, 45*(15), 6068-6077.

El-Hag Ali, A., & AlArifi, A. (2009). Characterization and in vitro evaluation of starch based hydrogels as carriers for colon specific drug delivery systems. *Carbohydrate Polymers, 78*(4), 725-730.

Fabregat-Santiago, F., Garcia-Belmonte, G., Mora-Sero, I., & Bisquert, J. (2011). Characterization of nanostructured hybrid and organic solar cells by impedance spectroscopy. *Physical Chemistry Chemical Physics, 13*(20), 9083-9118.

Fan, L., Kang, S., Wu, J., Hao, S., Lan, Z., & Lin, J. (2010). Quasi-Solid State Dye-sensitized Solar Cells Based on Polyvinylpyrrolidone With Ionic Liquid. *Energy Sources, Part A: Recovery, Utilization, and Environmental Effects, 32*(16), 1559-1568.

Flores, S., Haedo, A. S., Campos, C., & Gerschenson, L. (2007). Antimicrobial performance of potassium sorbate supported in tapioca starch edible films. *European Food Research and Technology, 225*(3), 375-384.

Fredriksson, H., Silverio, J., Andersson, R., Eliasson, A. C., & Åman, P. (1998). The influence of amylose and amylopectin characteristics on gelatinization and retrogradation properties of different starches. *Carbohydrate Polymers, 35*(3), 119-134.

Friedrich, D. (2011). *A Study of Charge Transfer Kinetics in Dye-sensitized Surface Conductivity Solar Cells*. (Doctor of Philosophy), Free University of Berlin, Germany.

Ganjyal, G. M., Reddy, N., Yang, Y. Q., & Hanna, M. A. (2004). Biodegradable packaging foams of starch acetate blended with corn stalk fibers. *Journal of Applied Polymer Science, 93*(6), 2627-2633.

Ghanbari, A., Tabarsa, T., Ashori, A., Shakeri, A., & Mashkour, M. (2018). Preparation and characterization of thermoplastic starch and cellulose nanofibers as green nanocomposites: Extrusion processing. *International Journal of Biological Macromolecules, 112*, 442-447.

Gorlov, M., & Kloo, L. (2008). Ionic liquid electrolytes for dye-sensitized solar cells. *Dalton Transactions,* (20), 2655-2666.

Grätzel, M. (2003). Dye-sensitized solar cells. *Journal of Photochemistry and Photobiology C: Photochemistry Reviews, 4*(2), 145-153.

Grillet, A., Wyatt, N., & M. Gloe, L. (2012). *Polymer Gel Rheology and Adhesion*. London, UK: IntechOpen Publishing.

Guo, M., Diao, P., Wang, X., & Cai, S. (2005). The effect of hydrothermal growth temperature on preparation and photoelectrochemical performance of ZnO nanorod array films. *Journal of Solid State Chemistry, 178*(10), 3210-3215.

Gupta, S., & Varshney, P. K. (2017). Effect of plasticizer concentration on structural and electrical properties of hydroxyethyl cellulose (HEC)-based polymer electrolyte. *Ionics, 23*(6), 1613-1617.

Hagfeldt, A., Boschloo, G., Sun, L., Kloo, L., & Pettersson, H. (2010). Dye-Sensitized Solar Cells. *Chemical Reviews, 110*(11), 6595-6663.

Hagfeldt, A., & Grätzel, M. (2000). Molecular Photovoltaics. *Accounts of Chemical Research, 33*(5), 269-277.

Hamsan, M. H., Shukur, M. F., & Kadir, M. F. Z. (2017). The effect of NH_4NO_3 towards the conductivity enhancement and electrical behavior in methyl cellulose-starch blend based ionic conductors. *Ionics, 23*(5), 1137-1154.

Han, G., Zhang, S., Boix, P. P., Wong, L. H., Sun, L., & Lien, S.-Y. (2017). Towards high efficiency thin film solar cells. *Progress in Materials Science, 87*, 246-291.

Han, X., Chen, S., & Hu, X. (2009). Controlled-release fertilizer encapsulated by starch/polyvinyl alcohol coating. *Desalination, 240*(1), 21-26.

Hauch, A., & Georg, A. (2001). Diffusion in the electrolyte and charge-transfer reaction at the platinum electrode in dye-sensitized solar cells. *Electrochimica Acta, 46*(22), 3457-3466.

Hočevar, M., Krašovec, U. O., Bokalič, M., Topič, M., Veurman, W., Brandt, H., & Hinsch, A. (2013). Sol-gel based TiO_2 paste applied in screen-printed dye-sensitized solar cells and modules. *Journal of Industrial and Engineering Chemistry, 19*(5), 1464-1469.

Hsu, Y. C., Tseng, L. C., & Lee, R. H. (2014). Graphene oxide sheet–polyaniline nanohybrids for enhanced photovoltaic performance of dye-sensitized solar cells. *Journal of Polymer Science Part B: Polymer Physics, 52*(4), 321-332.

Hu, X., Wei, B., Zhang, B., Xu, X., Jin, Z., & Tian, Y. (2013). Synthesis and characterization of dextrin monosuccinate. *Carbohydrate Polymers, 97*(1), 111-115.

Huang, K.-C., Chen, P.-Y., Vittal, R., & Ho, K.-C. (2011). Enhanced performance of a quasi-solid-state dye-sensitized solar cell with aluminum nitride in its gel polymer electrolyte. *Solar Energy Materials and Solar Cells, 95*(8), 1990-1995.

Huang, X., Liu, Y., Deng, J., Yi, B., Yu, X., Shen, P., & Tan, S. (2012). A novel polymer gel electrolyte based on cyanoethylated cellulose for dye-sensitized solar cells. *Electrochimica Acta, 80*, 219-226.

Hug, H., Bader, M., Mair, P., & Glatzel, T. (2014). Biophotovoltaics: Natural pigments in dye-sensitized solar cells. *Applied Energy, 115*, 216-225.

Hui, R., Qi-he, C., Ming-liang, F., Qiong, X., & Guo-qing, H. (2009). Preparation and properties of octenyl succinic anhydride modified potato starch. *Food Chemistry, 114*(1), 81-86.

Huo, W., Xie, G., Zhang, W., Wang, W., Shan, J., Liu, H., & Zhou, X. (2016). Preparation of a novel chitosan-microcapsules/starch blend film and the study of its drug-release mechanism. *International Journal of Biological Macromolecules, 87*, 114-122.

Huo, Z., Dai, S., Wang, K., Kong, F., Zhang, C., Pan, X., & Fang, X. (2007). Nanocomposite gel electrolyte with large enhanced charge transport properties of an I_3^-/I^- redox couple for quasi-solid-state dye-sensitized solar cells. *Solar Energy Materials and Solar Cells, 91*(20), 1959-1965.

Hwang, D., Kim, D. Y., Jo, S. M., Armel, V., MacFarlane, D. R., Kim, D., & Jang, S.-Y. (2013). Highly Efficient Plastic Crystal Ionic Conductors for Solid-state Dye-sensitized Solar Cells. *Scientific Reports, 3*, 3520.

Ikhmayies, S. (2018). *Advances in Silicon Solar Cells*. Berlin,German: Springer International Publishing.

Isaad, J., El Achari, A., & Malek, F. (2013). Bio-polymer starch thin film sensors for low concentration detection of cyanide anions in water. *Dyes and Pigments, 97*(1), 134-140.

Ito, B. I., Freitas, J. N. d., Paoli, M.-A. D., & Nogueira, A. F. (2008). Application of a composite polymer electrolyte based on montmorillonite in dye-sensitized solar cells. *Journal of the Brazilian Chemical Society, 19*, 688-696.

Ito, S., Zakeeruddin, S. M., Humphry-Baker, R., Liska, P., Charvet, R., Comte, P., Nazeeruddin, M. K., Péchy, P., Takata, M., Miura, H., Uchida, S., & Grätzel, M. (2006). High-Efficiency Organic-Dye- Sensitized Solar Cells Controlled by Nanocrystalline-TiO_2 Electrode Thickness. *Advanced Materials, 18*(9), 1202-1205.

Jacob, M. M. E., & Arof, A. K. (2000). FTIR studies of DMF plasticized polyvinyledene fluoride based polymer electrolytes. *Electrochimica Acta, 45*(10), 1701-1706.

Jacob, M. M. E., Prabaharan, S. R. S., & Radhakrishna, S. (1997). Effect of PEO addition on the electrolytic and thermal properties of PVDF-$LiClO_4$ polymer electrolytes. *Solid State Ionics, 104*(3), 267-276.

Jasmien, W., V., G. S., Ellen, F., & A., D. J. (2015). Starch blends and their physicochemical properties. *Starch - Stärke, 67*(1-2), 1-13.

Jayakumar, G. C., Mehta, A., Rao, J. R., & Fathima, N. N. (2015). Ionic liquids: new age materials for eco-friendly leather processing. *RSC Advances, 5*(40), 31998-32005.

Jin, L., & Chen, D. (2012). Enhancement in photovoltaic performance of phthalocyanine-sensitized solar cells by attapulgite nanoparticles. *Electrochimica Acta, 72*, 40-45.

Joly, D., Pellejà, L., Narbey, S., Oswald, F., Chiron, J., Clifford, J. N., Palomares, E., & Demadrille, R. (2014). A Robust Organic Dye for Dye Sensitized Solar Cells Based on Iodine/Iodide Electrolytes Combining High Efficiency and Outstanding Stability. *Scientific Reports, 4*, 4033.

Kalyanasundaram, K., Vlachopoulos, N., Krishnan, V., Monnier, A., & Graetzel, M. (1987). Sensitization of titanium dioxide in the visible light region using zinc porphyrins. *The Journal of Physical Chemistry, 91*(9), 2342-2347.

Kamat, P. V. (2013). Quantum Dot Solar Cells. The Next Big Thing in Photovoltaics. *The Journal of Physical Chemistry Letters, 4*(6), 908-918.

Kandiel, T. A., Robben, L., Alkaim, A., & Bahnemann, D. (2013). Brookite versus anatase TiO_2 photocatalysts: phase transformations and photocatalytic activities. *Photochemical & Photobiological Sciences, 12*(4), 602-609.

Kang, G., Choi, J., & Park, T. (2016). Pt-Free Counter Electrodes with Carbon Black and 3D Network Epoxy Polymer Composites. *Scientific Reports, 6*, 22987.

Katsaros, G., Stergiopoulos, T., Arabatzis, I. M., Papadokostaki, K. G., & Falaras, P. (2002). A solvent-free composite polymer/inorganic oxide electrolyte for high efficiency solid-state dye-sensitized solar cells. *Journal of Photochemistry and Photobiology A: Chemistry, 149*(1), 191-198.

Kaur, B., Ariffin, F., Bhat, R., & Karim, A. A. (2012). Progress in starch modification in the last decade. *Food Hydrocolloids, 26*(2), 398-404.

Kaur, L., Singh, J., & Liu, Q. (2007). Starch – A Potential Biomaterial for Biomedical Applications. In M. R. Mozafari (Ed.), *Nanomaterials and Nanosystems for Biomedical Applications* (pp. 83-98). Dordrecht: Springer Netherlands.

Kawano, R., & Watanabe, M. (2003). Equilibrium potentials and charge transport of an I^-/I_3^- redox couple in an ionic liquid. *Chemical Communications,* (3), 330-331.

Khalil, M. I., & Aly, A. A. (2004). Use of cationic starch derivatives for the removal of anionic dyes from textile effluents. *Journal of Applied Polymer Science, 93*(1), 227-234.

Khan, M. Z. H., Al-Mamun, M. R., Halder, P. K., & Aziz, M. A. (2017). Performance improvement of modified dye-sensitized solar cells. *Renewable and Sustainable Energy Reviews, 71*, 602-617.

Khan, R. A., Mariotti, P., Navarini, L., Gilli, R., & Konowicz, P. A. (1997). Process for the preparation of coal aqueous suspensions and new anionic dispersing agents contained therein: Google Patents.

Khanmirzaei, M. H., & Ramesh, S. (2014). Nanocomposite polymer electrolyte based on rice starch/ionic liquid/TiO_2 nanoparticles for solar cell application. *Measurement, 58*, 68-72.

Khanmirzaei, M. H., Ramesh, S., & Ramesh, K. (2015a). Hydroxypropyl Cellulose Based Non-Volatile Gel Polymer Electrolytes for Dye-Sensitized Solar Cell Applications using 1-methyl-3-propylimidazolium iodide ionic liquid. *Scientific Reports, 5*, 18056.

Khanmirzaei, M. H., Ramesh, S., & Ramesh, K. (2015b). Polymer electrolyte based dye-sensitized solar cell with rice starch and 1-methyl-3-propylimidazolium iodide ionic liquid. *Materials & Design, 85*, 833-837.

Khiar, A. S. A., & Arof, A. K. (2010). Conductivity studies of starch-based polymer electrolytes. *Ionics, 16*(2), 123-129.

Kim, J. K., Seo, H., Son, M. K., Shin, I., Choi, J. H., Choi, S. W., & Kim, H. J. (2011). The optimization of TiO_2 compact layer in dye-sensitized solar cell by the analysis of performance and internal impedance. *Physica Status Solidi C, 8*(2), 634-636.

Kim, S.-S., Nah, Y.-C., Noh, Y.-Y., Jo, J., & Kim, D.-Y. (2006). Electrodeposited Pt for cost-efficient and flexible dye-sensitized solar cells. *Electrochimica Acta, 51*(18), 3814-3819.

Kim, S. R., Parvez, M. K., & Chhowalla, M. (2009). UV-reduction of graphene oxide and its application as an interfacial layer to reduce the back-transport reactions in dye-sensitized solar cells. *Chemical Physics Letters, 483*(1), 124-127.

Koganti, N., Mitchell, J. R., Ibbett, R. N., & Foster, T. J. (2011). Solvent Effects on Starch Dissolution and Gelatinization. *Biomacromolecules, 12*(8), 2888-2893.

Komiya, R., Han, L., Yamanaka, R., Islam, A., & Mitate, T. (2004). Highly efficient quasi-solid state dye-sensitized solar cell with ion conducting polymer electrolyte. *Journal of Photochemistry and Photobiology A: Chemistry, 164*(1), 123-127.

Kondaveeti, S., Chejara, D. R., & Siddhanta, A. K. (2013). A facile one-pot synthesis of a fluorescent agarose-O-naphthylacetyl adduct with slow release properties. *Carbohydrate Polymers, 98*(1), 589-595.

Kondaveeti S., Chudasama N.A., Chaudhary J.P., Meena R., & A.K., S. (2015). Functional modification of agarose: Synthesis of nanosize half-esters of succinic, phthalic and maleic acids. *Indian Journal of Chemistry, 54A*, 10.

Kubo, W., Murakoshi, K., Kitamura, T., Yoshida, S., Haruki, M., Hanabusa, K., Shirai, H., Wada, Y., & Yanagida, S. (2001). Quasi-Solid-State Dye-Sensitized TiO_2 Solar Cells: Effective Charge Transport in Mesoporous Space Filled with Gel Electrolytes Containing Iodide and Iodine. *The Journal of Physical Chemistry B, 105*(51), 12809-12815.

Kumar, M., Tiwari, T., & Srivastava, N. (2012). Electrical transport behaviour of bio-polymer electrolyte system: Potato starch + ammonium iodide. *Carbohydrate Polymers, 88*(1), 54-60.

Kuwahara, S., Taya, S., Osada, N., Shen, Q., Toyoda, T., & Katayama, K. (2014). Effect of electrolyte constituents on the motion of ionic species and recombination kinetics in dye-sensitized solar cells. *Physical Chemistry Chemical Physics, 16*(11), 5242-5249.

Lam, C. X. F., Mo, X. M., Teoh, S. H., & Hutmacher, D. W. (2002). Scaffold development using 3D printing with a starch-based polymer. *Materials Science and Engineering: C, 20*(1), 49-56.

Law, C., Pathirana, S. C., Li, X., Anderson, A. Y., Barnes, P. R. F., Listorti, A., Ghaddar, T. H., & O′Regan, B. C. (2010). Water-Based Electrolytes for Dye-Sensitized Solar Cells. *Advanced Materials, 22*(40), 4505-4509.

Lee, J. G., Cheon, J. H., Yang, H. S., Lee, D. K., & Kim, J. H. (2012). Enhancement of Photovoltaic Performance in Dye-Sensitized Solar Cells with the Spin-Coated TiO_2 Blocking Layer. *Journal of Nanoscience and Nanotechnology, 12*(7), 6026-6030.

Lee, T. D., & Ebong, A. U. (2017). A review of thin film solar cell technologies and challenges. *Renewable and Sustainable Energy Reviews, 70*, 1286-1297.

Lee, Y.-L., Shanmugam, V., Tsai, M.-H., Lin, J.-C., Teng, H., & Liu, I. P. (2018). Highly Efficient Quasi-solid-state Dye-sensitized Solar cell using Polyethylene oxide (PEO) and Poly(methyl methacrylate) (PMMA)-based Printable Electrolytes. *Journal of Materials Chemistry A*.

Li, B., Wang, L., Kang, B., Wang, P., & Qiu, Y. (2006). Review of recent progress in solid-state dye-sensitized solar cells. *Solar Energy Materials and Solar Cells, 90*(5), 549-573.

Li, M. X., Wang, X. W., Yang, Y. Q., Chang, Z., Wu, Y. P., & Holze, R. (2015). A dense cellulose-based membrane as a renewable host for gel polymer electrolyte of lithium ion batteries. *Journal of Membrane Science, 476*(Supplement C), 112-118.

Liang, J., & Ludescher, R. D. (2015). Effects of glycerol on the molecular mobility and hydrogen bond network in starch matrix. *Carbohydrate Polymers, 115*, 401-407.

Liew, C.-W., & Ramesh, S. (2015). Electrical, structural, thermal and electrochemical properties of corn starch-based biopolymer electrolytes. *Carbohydrate Polymers, 124*, 222-228.

Lin, N., Huang, J., Chang, P. R., Anderson, D. P., & Yu, J. (2011). Preparation, Modification, and Application of Starch Nanocrystals in Nanomaterials: A Review. *Journal of Nanomaterials, 2011*, 13.

Lin, Y., Li, J., Liu, K., Liu, Y., Liu, J., & Wang, X. (2016). Unique starch polymer electrolyte for high capacity all-solid-state lithium sulfur battery. *Green Chemistry, 18*(13), 3796-3803.

Liska, P., Vlachopoulos, N., Nazeeruddin, M. K., Comte, P., & Graetzel, M. (1988). cis-Diaquabis(2,2'-bipyridyl-4,4'-dicarboxylate)ruthenium(II) sensitizes wide band gap oxide semiconductors very efficiently over a broad spectral range in the visible. *Journal of the American Chemical Society, 110*(11), 3686-3687.

Liu, C. F., Sun, R. C., Zhang, A. P., & Ren, J. L. (2007). Preparation of sugarcane bagasse cellulosic phthalate using an ionic liquid as reaction medium. *Carbohydrate Polymers, 68*(1), 17-25.

Liu, H., Adhikari, R., Guo, Q., & Adhikari, B. (2013). Preparation and characterization of glycerol plasticized (high-amylose) starch–chitosan films. *Journal of Food Engineering, 116*(2), 588-597.

Liu, I. P., Hou, Y.-C., Li, C.-W., & Lee, Y.-L. (2017). Highly electrocatalytic counter electrodes based on carbon black for cobalt(III)/(II)-mediated dye-sensitized solar cells. *Journal of Materials Chemistry A, 5*(1), 240-249.

Liu, Y., Hagfeldt, A., Xiao, X.-R., & Lindquist, S.-E. (1998). Investigation of influence of redox species on the interfacial energetics of a dye-sensitized nanoporous TiO_2 solar cell. *Solar Energy Materials and Solar Cells, 55*(3), 267-281.

Liu, Y., Sun, X., Tai, Q., Hu, H., Chen, B., Huang, N., Sebo, B., & Zhao, X.-z. (2011). Efficiency enhancement in dye-sensitized solar cells by interfacial modification of conducting glass/mesoporous TiO_2 using a novel ZnO compact blocking film. *Journal of Power Sources, 196*(1), 475-481.

Lopez, O., Garcia, M. A., Villar, M. A., Gentili, A., Rodriguez, M. S., & Albertengo, L. (2014). Thermo-compression of biodegradable thermoplastic corn starch films containing chitin and chitosan. *LWT - Food Science and Technology, 57*(1), 106-115.

Lu, D., Xiao, C., & Xu, S. J. (2009). Starch-based completely biodegradable polymer materials. *eXPRESS Polymer Letters, 3*, 366-375.

Ma, X., Yu, J., He, K., & Wang, N. (2007). The Effects of Different Plasticizers on the Properties of Thermoplastic Starch as Solid Polymer Electrolytes. *Macromolecular Materials and Engineering, 292*(4), 503-510.

Mahmood, A. (2015). Recent research progress on quasi-solid-state electrolytes for dye-sensitized solar cells. *Journal of Energy Chemistry, 24*(6), 686-692.

Manek, R. V., Builders, P. F., Kolling, W. M., Emeje, M., & Kunle, O. O. (2012). Physicochemical and Binder Properties of Starch Obtained from Cyperus esculentus. *AAPS PharmSciTech, 13*(2), 379-388.

Manthina, V., & Agrios, A. G. (2016). Blocking layers for nanocomposite photoanodes in dye sensitized solar cells: Comparison of atomic layer deposition and $TiCl_4$ treatment. *Thin Solid Films, 598*, 54-59.

Marcondes, R. F. M. S., D'Agostini, P. S., Ferreira, J., Girotto, E. M., Pawlicka, A., & Dragunski, D. C. (2010). Amylopectin-rich starch plasticized with glycerol for polymer electrolyte application. *Solid State Ionics, 181*(13), 586-591.

Masina, N., Choonara, Y. E., Kumar, P., du Toit, L. C., Govender, M., Indermun, S., & Pillay, V. (2017). A review of the chemical modification techniques of starch. *Carbohydrate Polymers, 157*, 1226-1236.

Mathew, S., & Abraham, T. E. (2007). Physico-chemical characterization of starch ferulates of different degrees of substitution. *Food Chemistry, 105*(2), 579-589.

Mathew, S., Yella, A., Gao, P., Humphry-Baker, R., Curchod, B. F. E., Ashari-Astani, N., Tavernelli, I., Rothlisberger, U., Nazeeruddin, M. K., & Grätzel, M. (2014). Dye-sensitized solar cells with 13% efficiency achieved through the molecular engineering of porphyrin sensitizers. *Nature Chemistry, 6*, 242.

Mattos, R. I., Tambelli, C. E., Donoso, J. P., & Pawlicka, A. (2007). NMR study of starch based polymer gel electrolytes: Humidity effects. *Electrochimica Acta, 53*(4), 1461-1465.

Mezger, T. G. (2006). *The Rheology Handbook: For Users of Rotational and Oscillatory Rheometers*. Hanover,Germany: Vincentz Network.

Miao, M., Li, R., Jiang, B., Cui, S. W., Zhang, T., & Jin, Z. (2014). Structure and physicochemical properties of octenyl succinic esters of sugary maize soluble starch and waxy maize starch. *Food Chemistry, 151*, 154-160.

Milan, R., Selopal, G. S., Cavazzini, M., Orlandi, S., Boaretto, R., Caramori, S., Concina, I., & Pozzi, G. (2017). Dye-sensitized solar cells based on a push-pull zinc phthalocyanine bearing diphenylamine donor groups: computational predictions face experimental reality. *Scientific Reports, 7*(1), 15675.

Mudgil, D., Barak, S., & Khatkar, B. S. (2014). Guar gum: processing, properties and food applications—A Review. *Journal of Food Science and Technology, 51*(3), 409-418.

Muljana, H., van der Knoop, S., Keijzer, D., Picchioni, F., Janssen, L. P. B. M., & Heeres, H. J. (2010). Synthesis of fatty acid starch esters in supercritical carbon dioxide. *Carbohydrate Polymers, 82*(2), 346-354.

Murai, S., Mikoshiba, S., Sumino, H., & Hayase, S. (2002). Quasi-solid dye-sensitized solar cells containing chemically cross-linked gel: How to make gels with a small amount of gelator. *Journal of Photochemistry and Photobiology A: Chemistry, 148*(1), 33-39.

Nagaraj, P., Sasidharan, A., David, V., & Sambandam, A. (2017). Effect of Cross-Linking on the Performances of Starch-Based Biopolymer as Gel Electrolyte for Dye-Sensitized Solar Cell Applications. *Polymers, 9*(12), 667.

Namazi, H., Fathi, F., & Dadkhah, A. (2011). Hydrophobically modified starch using long-chain fatty acids for preparation of nanosized starch particles. *Scientia Iranica, 18*(3), 439-445.

Nazeeruddin, M. K., Baranoff, E., & Grätzel, M. (2011). Dye-sensitized solar cells: A brief overview. *Solar Energy, 85*(6), 1172-1178.

Nazeeruddin, M. K., De Angelis, F., Fantacci, S., Selloni, A., Viscardi, G., Liska, P., Ito, S., Takeru, B., & Grätzel, M. (2005). Combined Experimental and DFT-TDDFT Computational Study of Photoelectrochemical Cell Ruthenium Sensitizers. *Journal of the American Chemical Society, 127*(48), 16835-16847.

Nazeeruddin, M. K., Kay, A., Rodicio, I., Humphry-Baker, R., Mueller, E., Liska, P., Vlachopoulos, N., & Graetzel, M. (1993). Conversion of light to electricity by cis-X2bis(2,2'-bipyridyl-4,4'-dicarboxylate)ruthenium(II) charge-transfer sensitizers (X = Cl^-, Br^-, I^-, CN^-, and SCN^-) on nanocrystalline titanium dioxide electrodes. *Journal of the American Chemical Society, 115*(14), 6382-6390.

Ninago, M. D., López, O. V., Lencina, M. M. S., García, M. A., Andreucetti, N. A., Ciolino, A. E., & Villar, M. A. (2015). Enhancement of thermoplastic starch final properties by blending with poly(ε-caprolactone). *Carbohydrate Polymers, 134*, 205-212.

Nirmale, T. C., Karbhal, I., Kalubarme, R. S., Shelke, M. V., Varma, A. J., & Kale, B. B. (2017). Facile Synthesis of Unique Cellulose Triacetate Based Flexible and High Performance Gel Polymer Electrolyte for Lithium Ion Batteries. *ACS Applied Materials & Interfaces, 9*(40), 34773-34782.

Nogueira, A. F., Longo, C., & De Paoli, M. A. (2004). Polymers in dye sensitized solar cells: overview and perspectives. *Coordination Chemistry Reviews, 248*(13), 1455-1468.

Norizuki, I. (1980). Modified Starch Industry in Japan. *Journal of the Japanese Society of Starch Science, 27*(4), 281-294.

O'Regan, B., & Grätzel, M. (1991). A low-cost, high-efficiency solar cell based on dye-sensitized colloidal TiO_2 films. *Nature, 353*, 737.

Papageorgiou, N., Athanassov, Y., Armand, M., Bonho$_x$te, P., Pettersson, H., Azam, A., & Grätzel, M. (1996). The Performance and Stability of Ambient Temperature Molten Salts for Solar Cell Applications. *Journal of The Electrochemical Society, 143*(10), 3099-3108.

Park, N.-G. (2010). Dye-Sensitized Metal Oxide Nanostructures and Their Photoelectrochemical Properties. *Journal of The Korean Chemical Society, 13*(1), 10-18.

Patel, S. K., Malone, S., Cohen, C., Gillmor, J. R., & Colby, R. H. (1992). Elastic modulus and equilibrium swelling of poly(dimethylsiloxane) networks. *Macromolecules, 25*(20), 5241-5251.

Peng, B., Jungmann, G., Jäger, C., Haarer, D., Schmidt, H.-W., & Thelakkat, M. (2004). Systematic investigation of the role of compact TiO_2 layer in solid state dye-sensitized TiO_2 solar cells. *Coordination Chemistry Reviews, 248*(13), 1479-1489.

Pérez-Higueras, P., Muñoz, E., Almonacid, G., & Vidal, P. G. (2011). High Concentrator PhotoVoltaics efficiencies: Present status and forecast. *Renewable and Sustainable Energy Reviews, 15*(4), 1810-1815.

Petrowsky, M., & Frech, R. (2008). Concentration Dependence of Ionic Transport in Dilute Organic Electrolyte Solutions. *The Journal of Physical Chemistry B, 112*(28), 8285-8290.

Petrowsky, M., & Frech, R. (2010). Salt concentration dependence of the compensated Arrhenius equation for alcohol-based electrolytes. *Electrochimica Acta, 55*(4), 1285-1288.

Qiao, D., Liu, H., Yu, L., Bao, X., Simon, G. P., Petinakis, E., & Chen, L. (2016). Preparation and characterization of slow-release fertilizer encapsulated by starch-based superabsorbent polymer. *Carbohydrate Polymers, 147*, 146-154.

Qin, Y., & Peng, Q. (2012). Ruthenium Sensitizers and Their Applications in Dye-Sensitized Solar Cells. *International Journal of Photoenergy, 2012*, 21.

Raga, S. R., Barea, E. M., & Fabregat-Santiago, F. (2012). Analysis of the Origin of Open Circuit Voltage in Dye Solar Cells. *The Journal of Physical Chemistry Letters, 3*(12), 1629-1634.

Rajendran, S., Babu, R. S., & Sivakumar, P. (2007). Effect of salt concentration on poly (vinyl chloride)/poly (acrylonitrile) based hybrid polymer electrolytes. *Journal of Power Sources, 170*(2), 460-464.

Ramesh, S., Shanti, R., & Morris, E. (2012). Studies on the plasticization efficiency of deep eutectic solvent in suppressing the crystallinity of corn starch based polymer electrolytes. *Carbohydrate Polymers, 87*(1), 701-706.

Ratner, M. A., & Shriver, D. F. (1988). Ion transport in solvent-free polymers. *Chemical Reviews, 88*(1), 109-124.

Reinders, A., Verlinden, P., Freundlich, A., & van Sark, W. (2017). *Photovoltaic Solar Energy: From Fundamentals to Applications*. New Jersey,USA: Wiley.

Richhariya, G., Kumar, A., Tekasakul, P., & Gupta, B. (2017). Natural dyes for dye sensitized solar cell: A review. *Renewable and Sustainable Energy Reviews, 69*, 705-718.

Ruban, A. V. (2009). Plants in light. *Communicative & Integrative Biology, 2*(1), 50-55.

Salgado, A. J., Coutinho, O. P., Reis, R. L., & Davies, J. E. (2007). In vivo response to starch-based scaffolds designed for bone tissue engineering applications. *Journal of Biomedical Materials Research Part A, 80A*(4), 983-989.

Santander-Ortega, M. J., Stauner, T., Loretz, B., Ortega-Vinuesa, J. L., Bastos-González, D., Wenz, G., Schaefer, U. F., & Lehr, C. M. (2010). Nanoparticles made from novel starch derivatives for transdermal drug delivery. *Journal of Controlled Release, 141*(1), 85-92.

Sarker, S., Ahammad, A. J. S., Seo, H. W., & Kim, D. M. (2014). Electrochemical Impedance Spectra of Dye-Sensitized Solar Cells: Fundamentals and Spreadsheet Calculation. *International Journal of Photoenergy, 2014*, 17.

Sato, T., Banno, K., Maruo, T., & Nozu, R. (2005). New design for a safe lithium-ion gel polymer battery. *Journal of Power Sources, 152*(Supplement C), 264-271.

Schoch, T. J., & Elder, A. L. (1955). Starches in the Food Industry *Use Of Sugars And Other Carbohydrates In The Food Industry* (Vol. 12, pp. 21-34): American Chemical Society.

Selvanathan, V., Azzahari, A. D., Abd. Halim, A. A., & Yahya, R. (2017). Ternary natural deep eutectic solvent (NADES) infused phthaloyl starch as cost efficient quasi-solid gel polymer electrolyte. *Carbohydrate Polymers, 167*, 210-218.

Selvanathan, V., Halim, M. N. A., Azzahari, A. D., Rizwan, M., Shahabudin, N., & Yahya, R. (2018). Effect of polar aprotic solvents on hydroxyethyl cellulose-based gel polymer electrolyte. *Ionics, 24*(7), 1955-1964.

Shalini, S., Balasundara prabhu, R., Prasanna, S., Mallick, T. K., & Senthilarasu, S. (2015). Review on natural dye sensitized solar cells: Operation, materials and methods. *Renewable and Sustainable Energy Reviews, 51*, 1306-1325.

Sharma, S., Bulkesh, S., Ghoshal, S. K., & Mohan, D. (2017). Dye sensitized solar cells: From genesis to recent drifts. *Renewable and Sustainable Energy Reviews, 70*, 529-537.

Shi, D., Pootrakulchote, N., Li, R., Guo, J., Wang, Y., Zakeeruddin, S. M., Grätzel, M., & Wang, P. (2008). New Efficiency Records for Stable Dye-Sensitized Solar Cells with Low-Volatility and Ionic Liquid Electrolytes. *The Journal of Physical Chemistry C, 112*(44), 17046-17050.

Shi, Y., Zhan, C., Wang, L., Ma, B., Gao, R., Zhu, Y., & Qiu, Y. (2009). The electrically conductive function of high-molecular weight poly(ethylene oxide) in polymer gel electrolytes used for dye-sensitized solar cells. *Physical Chemistry Chemical Physics, 11*(21), 4230-4235.

Shogren, R. L., & Biswas, A. (2006). Preparation of water-soluble and water-swellable starch acetates using microwave heating. *Carbohydrate Polymers, 64*(1), 16-21.

Shukur, M. F., Ibrahim, F. M., Majid, N. A., Ithnin, R., & Kadir, M. F. Z. (2013). Electrical analysis of amorphous corn starch-based polymer electrolyte membranes doped with LiI. *Physica Scripta, 88*(2), 025601.

Shukur, M. F., & Kadir, M. F. Z. (2015). Hydrogen ion conducting starch-chitosan blend based electrolyte for application in electrochemical devices. *Electrochimica Acta, 158*, 152-165.

Singh, S., Singh, A., & Kaur, N. (2016). Efficiency Investigations of Organic/Inorganic Hybrid ZnO Nanoparticles Based Dye-Sensitized Solar Cells. *Journal of Materials, 2016*, 11.

Song, A., Huang, Y., Zhong, X., Cao, H., Liu, B., Lin, Y., Wang, M., & Li, X. (2017). Gel polymer electrolyte with high performances based on pure natural polymer matrix of potato starch composite lignocellulose. *Electrochimica Acta, 245*, 981-992.

Sreekala, C. S. N. O. A., Indiramma, J., Kumar, K. B. S. P., Sreelatha, K. S., & Roy, M. S. (2013). Functionalized multi-walled carbon nanotubes for enhanced photocurrent in dye-sensitized solar cells. *Journal of Nanostructure in Chemistry, 3*(1), 19.

Ståkhandske, C. M. V., Mink, J., Sandström, M., Pápai, I., & Johansson, P. (1997). Vibrational spectroscopic and force field studies of N,N-dimethylthioformamide, N,N-dimethylformamide, their deuterated analogues and bis(N,N-dimethylthioformamide)mercury(II) perchlorate. *Vibrational Spectroscopy, 14*(2), 207-227.

Stojanović, Ž., Jeremić, K., Jovanović, S., & Lechner, M. D. (2005a). A Comparison of Some Methods for the Determination of the Degree of Substitution of Carboxymethyl Starch. *Starch - Stärke, 57*(2), 79-83.

Stojanović, Ž., Katsikas, L., Popović, I., Jovanović, S., & Jeremić, K. (2005b). Thermal stability of starch benzoate. *Polymer Degradation and Stability, 87*(1), 177-182.

Stoppe, N., & Horn, R. (2017). How far are rheological parameters from amplitude sweep tests predictable using common physicochemical soil properties? *Journal of Physics: Conference Series, 790*(1), 012032.

Su'ait, M. S., Rahman, M. Y. A., & Ahmad, A. (2015). Review on polymer electrolyte in dye-sensitized solar cells (DSSCs). *Solar Energy, 115*, 452-470.

Sudhakar, Y. N., & Selvakumar, M. (2012). Lithium perchlorate doped plasticized chitosan and starch blend as biodegradable polymer electrolyte for supercapacitors. *Electrochimica Acta, 78*, 398-405.

Sudhakar, Y. N., Selvakumar, M., & Bhat, D. K. (2015). Preparation and characterization of phosphoric acid-doped hydroxyethyl cellulose electrolyte for use in supercapacitor. *Materials for Renewable and Sustainable Energy, 4*(3), 10.

Sung, J. H., Park, D. P., Park, B. J., Choi, H. J., & Jhon, M. S. (2005). Phosphorylation of Potato Starch and Its Electrorheological Suspension. *Biomacromolecules, 6*(4), 2182-2188.

Suryanarayanan, V., Lee, K.-M., Ho, W.-H., Chen, H.-C., & Ho, K.-C. (2007). A comparative study of gel polymer electrolytes based on PVDF-HFP and liquid electrolytes, containing imidazolinium ionic liquids of different carbon chain lengths in DSSCs. *Solar Energy Materials and Solar Cells, 91*(15), 1467-1471.

Tachibana, Y., Haque, S. A., Mercer, I. P., Durrant, J. R., & Klug, D. R. (2000). Electron Injection and Recombination in Dye Sensitized Nanocrystalline Titanium Dioxide Films: A Comparison of Ruthenium Bipyridyl and Porphyrin Sensitizer Dyes. *The Journal of Physical Chemistry B, 104*(6), 1198-1205.

Tan, W., Li, Q., Dong, F., Qiu, S., Zhang, J., & Guo, Z. (2017). Novel 1,2,3-triazolium-functionalized starch derivatives: Synthesis, characterization, and evaluation of antifungal property. *Carbohydrate Polymers, 160*, 163-171.

Teli, M. D., Rohera, P., Sheikh, J., & Singhal, R. (2009). Application of germinated maize starch in textile printing. *Carbohydrate Polymers, 75*(4), 599-603.

Teoh, K. H., Lim, C.-S., Liew, C.-W., Ramesh, S., & Ramesh, S. (2015). Electric double-layer capacitors with corn starch-based biopolymer electrolytes incorporating silica as filler. *Ionics, 21*(7), 2061-2068.

Tesch, S., Gerhards, C., & Schubert, H. (2002). Stabilization of emulsions by OSA starches. *Journal of Food Engineering, 54*(2), 167-174.

Thelakkat, M., Schmitz, C., & Schmidt, H. W. (2002). Fully Vapor-Deposited Thin-Layer Titanium Dioxide Solar Cells. *Advanced Materials, 14*(8), 577-581.

Tributsch, H. (2004). Dye sensitization solar cells: a critical assessment of the learning curve. *Coordination Chemistry Reviews, 248*(13), 1511-1530.

Usui, H., Matsui, H., Tanabe, N., & Yanagida, S. (2004). Improved dye-sensitized solar cells using ionic nanocomposite gel electrolytes. *Journal of Photochemistry and Photobiology A: Chemistry, 164*(1), 97-101.

Varshney, P. K., & Gupta, S. (2011). Natural polymer-based electrolytes for electrochemical devices: a review. *Ionics, 17*(6), 479-483.

Veerappan, G., Bojan, K., & Rhee, S.-W. (2012). Amorphous carbon as a flexible counter electrode for low cost and efficient dye sensitized solar cell. *Renewable Energy, 41*, 383-388.

Venkatesan, S., Obadja, N., Chang, T.-W., Chen, L.-T., & Lee, Y.-L. (2014). Performance improvement of gel- and solid-state dye-sensitized solar cells by utilization the blending effect of poly (vinylidene fluoride-co-hexafluropropylene) and poly (acrylonitrile-co-vinyl acetate) co-polymers. *Journal of Power Sources, 268*, 77-81.

Vondrák, J., Reiter, J., Velická, J., Klápště, B., Sedlaříková, M., & Dvořák, J. (2005). Ion-conductive polymethylmethacrylate gel electrolytes for lithium batteries. *Journal of Power Sources, 146*(1), 436-440.

Waita, S. M., Aduda, B. O., Mwabora, J. M., Niklasson, G. A., Granqvist, C. G., & Boschloo, G. (2009). Electrochemical characterization of TiO_2 blocking layers prepared by reactive DC magnetron sputtering. *Journal of Electroanalytical Chemistry, 637*(1), 79-83.

Wang, H., & Hu, Y. H. (2012). Graphene as a counter electrode material for dye-sensitized solar cells. *Energy & Environmental Science, 5*(8), 8182-8188.

Wang, H., & Peter, L. M. (2012). Influence of Electrolyte Cations on Electron Transport and Electron Transfer in Dye-Sensitized Solar Cells. *The Journal of Physical Chemistry C, 116*(19), 10468-10475.

Wang, L., Fang, S., Lin, Y., Zhou, X., & Li, M. (2005a). A 7.72% efficient dye sensitized solar cell based on novel necklace-like polymer gel electrolyte containing latent chemically cross-linked gel electrolyte precursors. *Chemical Communications,* (45), 5687-5689.

Wang, M., Lin, Y., Zhou, X., Xiao, X., Yang, L., Feng, S., & Li, X. (2008). Solidification of liquid electrolyte with imidazole polymers for quasi-solid-state dye-sensitized solar cells. *Materials Chemistry and Physics, 107*(1), 61-66.

Wang, P., Zakeeruddin, S. M., Comte, P., Exnar, I., & Grätzel, M. (2003a). Gelation of Ionic Liquid-Based Electrolytes with Silica Nanoparticles for Quasi-Solid-State Dye-Sensitized Solar Cells. *Journal of the American Chemical Society, 125*(5), 1166-1167.

Wang, P., Zakeeruddin, S. M., Moser, J. E., Nazeeruddin, M. K., Sekiguchi, T., & Grätzel, M. (2003b). A stable quasi-solid-state dye-sensitized solar cell with an amphiphilic ruthenium sensitizer and polymer gel electrolyte. *Nature Materials, 2*, 402.

Wang, Q., Ito, S., Grätzel, M., Fabregat-Santiago, F., Mora-Seró, I., Bisquert, J., Bessho, T., & Imai, H. (2006). Characteristics of High Efficiency Dye-Sensitized Solar Cells. *The Journal of Physical Chemistry B, 110*(50), 25210-25221.

Wang, Q., Moser, J.-E., & Graetzel, M. (2005b). *Electrochemical Impedance Spectroscopic Analysis of Dye-Sensitized Solar Cells* (Vol. 109).

Wang, X., Deng, R., Kulkarni, S. A., Wang, X., Pramana, S. S., Wong, C. C., Gratzel, M., Uchida, S., & Mhaisalkar, S. G. (2013a). Investigation of the role of anions in hydrotalcite for quasi-solid state dye-sensitized solar cells application. *Journal of Materials Chemistry A, 1*(13), 4345-4351.

Wang, X., Kulkarni, S. A., Ito, B. I., Batabyal, S. K., Nonomura, K., Wong, C. C., Grätzel, M., Mhaisalkar, S. G., & Uchida, S. (2013b). Nanoclay Gelation Approach toward Improved Dye-Sensitized Solar Cell Efficiencies: An Investigation of Charge Transport and Shift in the TiO_2 Conduction Band. *ACS Applied Materials & Interfaces, 5*(2), 444-450.

Wanninayake, W. M. N. M. B., Premaratne, K., Kumara, G. R. A., & Rajapakse, R. M. G. (2016). Use of lithium iodide and tetrapropylammonium iodide in gel electrolytes for improved performance of quasi-solid-state dye-sensitized solar cells: Recording an efficiency of 6.40%. *Electrochimica Acta, 191*, 1037-1043.

Wiberg, K. B., & Rablen, P. R. (1993). Substituent effects. 5. Vinyl and ethynyl derivatives. An examination of the interaction of amino and hydroxy groups with carbon-carbon double and triple bonds. *Journal of the American Chemical Society, 115*(20), 9234-9242.

Wilpiszewska, K., & Spychaj, T. (2007). Chemical modification of starch with hexamethylene diisocyanate derivatives. *Carbohydrate Polymers, 70*(3), 334-340.

Winther-Jensen, B., Winther-Jensen, O., Forsyth, M., & MacFarlane, D. R. (2008). High Rates of Oxygen Reduction over a Vapor Phase–Polymerized PEDOT Electrode. *Science, 321*(5889), 671-674.

Wu, J., Lan, Z., Hao, S., Li, P., Lin, J., Huang, M., Fang, L., & Huang, Y. (2008). Progress on the electrolytes for dye-sensitized solar cells *Pure and Applied Chemistry* (Vol. 80, pp. 2241).

Wu, J., Lan, Z., Lin, J., Huang, M., Huang, Y., Fan, L., & Luo, G. (2015). Electrolytes in Dye-Sensitized Solar Cells. *Chemical Reviews, 115*(5), 2136-2173.

Wu, J. H., Hao, S. C., Lan, Z., Lin, J. M., Huang, M. L., Huang, Y. F., Fang, L. Q., Yin, S., & Sato, T. (2007a). A Thermoplastic Gel Electrolyte for Stable Quasi-Solid-State Dye-Sensitized Solar Cells. *Advanced Functional Materials, 17*(15), 2645-2652.

Wu, J. H., Lan, Z., Lin, J. M., Huang, M. L., Hao, S. C., Sato, T., & Yin, S. (2007b). A Novel Thermosetting Gel Electrolyte for Stable Quasi-Solid-State Dye-Sensitized Solar Cells. *Advanced Materials, 19*(22), 4006-4011.

Xia, J., Masaki, N., Jiang, K., & Yanagida, S. (2007). Sputtered Nb_2O_5 as a Novel Blocking Layer at Conducting Glass/TiO_2 Interfaces in Dye-Sensitized Ionic Liquid Solar Cells. *The Journal of Physical Chemistry C, 111*(22), 8092-8097.

Xu, S., Luo, Y., & Zhong, W. (2011). Investigation of catalytic activity of glassy carbon with controlled crystallinity for counter electrode in dye-sensitized solar cells. *Solar Energy, 85*(11), 2826-2832.

Xu, Y. X., Kim, K. M., Hanna, M. A., & Nag, D. (2005). Chitosan–starch composite film: preparation and characterization. *Industrial Crops and Products, 21*(2), 185-192.

Yan, S. G., & Hupp, J. T. (1997). Energetics of Electron Transfer at the Nanocrystalline Titanium Dioxide Semiconductor/Aqueous Solution Interface: pH Invariance of the Metal-Based Formal Potential of a Representative Surface-Attached Dye Couple. *The Journal of Physical Chemistry B, 101*(9), 1493-1495.

Yang, Y., Hu, H., Zhou, C.-H., Xu, S., Sebo, B., & Zhao, X.-Z. (2011). Novel agarose polymer electrolyte for quasi-solid state dye-sensitized solar cell. *Journal of Power Sources, 196*(4), 2410-2415.

Yeh, M.-H., Lin, L.-Y., Sun, C.-L., Leu, Y.-A., Tsai, J.-T., Yeh, C.-Y., Vittal, R., & Ho, K.-C. (2014). Multiwalled Carbon Nanotube@Reduced Graphene Oxide Nanoribbon as the Counter Electrode for Dye-Sensitized Solar Cells. *The Journal of Physical Chemistry C, 118*(30), 16626-16634.

Yeh, N., & Yeh, P. (2013). Organic solar cells: Their developments and potentials. *Renewable and Sustainable Energy Reviews, 21*, 421-431.

Yoon, I.-N., Song, H.-k., Won, J., & Kang, Y. S. (2014). Shape Dependence of SiO_2 Nanomaterials in a Quasi-Solid Electrolyte for Application in Dye-Sensitized Solar Cells. *The Journal of Physical Chemistry C, 118*(8), 3918-3924.

Yu, H., Zhang, S., Zhao, H., Will, G., & Liu, P. (2009). An efficient and low-cost TiO_2 compact layer for performance improvement of dye-sensitized solar cells. *Electrochimica Acta, 54*(4), 1319-1324.

Yu, Z., Vlachopoulos, N., Gorlov, M., & Kloo, L. (2011). Liquid electrolytes for dye-sensitized solar cells. *Dalton Transactions, 40*(40), 10289-10303.

Yun, S., Freitas, J. N., Nogueira, A. F., Wang, Y., Ahmad, S., & Wang, Z.-S. (2016). Dye-sensitized solar cells employing polymers. *Progress in Polymer Science, 59*, 1-40.

Yusuf, S. N. F., Azzahari, A. D., Selvanathan, V., Yahya, R., Careem, M. A., & Arof, A. K. (2017). Improvement of N-phthaloylchitosan based gel polymer electrolyte in dye-sensitized solar cells using a binary salt system. *Carbohydrate Polymers, 157*, 938-944.

Zakeeruddin, S. M., & Grätzel, M. (2009). Solvent-Free Ionic Liquid Electrolytes for Mesoscopic Dye-Sensitized Solar Cells. *Advanced Functional Materials, 19*(14), 2187-2202.

Zama, I., Martelli, C., & Gorni, G. (2017). Preparation of TiO_2 paste starting from organic colloidal suspension for semi-transparent DSSC photo-anode application. *Materials Science in Semiconductor Processing, 61*, 137-144.

Zarski, A., Ptak, S., Siemion, P., & Kapusniak, J. (2016). Esterification of potato starch by a biocatalysed reaction in an ionic liquid. *Carbohydrate Polymers, 137*, 657-663.

Zhang, B., Zhou, Y., Li, X., Wang, J., Li, G., Yun, Q., & Wang, X. (2014a). Li^+-molecule interactions of lithium tetrafluoroborate in propylene carbonate + N,N-dimethylformamide mixtures: An FTIR spectroscopic study. *Spectrochimica Acta Part A: Molecular and Biomolecular Spectroscopy, 124*(Supplement C), 40-45.

Zhang, M. Y., Li, M. X., Chang, Z., Wang, Y. F., Gao, J., Zhu, Y. S., Wu, Y. P., & Huang, W. (2017). A Sandwich PVDF/HEC/PVDF Gel Polymer Electrolyte for Lithium Ion Battery. *Electrochimica Acta, 245*(Supplement C), 752-759.

Zhang, Z., Macquarrie, D. J., Clark, J. H., & Matharu, A. S. (2014b). Chemical modification of starch and the application of expanded starch and its esters in hot melt adhesive. *RSC Advances, 4*(79), 41947-41955.

Zheng, W., Qi, T., Zhang, Y.-c., Shi, H.-y., & Tian, J.-q. (2015). Fabrication and characterization of a multi-walled carbon nanotube-based counter electrode for dye-sensitized solar cells. *New Carbon Materials, 30*(5), 391-396.

Zhiguan, Y., Daniel, G., & Ramani, N. (2013). Extrusion of humidity-resistant starch foam sheets. *Polymer Engineering & Science, 53*(4), 857-867.

Zhong, Y., Song, X., & Li, Y. (2011). Antimicrobial, physical and mechanical properties of kudzu starch–chitosan composite films as a function of acid solvent types. *Carbohydrate Polymers, 84*(1), 335-342.

Zhou, J., Ren, L., Tong, J., Xie, L., & Liu, Z. (2009). Surface esterification of corn starch films: Reaction with dodecenyl succinic anhydride. *Carbohydrate Polymers, 78*(4), 888-893.

Zhu, Z. (2003). Starch mono-phosphorylation for enhancing the stability of starch/PVA blend pastes for warp sizing. *Carbohydrate Polymers, 54*(1), 115-118.

Zistler, M., Wachter, P., Wasserscheid, P., Gerhard, D., Hinsch, A., Sastrawan, R., & Gores, H. J. (2006). Comparison of electrochemical methods for triiodide diffusion coefficient measurements and observation of non-Stokesian diffusion behaviour in binary mixtures of two ionic liquids. *Electrochimica Acta, 52*(1), 161-169.

LIST OF PUBLICATIONS AND PAPERS PRESENTED

Publications:

Selvanathan, V., Halim, M. N. A., Azzahari, A. D., Rizwan, M., Shahabudin, N., & Yahya, R. (2018). Effect of polar aprotic solvents on hydroxyethyl cellulose-based gel polymer electrolyte. *Ionics,*24,1955-1964.

Selvanathan, V., Azzahari, A. D., Abd. Halim, A. A., & Yahya, R. (2017). Ternary natural deep eutectic solvent (NADES) infused phthaloyl starch as cost efficient quasi-solid gel polymer electrolyte. *Carbohydrate Polymers*, 167, 210-218.

Conferences:

Selvanathan, V. & Yahya, R., Effect Of Rheological Properties Of Polysaccharide Based Gel Polymer Electrolyte On Quasi-Solid Dye Sensitized Solar Cell Performance, 3rd International Conference on Science and Engineering Materials (ICSEM), 6-8th January 2018, Sharda University, Delhi,India – Oral presenter

Selvanathan, V. & Yahya, R., Effect Of Polar Aprotic Solvents On Hydroxyethyl Cellulose-Based Gel Polymer Electrolyte, 6th International Conference on Functional Materials and Devices (ICFMD), 15-18th August 2017, Bayview Hotel, Melaka, Malaysia – Oral presenter